9-2023

Utilizing the 3D Environment to Facilitate Learning of Complex Visual Neural Pathways in the Avian Brain

Parker Straight
University of Arkansas-Fayetteville

Utilizing the 3D Environment to Facilitate Learning of Complex Visual Neural Pathways in the Avian Brain

A thesis submitted in partial fulfillment
of the requirements for the degree of
Master of Science in Poultry Science

by

Parker Straight
University of Arkansas
Bachelor of Science in Poultry Science, 2020

December 2022
University of Arkansas

This thesis is approved for the recommendation to the Graduate Council.

_____
Wayne Kuenzel, Ph.D.
Thesis Director

_____
Adnan Alrubaye, Ph.D.
Committee Member

_____
Paul Gignac, Ph.D.
Ex-Officio Committee Member

_____
Xiaolun Sun, Ph.D.
Committee Member

Abstract

Neuroanatomical pathways are difficult to study often due to the limit of methods used to visualize the anatomical and physiologic characteristics. In many studies, a neural pathway is presented using 2D representations for structural connectivity. A problem is deciding which of three planes: coronal, sagittal, or horizontal is best for visualizing the pathway's components clearly and spatially precise for those wanting to learn and utilize that information. A 3D environment would be imperative in solving this issue. We therefore attempted to develop a means of accurately presenting detailed anatomical structures within the 3D regions they occurred. It is our hope that accurate, spatial representations of visual neural pathways will result in learning specific structures, their subdivisions, and their spatial organizations. Advancements in imaging techniques address this issue and have allowed for a new avenue of investigation for studying the morphology of anatomical systems. One such technique, diffusible iodine-based contrast-enhanced computed tomography (diceCT), has allowed for nondestructive visualization of an appropriately fixed brain. In other words, it allows one to image the entire brain, and visualize any of the three planes without damaging the specimen.

We have chosen the visual tectofugal and thalamofugal pathways in an avian brain as they are some of the most well studied systems that seems to have much disparity in their anatomical organization and connectivity. The tectofugal pathway begins in the eyeball with retinal ganglion cells projecting to the optic tectum which in turn send projections to a thalamic nucleus. This thalamic nucleus then projects to a region of the forebrain, completing the ascending pathway. The thalamofugal pathway begins in the eyeball with retinal ganglion cells projecting to the lateral geniculate complex, which in turn projects bilaterally to a large terminal forebrain structure occupying the dorsomedial brain surface. For our investigation we employed two

techniques: (1) a series of stacked histologic sections of four chick brains, and (2) a diceCT stained whole brain of a chick. For histological sections, we used series of coronal, sagittal, and horizontal sections stained with Nissl (cell bodies revealed) and Luxol Fast Blue or Gallyas silver myelin (fiber tracts revealed). Sections were imported into Brainmaker (Microbrightfield Biosciences), a software that stacks image sequences and reconstructs volumes based on sequential contours. For our diceCT investigation, we rendered the eyeball and brain within the skull of the bird. This allowed an accurate spatial representation of the eyeball with respect to the brain. Post model processing was essential to integrate detailed 2D images in the appropriate plane of the 3D environment. Using the histological image stacks, diceCT scanned eye and brain, and 3D editing software, we created an interactive 3D model of the avian visual tectofugal and thalamofugal pathways. The combination of histochemical sections with diceCT 3D modeling is necessary when detailed anatomical and spatial organization of complex neural pathways such as the tectofugal visual system are desired.

Acknowledgements

I would like to first express my gratitude to my major advisor, Dr. Wayne Kuenzel, for his continuous guidance and support during my master's program. I am thankful for the opportunity he has given me to grow as an individual, and as a researcher. This accomplishment would not be possible without his encouragement and support.

I wish to thank Dr. Paul Gignac for his consistent support at each step of this project. His expertise and advice were imperative for the completion of this project. It was truly an honor to work alongside such a brilliant mind.

I would like to thank the members of my committee, Dr. Sun, Dr. Alrubaye, and Dr. Gignac for spending their time and effort reviewing my thesis work.

I would like to thank my family for their relentless reassurance and love. Special thanks to my mom and dad, for giving me the tools to achieve greatness. You have instilled in me integrity, rigor, and empathy among many qualities that were vital to my success.

Finally, I would like to thank my fiancé, Hagen Delaney, for your endless love and support even from 300 miles away. Our weekends together, whether it meant going on a dinner date, seeing a movie, shopping on the square, or staying inside, I will always cherish those moments with you.

Dedication

This thesis work is dedicated to my late grandmother, Elizabeth E. Johnston (July 2, 1940 -- March 14, 2017). Your kindness and strength were inspiring, and I hope I can be a fraction of the person you were. You will forever be in my heart.

Epigraph

“As long as our brain is a mystery, the universe, the reflection of the structure of the brain will also be a mystery.”
— Santiago Ramón y Cajal

Table of Contents

Nomenclature

ac, anterior commissure

AD, dorsal arcopallium

AI, intermediate arcopallium

AId, dorsal subdivision of the of the intermediate arcopallium

AIv, ventral subdivision of the intermediate arcopallium

ARP, arcopallium

CEV, cresylecht violet

ChAT, choline acetyltransferase

csm, corticoseptomesencephalic tract

diceCT, diffusible iodine-based contrast-enhanced computed tomography

DLAlr, dorsolateral anterior thalamus, lateral rostral part

DLAmc, dorsolateral anterior thalamus, magnocellular part

DLL, dorsolateral anterior thalamus, lateral part

DLLd, dorsal division of the dorsolateral anterior thalamus, lateral part

DLLv, ventral division of the dorsolateral anterior thalamus, lateral part

dsd, dorsal supraoptic decussation

Eb, belt of the entopallium

Ee, external core of the entopallium

Ei, internal core of the entopallium

Ento, entopallium

GABA, γ-Aminobutyric acid

GAD, glutamic acid decarboxylase

GLd, dorsal lateral geniculate nuclear complex

GSM, gallyas silver myelin

HA, apical hyperpallium

HAI, intercalated nucleus of the apical hyperpallium

HD, densocellular hyperpallium

HF, hippocampal formation

HIS, superior intercalatum hyperpallium

iit, intra-isthmal tract

Imc, nucleus isthmus, magnocellular part

IMM, internal medial mesopallium

iot, isthmo-optic tract

Ipc, nucleus isthmus, parvocellular part

ISPT, intermediate subpretectal nucleus

LdOPT, lateral dorsal principal optic thalamus

lfb, lateral forebrain bundle

LFBS, luxol fast blue

MVL, ventral lateral mesopallium

N, nissl

NCL, caudal lateral nidopallium

NFL, frontal lateral nidopallium

NI, intermediate nidopallium

NIL, intermediate lateral nidopallium

omt, occipital mesencephalic tract

OPT, principal optic nucleus of the thalamus

pspt, pretecto-subpretectal tract

PT, pretectal nucleus

RGCs, retinal ganglion cells

ROT/Rt, nucleus rotundus

ROTd, dorsal subdivision of the nucleus rotundus

ROTi, intermediate subdivision of the nucleus rotundus

ROTlp, lateral posterior subdivision of the nucleus rotundus

ROTv, ventral subdivision of the nucleus rotundus

SLu, semilunar nucleus

SP, subpretectal nucleus

SPC, superficial parvocellular nucleus

SpROT, suprarotundus

SROT, subrotundus

T, triangularis

TeO, optic tectum

TGC, tectal ganglion cell

csm, corticoseptomesencephalic tract

ttt, tectothalamic tract

vat, ventral arcopallial tract

VGLuT2, glutamate vesicular transporter 2

W, wulst

List of Figures

List of Tables

Chapter 1. Introduction

Vision is a very important sensory modality for most amniotes and the pathways utilized for processing vision share many similarities (Ott 2005). Vision is especially important in avian species, being utilized for a variety of complex behaviors such as predator detection, mating, foraging or hunting, and migratory navigation or homing. Because birds have such highly specialized visual processing components, this makes them excellent candidates for studying their visual morphology and how these changes in morphology generate functional differences.

The pathways processing visual information required for these complex behaviors have been well documented in several species including the chicken (Koshiba et al., 2002), pigeon (Benowitz and Karten, 1976), zebra finch (Watanabe et al., 2011), owl (Gutierrez-Ibanez et al., 2012), and starling (Hart et al., 1998) among others. However, there is a number of structural and therefore functional differences among species likely due to the distinct visual ecologies a species might possess. For example, it would be advantageous for a ground foraging bird such as the chicken or pigeon to have a highly developed set of components to process differential patterns to discriminate food versus non-food in the binocular field while having a set of developed components to detect incoming predators in their lateral field. Conversely, raptorial species likely have well-developed components needed to process time to collision for prey capture.

Here we will review the current understanding of the anatomical structures, their spatial organization, and connectivity that provide the basis for visual processing in birds. We will first discuss the diversity of perceptive visual fields and retinal organization and how they ultimately determine the contribution of which visual system dictates processing. We will then discuss previous research investigating the anatomical and functional characteristics of the tectofugal

and thalamofugal pathways. Finally, we discuss more recent research investigating higher visual associative areas and how they could act as points of integration or communication between the distinct visual pathways. This provides us the necessary information to create current comprehensive visual system models for use in both research and education.

Chapter 2. Literature Review

2.1 Visual Fields and the Retina

Birds are highly visual organisms that experience a wide range of visual ecologies owing to the diversity of their visual processing mechanisms. The systems performing visual processing have been fine-tuned to enhance collecting and processing of input from the visual fields. Visual fields are defined as the three-dimensional space that is visually perceptive to the eye at any given moment. For most avian species, the lateral field is much more extensive than the frontal field and therefore do not have considerable binocular overlap. However, birds of prey often have more frontally placed eyes, allowing for extensive binocular overlap. The configuration of the visual fields can essentially be divided into three groups: (1) binocular field ranges from 20° to 30° with the beak projecting centrally or below the center of the field, (2) binocular field ranges ≤ 10° with the beak laying outside of the visual field, and (3) binocular field ranged around 50° which is typically found in owls (Martin, 2007; see Fig 2.1). It is thought that food acquirement is the primary driver of the differences in visual field configuration. For example, the pigeon has a binocular field range of 27° (Martin and Young 1983) and the chicken has a binocular field range of 15° to 20°, whereas the eagles have a binocular field range of 33° to 40° (O'Rourke et al., 2010; Martin and Katzir, 1999).

Figure 2.1. Visual field of the chicken, pigeon, zebra finch and owl along with their retinal makeup.

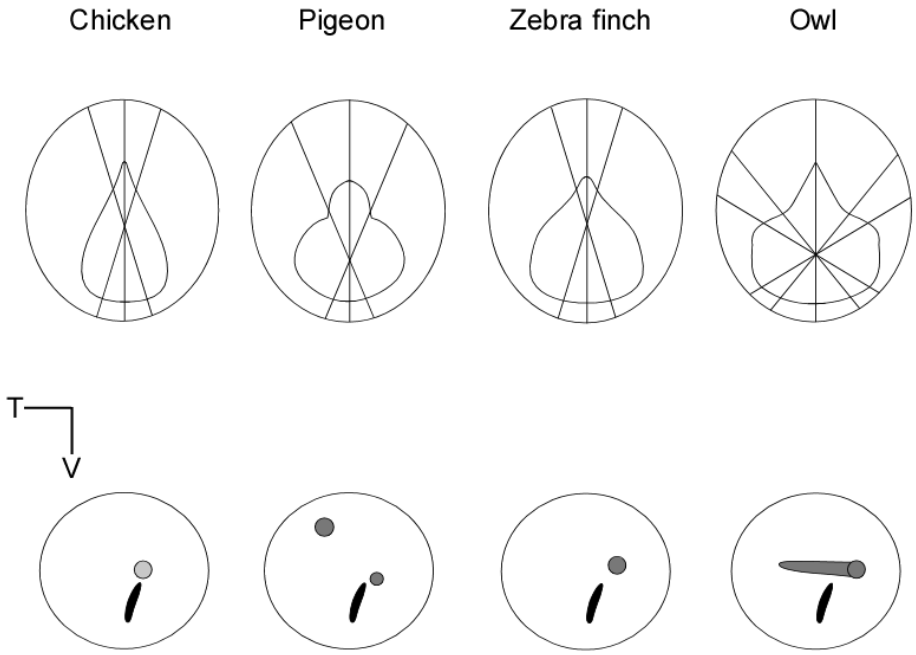

Diagram of the visual field showing monocular lateral and binocular frontal vision of the chicken, pigeon, zebra finch, and owl. Below are retinal maps for each species showing the pecten (black) and the areas of high photoreceptor density such as foveae or horizontal streaks.

The visual stimuli characteristics that are perceptive in the diverse visual fields must be processed to elicit behavioral response. This processing begins within the retina. The structure of the vertebrate retina is complex and consists of several layers. Avian species follow the typical structure of the retina, containing the ganglion cell layer, the inner nuclear layer, the outer nuclear layer, the inner plexiform layer, the outer plexiform layer, and the retinal nerve fiber layer (Seifert et al., 2020; Yamagata et al., 2021; Hayes 1982). The two major pathways that are involved in retinal visual input processing are the vertical and horizontal pathways. The vertical pathway is composed of bipolar cells that are connected to the retinal ganglion cells. On the other hand, the horizontal pathways are composed of amacrine cells and horizontal cells which regulate several processes, such as directional selectivity (Seifert et al., 2020). Retinal processing of visual input begins with stimulation of several classes of photoreceptors. Studies utilizing

electron microscopy, gene expression, phase contrast microscopy, and microspectrophotometry have discovered six classes of photoreceptors (Meyer and Cooper, 1966; Morris and Shorey, 1967; Das et al., 1999; Hart et al., 1998; Tyrell et al., 2019; Bowmaker et al., 1997). These classes include rods, doubles cones, and four types of single cones. The four types of single cones can be differentiated based on the functional photosensitive pigment they contain (long wavelength sensitivity, LWS; middle wavelength sensitivity, MWS; short wavelength sensitivity, SWS1 and SWS2). Double cones have been shown to possess the LWS opsin (Goldsmith and Butler, 2005) while the rods present rhodopsin which is functionally similar to the MWS cones (Okano et al., 1992). Additionally, all classes of cones contain oil droplets which act as a spectral filter, increasing or decreasing absorbance levels of the cone opsins (Stavenga and Wilts 2014). These oil droplets contain differing levels of carotenoids and allow for dividing oil droplets into several classes, with each class being associated with a specific cone class. Together, these generate interspecific as well as intraspecific variations in the distribution of oil droplet classes as well distribution of photoreceptor classes. The variable distribution of photoreceptors often leads to specialized functional regions. One such region is the fovea, a depression within the retina due to displacement of the inner layers. Birds can have one, two, or no fovea as well as visual horizontal streaks. For example, pigeons have a central pitted fovea and a shallow dorsotemporal fovea (Hayes 1982), chickens have no fovea (Ehrlich 1981), budgerigars have a central pitted fovea and a shallow nasal fovea (Mitkus et al., 2014), and geese contain a central fovea and horizontal streak (Moore et al., 2012). These specialized regions are characterized as having higher photoreceptor density. The increase in photoreceptor density is paralleled by an increase in retinal ganglion cell density (Seifert et al., 2020). Several studies across a range of orders and species have investigated the distributions of oil droplets, photoreceptors, and retinal

ganglion cells, but more research is needed to better understand the impacts of visual ecology on visual system morphological variations at the level of the retina.

Figure 2.2. Diversity of avian photoreceptors.

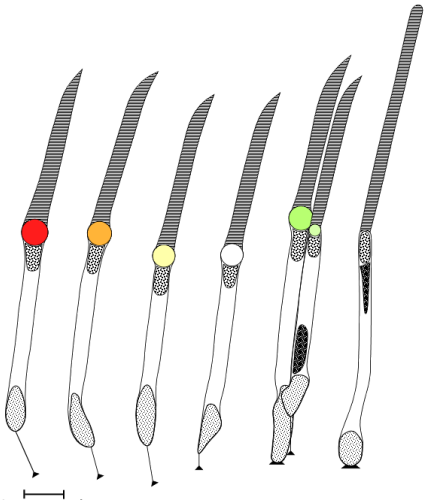

Representation of the various photoreceptor types found in avian species. Shown are the four classes of single cones, double cone and rod (from left to right). Each cone has one or more different oil droplets. Scale bar = 5 um.

2.2 Tectofugal Pathway

2.2.1 Retinotopic Transfer and the Optic Tectum

The optic tectum is a large, 15 layered structure whose layers can be differentiated based on electrophysiology, connectivity, neuropeptide expression, and morphology (Gu et al., 2000; Gunturken, 1997; Reperant and Angaut, 1977; Hardy et al., 1985; Treubert-Zimmermann, 2002; Sebesteny et al., 2002). The optic tectum represents the first step of the tectofugal pathway, receiving retinal input from small retinal ganglion cells of the contralateral retina (Remy and Gunturken, 1991). The topographic layout of the retino-tectal projection has been superficially studied using anatomical and electrophysiological methods (Clarke and Whitteridge, 1976; Hamdi and Whiteridge, 1954). These investigations demonstrate a double inversion along the dorso-ventral and anterior-posterior axes of the retina, with the dorsal retina projecting to the

ventral tectum and the anterior retina projecting to the posterior tectum. However, these early investigations did not provide highly detailed topographic maps, and often did not provide orientation of the brain or eye. Later studies using local field potentials and reverse retinoscopy (Letelier et al., 2004) addressed the issue of orientation of the brain and eyeball within the skull and produced a detailed topographic map of the visual field. However, this study documented the visual field transfer to the optic tectum in live birds and were only able to produce a detailed map on the accessible dorsal tectum, a triangular region covering a portion of the lateral tectum.

Figure 2.3. Histological section of the tectum.

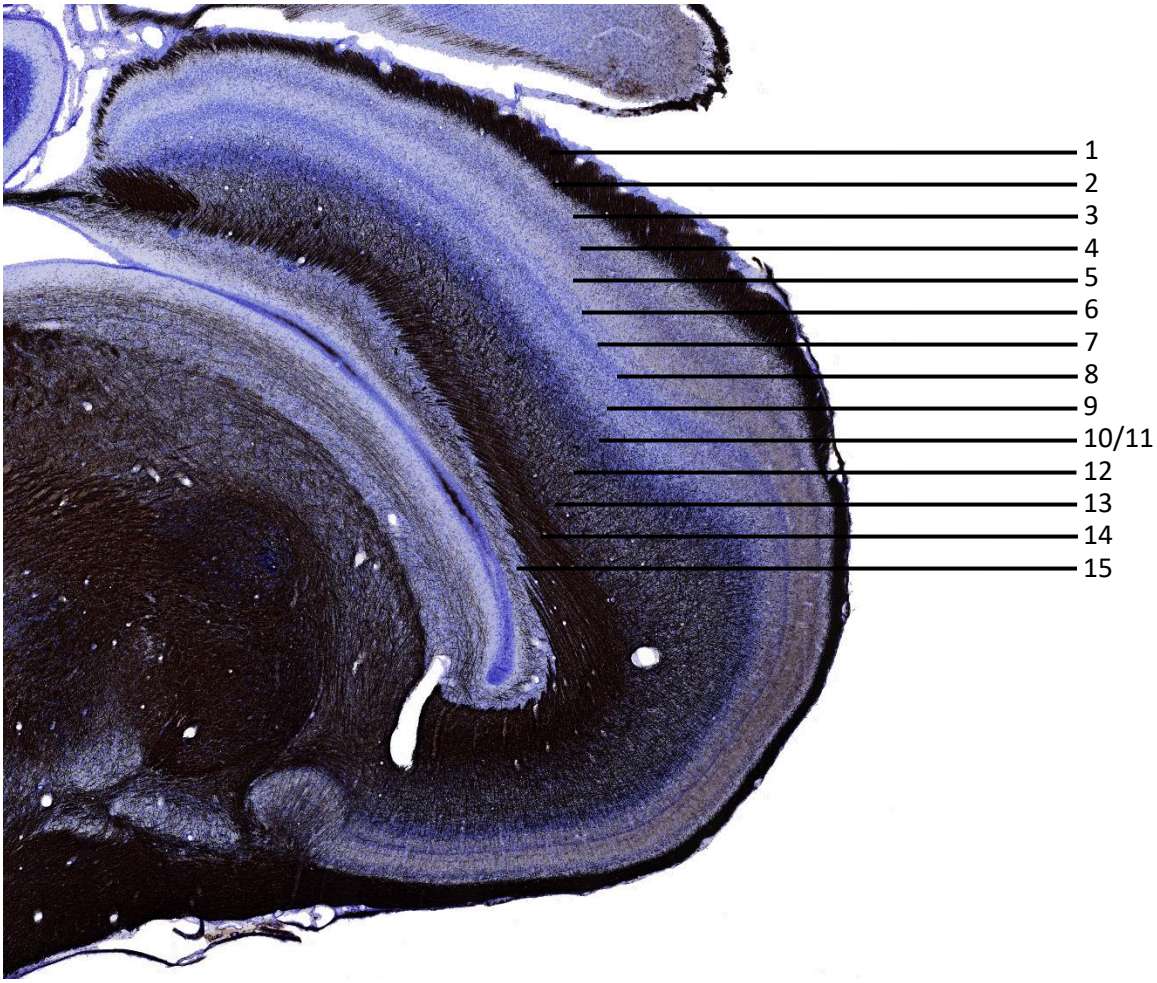

Histological section of the optic tectum at atlas coordinate A4.4 (Kuenzel and Masson, 1988) with the different layers labeled.

The retinal ganglion cell terminals that constitute this retinotopic map synapse within the superficial tectal layers 2-7. Reperant and Angaut (1977) described these terminations in detail, providing five types of retinal terminations varying in terminal field configuration and tectal layer they synapse in. With regard to the tectofugal pathway, several of the retinal terminal field classes make unique monosynaptic and polysynaptic connections with the dendrites of tectal ganglion cells (Karten et al., 1997). The tectal ganglion cells (TGC) soma reside within tectal layer 13 and consist of several subclasses. Initial studies of the TGC classes defined three different classes on the basis of dendritic field configuration, location of the somal body in layer 13, and the layer that their dendrites terminate in (Karten et al., 1997, Luksch et al., 1998). Type I TGC are located superficially within layer 13 and have a round dendritic profile that terminates in layer 5b. Type II TGC are located deep within layer 13 and have ellipsoid shaped dendritic profiles that terminate in the intermediate tectal layers 8 and 9. Type III TGC are located variably within layer 13 and had dendritic profiles that terminated in layer 4 of the tectum. All three types have unique bottlebrush endings on their dendritic profiles and had dendritic field diameters greater than 1 mm (Karten et al., 1997; Luksch et al., 1998). A subsequent study in the pigeon found two additional TGC classes (Type IV and V) after retrograde tracing into the rotundus (Hellmann and Gunturken 2001). Type IV TGC was characterized by having dendritic profile terminations in layer 5a whereas type V TGC was characterized as having dendritic profile terminations in layers 6, 5a, and 3. At the level of the deep tectum, the retinotopic map is replaced with a functionotopic map composed of parallel functional pathways arising from the different classes of TGCs that will project to the thalamic rotundus (Karten et al.., 1997; Luksch et al., 1998; Hellmann and Gunturken, 2001; Hellmann et al., 2004). This change from retinotopic to functionotopic occurs when TGCs project to the rotundus. According to an early

study done by Hellmann and Gunturken (1999), the dorsal and ventral tectal region were thought to project differentially to structures of the thalamus with the dorsal tectum projecting to the dorsal lateral geniculate nucleus (GLd) and the ventral tectum projecting to the rotundus. However, these findings were refuted by several studies (Hellmann et al., 2004; Hu et al., 2003; Deng and Rogers, 1998; Hellmann and Gunturken, 2001; Luksch et al., 1998) showing that the full dorsoventral extent of the optic tectum projects to the rotundus.

Figure 2.4. High magnification of the differential synapsing of retinal ganglion cells and tectal ganglion cells

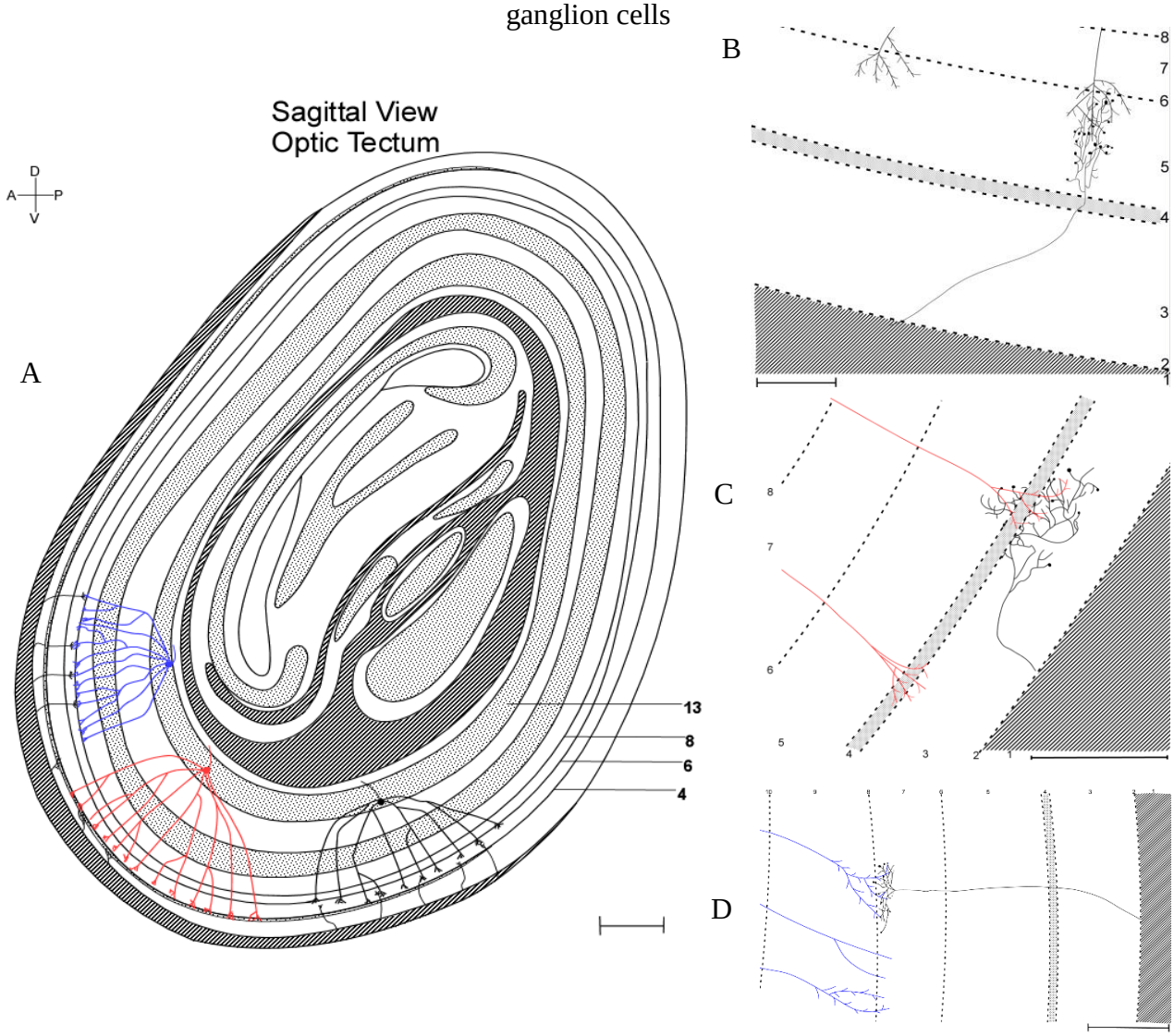

Sagittal slice, **A**, through the tectum showing the 3 primary TGC classes that have been described in the chicken and high magnification visualizations of RGC terminals synapsing on a dendritic branch of a TGC, **BCD**. Scale bar in **A** = 500um. Scale bar in **B,C,D** = 25 um.

Functionally, several studies have investigated tectal response to various visual stimuli. An early study from Hodos and Karten (1974) utilized gross lesions of the optic tectum that produced severe deficits in visual discrimination likely attributed to a combination of destruction of local tectal visual processing mechanisms and reduction in the transfer of visual input to higher visual processing centers such as the rotundus. Frost and DiFranco (1976) found tectal cells to respond more vigorously to dynamic versus static stimuli and that a majority of these cells had preferential responses to motion in a specific direction. A subsequent study found that motion sensitive cells can detect motion from a pattern composed of absolute color contours (Sun and Frost, 1997). Wu et al., (2005) found the tectum to have 3 classes of looming (motion in depth) sensitive neurons (rho, eta, tau). The authors show evidence that rho and eta class neurons signal initial warning of imminent collision while tau cells trigger avoidance behaviors. Additionally, the optic tectum comprises a major role in stimulus selection and spatial orientation in conjunction with the isthmi nuclei (Marin et al., 2007, 2012).

2.2.2 Nucleus Rotundus

The nucleus rotundus is the second major relay station of the tectofugal pathway residing in the thalamus. This structure receives bilateral input from the optic tecum via direct and indirect pathways (Deng and Rogers, 1998; Schmidt and Bischof, 2001). Direct input from the TGC classes of layer 13 of the optic tectum enters the rotundus caudally via the tectothalamic tract (ttt). Indirect pathways arise as axon collaterals of TGC classes. These collaterals exit the ttt and enter the pretecto-subpretecto tract, terminating in the subpretectal nucleus (SP), intermediate subpretectal nucleus (ISPT), or the pretectal nucleus (PT) (Theiss et al., 2003). The PT and SP/ISPT complex have reciprocal connections (Acerbo et al., 2012). The SP/ISPT complex in turn sends GABAergic projections bilaterally to the nucleus rotundus (Mpodozis et al., 1996).

This indirect flow of information likely serves to modulate processing in the rotundus. Several studies using anterograde and retrograde tracers have shown that the rotundus can be divided into anatomical subunits that receive input from a unique class of TGC (Karten et al., 1997; Deng and Rogers, 1998; Hellmann and Gunturken, 2001). Benowitz and Karten (1976) were the first to divide the rotundus on the basis of tract tracing noting five subdivisions in the pigeon. Subsequent studies using tract tracing also found anatomical domains in the rotundus. Deng and Rogers (1998) and Hu et al., (2003) found four divisions depending on tectal input whereas Fredes et al., (2010) found three subdivisions. These differences in divisions using tract tracing are likely due to the sensitivity of the anterograde or retrograde tracer used as well as the amount of tracer injected. Using acetylcholinesterase staining, Martinez-de-la-Torre et al., (1990) found six subdivisions while Redies and Becker (2003) found four subdivisions on the basis of differential cadherin expression. Interestingly, other studies using chemoarchitectonic methods have typically found homogenous expression throughout the rotundus (GABA, Domenici et al., 1988; parvalbumin, Braun et al., 1985; NADH-diaphorase, Martinez-de-la-Torre 1990; cytochrome oxidase, Braun et al., 1985; monoaminoxidase, Kusunoki, 1970).

Table 2.1 Divisions of the nucleus rotundus based on differential investigatory techniques

Species	Methods Used	# Subdivsions	Source
Pigeon	Anterograde and retrograde tract tracing; calbindin and parvalbumin immunoreactictivity	3	Marin et al., 2003
Pigeon	Retrograde tracing	5	Hellmann and Gunturken, 2001
Chicken	Cahderin expression	4	Redies and Becker, 2003
Chicken	Differential acetylcholinesterase immunoreactivity	7	Martinez-de-la-Torre et al., 1990
Pigeon	Retrograde tracing	3	Fredes et al., 2010
Pigeon	Electrophysiology	2	Yazulla and Grana, 1974
Pigeon	Retrograde tracing	5	Benowitz and Karten, 1976
Pigeon	Electrophysiology	4	Wang et al., 1993
Zebra Finch	Retrograde tracing	4	Nixdorf and Bischof, 1982
Chicken	Anterograde and retrograde tract tracing	4	Hu et al., 2003
Chicken	Retrograde tracing	4	Deng and Rogers, 1998

Functional domains have also been determined within the rotundus, often overlapping considerably with the anatomical domains. Revzin et al., (1979) discovered that the cells of the

rotundus display directional selectivity in the anterior half and nondirectional selectivity in the posterior half when subject to moving stimuli. Wang and Frost (1992) found cells within the dorsal posterior rotundus to be responsive to motion in depth. Additionally, Ganda and Yazulla (1971) found evidence that the rotundus contains cells that were wavelength selective, with some cells responding in opposition to long wavelength and short wavelength light. Wang et al., (1993) performed one of the most detailed functional compartmentalization studies in the rotundus. Using various visual stimuli (e.g. moving spots/bars, colors, luminance, object motion in depth), Wang et al., quantified single-cell responses throughout the rotundus and revealed distinct functional domains. They found the rostral anterior rotundus to be preferentially responsive to color or luminance changes whereas the ventral and dorsal posterior rotundus were preferentially responsive to object motion and looming motion respectively. These functional domains further support the idea of a retinotopic to functionotopic transition between the superficial tectum and the rotundus via TGCs. Supporting this functional compartmentalization, Laverghetta and Shimizu (1999) found the rostral rotundus had reduced color discrimination post lesioning whereas the caudal rotundus had reduced motion discrimination post lesioning. However, Hu and Wang (2001) found evidences for only two types of physiologically distinct classes of rotundal cells. Interestingly, although the rotundal cells have different physiological properties, they are homogenous in terms of morphology (Thin et al., 1992; Hu and Wang, 2001). Rotundal neurons are characterized as being medium to large multipolar neurons with five to eight primary dendrites giving off the occasional side branch (chicken, Thin et al., 1992; pigeon, Hu and Wang 2001). Axons of these cells travel dorsally where they congregate as fiber bundles and utilize the lateral forebrain bundle to travel to the terminal tectofugal structure.

2.2.3 Isthmic nuclei: midbrain selection network

The isthmic nuclei serve as a mediator for the specific calculations carried out by the midbrain network, which are crucial for stimulus-driven selection and orientation within space. The primary components of this midbrain network are the nucleus isthmus, parvocellular part (Ipc) and nucleus isthmus, magnocellular part (Imc) with the lesser components being the semilunar nucleus (SLu) and the isthmo-optic nucleus (ION). These nuclei receive ipsilateral tectal input from specialized neurons of tectal layers 10/11, termed Shepherd's crook neurons. The dendrites of these neurons project into tectal layer 7 and receive visual input which is relayed topographically to the isthmic nuclei. The Ipc was first described as receiving topographic projections from the optic tectum by Hunt and Kunzle (1976). Subsequent studies confirmed this observation and also noted that the Ipc reciprocally projects back onto the optic tectum, terminating in the superficial layers in a columnar, homotopic fashion (Wang et al., 2005; Marin et al., 2012). Initial neurochemical studies using uptake-release assays described the Ipc as being GABAergic and glycinergic (Wang et al., 1995). However, later studies using modern neurochemical methods determined that the Ipc displayed ChAT expression. However, Islam and Atoji (2008) found a high expression of VGLuT2 within the Ipc. Further investigation by Gonzalez-Cabrera et al., (2015) and Reyes-Pinto et al., (2021) suggest that acetylcholine is important for development of Ipc terminals, which is followed by a corelease of acetylcholine and glutamate, ending with primarily glutamate release to modulate ascending visual input. Similar to the Ipc, the SLu has been shown to homotopically project back to the superficial tectum (Hellmann et al., 2001). Interestingly, the SLu also sends bilateral projections to the rotundus. This projection seems to maintain rough topography with the ventral SLu projecting to the ventral rotundus and the dorsal SLu projecting to the dorsal rotundus and is likely modulating

visual input (Hellmann et al., 2001). Neurochemical analyses have strongly supported a cholinergic function of SLu neurons (Hellmann et al., 2001; Medina and Reiner, 1994; Gonzalez-Cabrera et al., 2015). The Imc afferent projections to the tectum are different than the Ipc and SLu as they are heterotopically organized and projects to the intermediate and deep tectal layers (Tombol et al., 2005; Hunt et al., 1977). Additionally, Imc neurons also send projections to the Ipc and SLu (Wang et al., 2004). Neurochemical analysis of the Imc showed intense GABA labeling (Sun et al., 2005; Tombol and Nemeth 1998; Braun et al., 1988). These large GABAergic terminal fields of Imc neurons provide wide-field inhibition in the deep tectal layers, Ipc, and SLu (Wang et al., 2004). The Imc cells that these projections arise from can be broken into two subpopulations: one that projects to the tectum and the other that projects to the Ipc and SLu (Faunes et al., 2013). Faunes et al., (2013) postulate that the different Imc subpopulations may receive unique tectal inputs and function as independent synchronized ensembles, carrying inhibitory signals at varying frequencies to their respective targets.

The midbrain selection network is composed of the Ipc, Imc, and SLu. These nuclei work in conjunction with the optic tectum via a network of reciprocal connection to selectively enhance and suppress stimuli within the visual field (Marin et al., 2012; Garrido-Charad et al., 2018). Two primary stages for the tecto-isthmo-tectal circuit's activity are performed when retinal activation of shepherd's crook neurons occurs. The first is the concurrent activation of Ipc and SLu parallel reentrant signals to the tectum, enhancing the retinal input on the TGC dendrites to the rotundus and entopallium of the ascending tectofugal pathway. The second stage includes the stimulation of Imc neurons that send GABAergic projections to the tectum, Ipc, and SLu to suppress the reentrant Ipc and SLu signals to tectal regions receiving lesser retinal input (Marin et al., 2012; Garrido-Charad et al., 2018). Together, this neural circuit permits global competitive

stimulus selection. In other words, RGCs project a map of the visual field onto the superior layers of the optic tectum. Cells from tectal layers 10/11 sample the input and project to the Ipc, Imc and SLu. The neurons of the Ipc and SLu will send excitatory projections back to the portion of the superior optic tectum they received input from. The neurons of the Imc will send inhibitory projections to the intermediate layers of the optic tectum including layer 13 which is responsible for the ascending visual flow of information to the rotundus. The Ipc and SLu will selectively enhance and boost the strongest visual input from RGCs to TGCs while the Imc will inhibit the weaker visual input by inhibiting layer 13 neurons as well as portions of neurons in the SLu and Ipc. Therefore, these interactions form the basis for competitive stimulus selection within the tectum by means of reciprocal projections of the tectum and isthmi nuclei.

The isthmo optic nucleus (ION) is similar to the other isthmic nuclei in that it receives projections from shepherd's crook neurons of tectal layer 9 and 10 (Woodson et al., 1991). However, it is different from its counterparts in that rather than projecting back onto the tectum, it projects to the ventral contralateral retina, where it is thought to terminate on amacrine cells (Maturana and Frenk, 1965; Miceli et al., 1999). However, reinvestigation of the ION terminals in the retina revealed that the cells receiving projections from the ION (termed IOTCs) are not amacrine cells (Uchiyama et al., 2004). The functional importance of the ION has been debated with no complete understanding presently. Early studies varied in suggested functional roles of the ION including modulation of retinal sensitivity (Uchiyama et al., 1995) and food searching (Miceli et al., 1999). Lesioning of the ION (Uchiyama et al., 2012) dramatically reduced response accuracy of target selection during competitive visual search. A subsequent study from Uchiyama et al., (2022) found that the ION projections enhance the ability to detect visual stimuli and discriminate the target stimulus. This study confirms the role of ION in attentional

facilitation at the level of the retina, reminiscent of the Ipc/Imc attentional capture and stimulus selection in the optic tectum.

2.2.4 Pretectum: inhibitory modulation complex

The components of the pretectum comprising the indirect inhibitory sidepath between the optic tectum and the rotundus includes the subpretectal nucleus (SP), the intermediate subpretectal nucleus (ISPT) and the pretectal nucleus (PT). The SP and ISPT are intrinsic to the ttt and are often referred to as the bed nuclei of the ttt. Several early studies investigating the tectorotundal pathway noted labeling of tectal terminals within the pretectum (Karten et al., 1997; Bischof and Niemann, 1990; Mpodozis et al., 1996). The SP and ISPT components have been shown to receive a dense ipsilateral input from the tectum with a much sparser input from the contralateral tectum (Bischof and Niemann, 1990). Deng and Rogers (1998) used retrograde tract tracing from the rotundus and found that the SP/ISPT complex has roughly topographic projections to the ipsilateral rotundus. Injections into the dorsal rotundus labeled the dorsal SP, whereas injections into the middle and ventral rotundus labeled the middle and ventral SP. They did note that the ISPT was only labeled after injections to the dorsal most rotundus, likely due to diffusion of the tracer into the triangularis, the dorsomedial extension of the rotundus. These results differed from the early study of Benowitz and Karten (1976) who reported that only the ventral division of the rotundus receives input from the SP/ISPT complex. However, histochemical studies have found homogenous distribution of GABAergic fibers within the rotundus, agreeing with the observations of Deng and Rogers (1998).

The functionality of the nuclei of the SP/ISPT complex and their role as a sidepath in the transfer of visual input from the tectum to the rotundus is much less understood. Mpodozis et al., (1996) found that neurons of the SP and ISPT were intensely glutamic acid decarboxylase-

immunoreactive (GAD-ir) and electrolytic lesions to the SP/ISPT complex markedly reduced GAD-ir in the ipsilateral rotundus and little to no reduction in the contralateral rotundus occurred. GAD is responsible for catalyzing the production of the inhibitory neurotransmitter γ-Aminobutyric acid. This study suggests the SP/ISPT as having a role in inhibitory modulation at the level of the rotundus. Acerbo et al., (2012) used several static figure-ground cues to determine the role of SP, ISPT, and PT modulation of the rotundus during figure-ground segregation, shape discrimination, and color discrimination. They found that the rotundus plays a primary role in figure-ground discrimination with modulatory control by the SP/ISPT complex but not by the PT. This may be due to inhibitory projections of the SP/ISPT complex onto the PT, reducing its activity (Theiss et al., 2003). A striking result from this study was that none of the nuclei of the pretectum displayed modulatory control during color and shape discrimination tasks, and the authors suggested that this may indicate that the rotundus is not directly involved in color or shape discrimination.

The PT also receives excitatory axon collaterals from cells of tectal layer 13 (Gamlin et al., 1996). The PT then sends projections to the SP/ISPT complex and bilateral projections back onto the tectum, terminating in layer 5b (Gamlin et al. 1996). This suggests binary modulation of ascending excitatory visual input. The PT is responsible for the neuropeptide Y labeling within layer 5b and was confirmed after enucleation and lesioning of the PT (Gamlin et al., 1996). The functional significance of the PT in regards to the tectofugal system has been understudied. The capacity of birds to engage in actions like tracking and pecking at moving stimuli was shown to be impacted by combined lesions of the lateral spiriform nucleus and the PT (Bugbee 1979). Pretectal lesions in toads abolish avoidance behavior and reduce inhibitory prey-catching reactions to visual cues, and a similar functional system may occur in birds (Gamlin et al., 1996).

It is likely the PT is important for food searching in the visual field and may play a role in identifying and selecting food targets within the visual field at the level of the tectum. This could be further supported by the reciprocal connections of the PT with the SP/ISPT complex as this complex is involved in figure-ground segregation which would be important for discriminating a food item from the background behind it.

2.2.5 Entopallium

The entopallium is the terminal structure of the ascending tectofugal pathway and resides within the avian pallium. The entopallium receives massive ipsilateral projections from the rotundus. Several studies using a variety of methods have divided the entopallium into two to four divisions (Table 2.2). Benowitz and Karten (1976) divided the entopallium on the basis of anterograde projections in the rotundus. They show the rotundal domains are roughly maintained at the level of the entopallium in that the anterior entopallium will receive projections from the anterior rotundus, the intermediate entopallium will receive projections from the intermediate rotundus, and the posterior entopallium will receive projections from the posterior rotundus. Husband and Shimizu (1999) and Laverghetta and Shimizu (2003) also found an anterior-posterior organization of rotundal innervation of the entopallium. Conversely, Krutzfeldt and Wild (2004,2005) displayed a dorsoventral partitioning of the entopallium on the basis of cell density, differential neurochemical staining, and tract tracing. They did support the anterior-posterior rotundal innervation of the entopallium, but they also found a dorsal-ventral partitioning from retrograde tracer injections in the mesopallium. To complement and replicate the dorsal-ventral partitioning, Ahumada-Galleguillos et al., (2015) found that the ventral entopallium projects to the intermediate nidopallium and mesopallium while the dorsal entopallium projects back down into the lateral striatum on the basis of afferent connectivity.

Table 2.2 Divisions of the entopallium based on differential investigatory techniques

Species	Methods Used	# Subdivsions	Source
Quail	Anterograde tracing	2	Watanabe et al., 1985
Pigeon	Anterograde tracing	3	Fredes et al., 2010
Zebra Finch	Anterograde and retrograde tracing	3	Laverghetta and Shimizu, 2003
Pigeon	Electrophysiology and lesion	2	Nguyen et al., 2004
Pigeon	Electrophysiology and lesion	2	Cook et al., 2013
Chicken	Differential GABA and calbindin expression	3	Suarez et al., 2005
Pigeon	Anterograde tracing	3	Benowitz and Karten, 1976
Pigeon	Cell density; parvalbumin, calretinin, and cytochrome oxidase immunoreactivity	2--3	Krutzfeldt and Wild, 2005
Zebra Finch	Cell density; parvalbumin, calretinin, and cytochrome oxidase immunoreactivity	2--3	Krutzfeldt and Wild, 2004
Chicken	Anterograde and retrograde tracing	3	Ahumada-Gallaguillos et al., 2015

Few studies have attempted to ascertain if the functional domains present in the rotundus are transferred to the entopallium, thereby supporting the anterior-posterior entopallial partitioning. Early functional studies found that after lesioning the entopallium, there were subsequent deficits in intensity and pattern discrimination (Hodos and Karten, 1970; Hodos et al., 1988; Laverghetta and Shimizu 1999). However, these lesions were large and likely affected several divisions of the entopallium as well as the overlying nidopallium and mesopallium visual centers. More recent studies utilizing smaller lesions (Nguyen et al., 2004) found that lesions to the posterior entopallium caused performance deficits in the motion task whereas lesions to the anterior caused performance deficits in the spatial-pattern task. This indicated that the entopallium likely maintains the functional compartmentalization that occurs in the rotundus with more posterior regions important for motion processing and more anterior regions important for pattern discrimination (color, luminance). Xiao et al., (2006), using electrophysiology, found several types of looming sensitive neurons in the caudal entopallium which is reminiscent of cells of the posterior rotundus (Wang et al., 1993). Additional support for this compartmentalization of functions comes from Cook et al., (2013) in which birds were trained to perform a specific task (textured target localization, dynamic shape discrimination, where/what discrimination task) prior to electrolytic lesions to the entopallium. They found that lesions of the anterior

entopallium markedly reduced performance in the texture discrimination task (assesses ability to discriminate between different textures) while lesions of the posterior entopallium adversely affected the dynamic shape discrimination task (assesses ability to discriminate between moving objects based on their shape). Interestingly, Cook et al., (2013) found that posterior lesions also caused deficits in static shape discrimination (assesses ability to discriminate between nonmoving objects based on their shape). These studies provide the support that the functional domains of the rotundus maintain their topography suggesting a system for parallel processing of visual attributes. These parallel pathways may continue into the higher visual associative areas that the entopallium projects to.

2.3 Thalamofugal Pathway

2.3.1 GLd

The dorsal lateral geniculate nuclear complex (GLd), previously named the principal optic thalamus (OPT, see Karten et al., 1973), is a complex of several nuclei that resides within the dorsal thalamus. The nuclei that make up this complex include: suprarotundus (SpROT), dorsolateral anterior thalamus, lateral part (DLL), lateral dorsal principal optic thalamus (LdOPT), dorsolateral anterior thalamus, magnocellular part (DLAmc), superficial parvocellular nucleus (SPC), dorsolateral anterior thalamus, rostrolateral part (DLAlr). The nuclei of the GLd receive contralateral retinal input from medium-sized retinal ganglion cells (Remy and Gunturken, 1991). The distribution of these retinal ganglion cells was primarily in the central retina with very few being labeled in the dorsal temporal retina (Remy and Gunturken, 1991). These findings were confirmed by Miceli et al., (2006) who used retrograde transneuronal transport to determine distribution of retinal ganglion cells that project to the thalamofugal system. This suggests preferential sampling and subsequent processing of visual input from the

monocular lateral field. Of interest, studies in birds of prey revealed that retinal ganglion cells from the temporal retina project to the GLd nuclei (Pettigrew 1978, 1979; Porciatti et al., 1990). This is likely due to the placement of the eyes (with frontally directed vision vs laterally directed vision) and the amount of binocular overlap. Retinal innervation varies between the nuclei with the suprarotundus (SpROT), dorsolateral anterior thalamus, lateral part (DLL), and dorsal lateral principal optic thalamus (LdOPT) receiving dense retinal input whereas the dorsolateral anterior thalamus, magnocellular part (DLAmc), superficial parvocellular nucleus (SPC), and dorsolateral anterior thalamus, rostrolateral part (DLAlr) receiving much sparser retinal input (Krabichler et al., 2014; Ehrlich and Mark, 1984; Miceli et al., 1975; Miceli et al., 2008; Gunturken and Karten 1991).

The nuclei of the GLd can be grouped into ipsilaterally, contralaterally, or bilaterally projecting features. In general, the SpROT, DLLv, and the DLAda project ipsilaterally to the Wulst using the lfb. The DLAlr, DLLd, SPC, and LdOPT primarily project to the contralateral Wulst using the dorsal supraoptic decussation (dsd) and lfb. The DLAmc projects bilaterally to the Wulst using different cell populations (Koshiba et al., 2005; Rogers et al., 1993; Miceli et al., 1975; Strockens et al., 2012; Miceli et al., 1990; Miceli et al., 2006). Aside from delineating these nuclei based on afferent or efferent projections, some studies have also characterized these divisions using histochemistry. Gunturken and Karten (1991) characterized the nuclei using choline acetyltransferase (ChAT-ir), cholecystokinin (CCK-ir), neurotensin (NT-ir), glutamic acid decarboxylase (GAD-ir), serotonergic (S-ir), neuropeptide Y (NPY-ir), and substance P (SP-ir) immunoreactivities among others. Results of this study demonstrate high numbers of ChAT-ir and CCK-ir perikarya within the entire GLd. Additional findings include dividing the DLL on the basis of ChAT and GAD immunoreactivity, dense NPY-ir in the SPC, dense serotonergic like

(S-li) fibers in the DLAmc, and dense GAD-li neuropil in the LdOPT. Additionally, Miceli et al., (2008) found that GABA-ir was present in all GLd components with densest labeling located in the DLLv.

There are very few functional studies investigating precise roles of the GLd nuclei in visual attribute processing. This is likely due to overlap of nuclear boundaries making it difficult to perform precise electrophysiology, or add nucleus-specific lesions. Despite these obstacles, several recent studies have aimed to understand the role of the DLL, the largest component of the GLd, in visually guided behavior. After anterograde injections into the retina and retrograde injections into Cluster N (region of the Wulst active during nighttime migration), Heyers et al., (2007) found colocalization of these tracers within the DLL suggesting this nuclear component of the GLd comprises a role in nighttime migration. A separate study measuring neuronal activation after exposure to environmental stimuli associated with navigation found significant interaction of the DLL, suggesting this nucleus is important for migratory navigation and homing (Jorge et al., 2017). Together, these studies provide evidence that the retina-DLL-wulst pathway represents a subsystem for processing a specific visual attribute and suggest that there are likely other subsystems through the other GLd nuclei acting in parallel, reminiscent of the parallel processing seen in the tectofugal system.

2.3.2 Wulst

The wulst is the terminal structure of the thalamofugal pathway that occupies an extensive portion of the dorsomedial pallial brain surface. The visual wulst is laminated and can be divided into at least four layers based on cell morphology and density (Denton 1981; apical hyperpallium, HA; and intercalated nucleus of the hyperpallium, HAI; superior intercalated hyperpallium, HIS; and densocellular hyperpallium, HD). The rostral wulst has been shown to be

involved in somatosensory/motor function and the posterior wulst functions in visual processing (Den and Wang, 1992, 1993). The boundary between the two domains is not explicit, as there is a portion of the wulst that responds to both visual and somatosensory stimulation. However, according to research, we suggest the transitional boundary between somatosensory and visual divisions seems to occur between atlas plates A10.4 and A10.8 of the chick brain atlas of Kuenzel and Masson (1988). The GLd provides an immense bilateral input to the visual wulst using the lateral forebrain bundle (lfb). The GLd projections terminate in HD and HIS/HAI divisions of the wulst. The HD and HIS/HAI project to the HA, the primary division for intratelencephalic and extratelencephalic projections (Shimizu et al., 1995; Deng and Rogers 1998; Stacho et al., 2020). The visual wulst can be subdivided by means of immunohistochemistry. Shimizu and Karten (1990) used ChAT-ir, GAD-ir, SP-ir, CCK-ir, and others neuromolecules to differentiate the wulst. Some key findings from this study were the distinct laminar patterns for several of the substances investigated, the extensive variety of expressed neurotransmitters, receptors, and neuropeptides within the visual wulst, and several neuroactive substances displaying regional variance. For example, SP-ir cells were primarily located in the HA of the wulst. Differential GAD staining was also apparent and followed the cytoarchitectonic laminar organization.

Early functional investigations of the wulst often utilized gross lesions to determine deficits in performance during visual tasks. Such studies (Hodos et al., 1973; Pritz et al., 1970) found that lesions to the wulst had little to no effect on pattern and intensity discrimination. However, a later study (Budzynski and Bingman, 2004) found that pigeons with lesions of the wulst have impaired visual pattern discrimination. The discrepancy between the studies is due to the use of a pecking key as the final operant in the former study. A pecking key is processed by the

dorsotemporal retina, which does not have major connections with the thalamofugal pathway, but instead with the tectofugal pathway. Another study performed by Budzynski et al., (2002) also found the wulst to be involved in sun-compass orientation. This is further supported by Watanabe (2003) who found lesions to the wulst caused deficits in spatial acquisition and discrimination.

2.4 Higher Visual Associative Areas

Several early studies involving tracing the tectofugal pathway found many regions of the pallium to receive direct or indirect axonal projections from the entopallium (Dubbledam et al., 1997; Husband and Shimizu, 1999; Krutzfeldt and Wild, 2004, 2005). Similarly, tract tracing in the thalamofugal pathway found many pallial regions to receive input from the wulst (Shimizu et al., 1995; Alpar and Tombol, 1998; Deng and Rogers, 2000). The areas involved in the tectofugal system include the intermediate nidopallium (NI), frontolateral nidopallium (NFL), intermediolateral nidopallium (NIL), caudolateral nidopallium (NCL), ventrolateral mesopallium (MVL), and the intermediate arcopallium (AI). The areas involved in the thalamofugal pathway include frontolateral nidopallium (NFL), the caudolateral nidopallium (NCL), the intermediate arcopallium (AI), the hippocampal formation (Hp), ventral hyperpallium (HV), and the medial mesopallium (IMM). Additionally, there are extratelencephalic connections stemming directly from the Wulst to the optic tectum, GLd, pretectal nuclei, and the nucleus of the basal optic root (Rio et al., 1983; Reiner and Karten, 1983; Mestrus and Delius, 1982). On the other hand, no direct extratelencephalic projects have been shown to stem from the entopallium (Alpar and Tombol, 1998; Husband and Shimizu, 1999). A point of interest is the overlap of tectofugal and thalamofugal pathways in the NFL, NCL, and AI. These may serve as integration centers for visual information between the two pathways.

Later studies further detailed the intratelencephalic connections stemming from the wulst or entopallium. With respect to the tectofugal pathway, the general flow of ascending information begins with the ventral entopallium projecting to intermediate nidopallium and ventrolateral mesopallium. The MVL sends reciprocal projections to the entopallium and potentially collaterals to the intermediate nidopallium (Ahumada-Galleguillos et al., 2015; Fernandez et al., 2019; Stacho et al., 2020). These studies provide evidence of reciprocal, homotopic columnar projections between tangentially oriented layers which is reminiscent of the organization of the mammalian cortex. Aside from the projections between the entopallium, NI, and MVL, the NI also maintains reciprocal projections with three regions of the lateral nidopallium (Fernandez et al., 2019). Additionally, the AI also receives a large projection from the NI. Similar reciprocal, columnar organization is also apparent within the thalamofugal pallial circuits (Stacho et al., 2020). These circuits arise from reciprocal, topographic projections between the HD, HIS, and HA. An additional tangentially organized system between the HD and IMM and a long-range columnar organized circuit from the wulst to the dorsal mesopallium, to the NCL and AI were also noted (Stacho et al., 2020). A point of interest is the overlap of tectofugal and thalamofugal visual input in the NFL, NCL, and AI. These regions likely act as integration centers of information between the two visual pathways; however, research on the functional importance of this integration is incipient, and more research is needed to understand the functional mechanisms that occur due to this integration.

Several of these higher visual associative pallial areas have been rudimentarily studied in regard to their functional importance. The intermediate arcopallium (AI) has a significant projection to the optic tectum and is thought to be involved in top-down modulation of ascending visual input (Manns et al., 2007; Fernandez et al., 2019). Fernandez et al., (2019) have

hypothesized that the AI projections that terminate in the optic tectum may contact TGCs or shepherd's crook neurons to selectively modulate ascending tectal output to the rotundus. The NFL has been implicated in context encoding and extinction learning as transient inactivation of NFL neurons using tetrodotoxin reduced extinction learning and eliminated the renewal effect (Gao et al., 2019). After lesioning the NCL, Hartmann and Gunturken (1998) suggested the involvement of this structure in reversal learning (assesses ability to stop reward-related responses and stop current behavior when presented a stimulus). Additional functional studies of the NCL also provide evidence of its involvement in working memory and executive functioning (assesses ability to plan, monitor and execute behaviors to achieve a goal) (Johnston et al., 2017) and color perception (Hsiao et al., 2020). The MVL has been shown to be functionally similar to the entopallium and can process more complex visual stimuli (Azizi et al., 2019). The IMM, a target of the thalamofugal pathway, has been shown to be involved in imprinting (Maekawa et al., 2006). An additional thalamofugal target, the Hp, has been under recent investigation for its involvement in spatial memory formation (Gagliardo et al., 2005). Together these targets of the tectofugal and thalamofugal systems act to process visually complex attributes and contribute to complex cognitive functions that then facilitate complex behavioral output necessary for survival.

2.6 Plans to update progress of the two major visual pathways in birds

The review of research on the components of the primary visual pathways in birds (tectofugal and thalamofugal) provides the necessary foundation for generating 3D model representations of the complex systems. To generate comprehensive 3D atlases of the visual systems in birds we implemented a multi-modal image reconstruction protocol with the following aims for this research project: (1) describe the retinotopic projections from the retina to the superficial optic

tectum as defined by the quadrant theory, (2) reconstruct primary and secondary components of the tectofugal system and their connectivity, and (3) reconstruct the primary and secondary components of the thalamofugal system and their connectivity.

Figure 2.5 Overview of the tectofugal visual pathway.

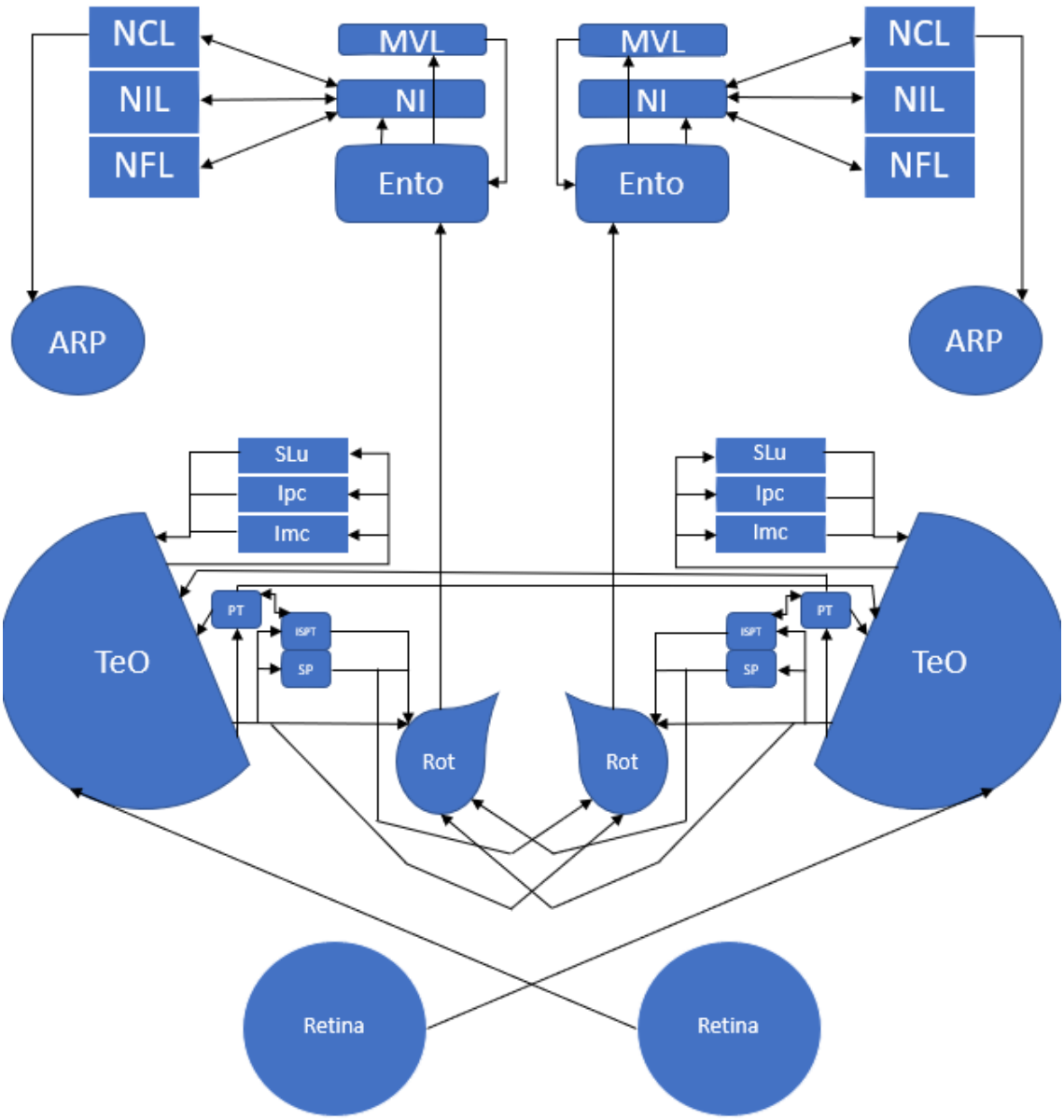

Figure 2.6 Overview of the thalamofugal visual pathway.

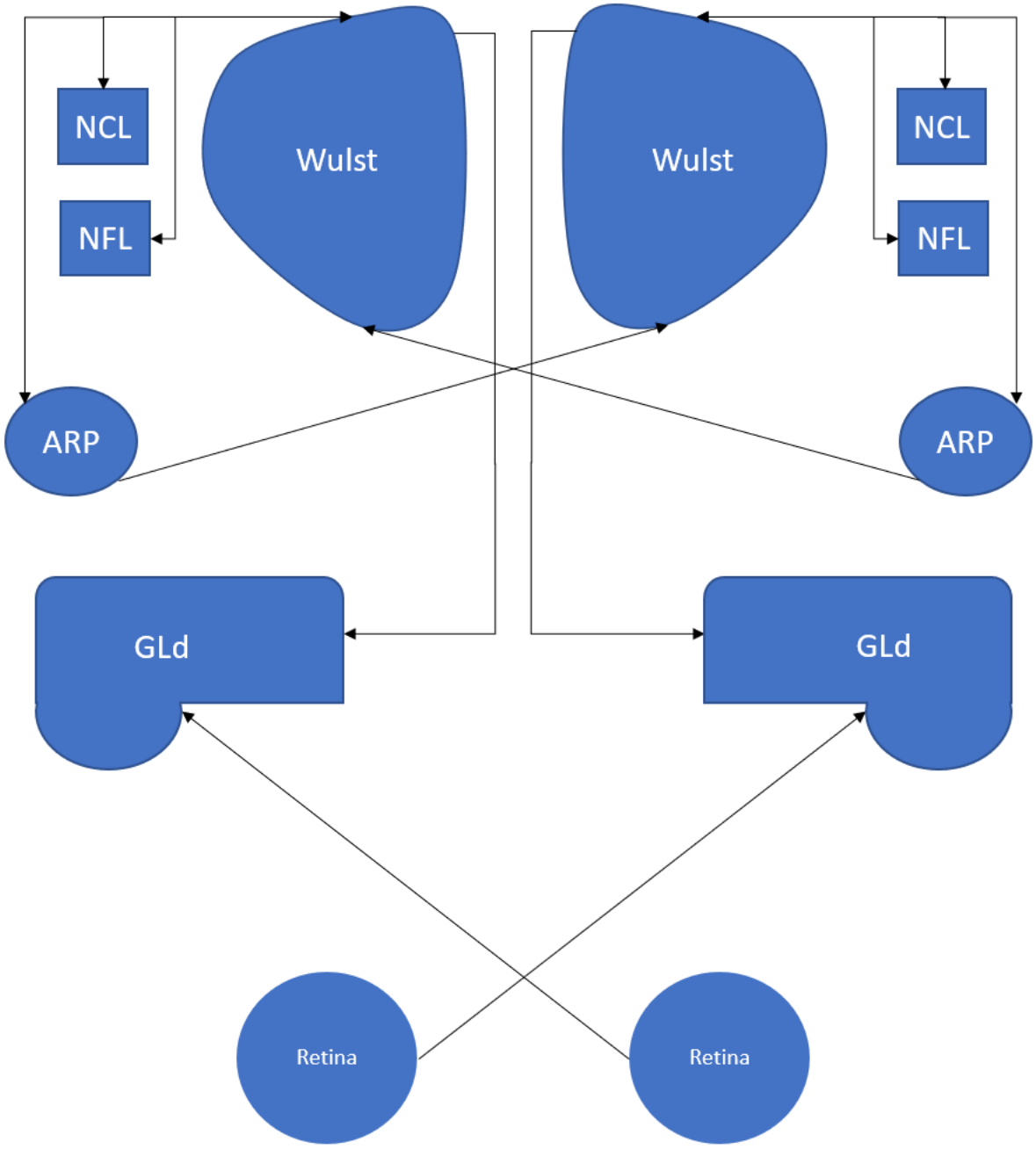

2.5 References

Acerbo, M. J., Lazareva, O. F., McInnerney, J., Leiker, E., Wasserman, E. A., & Poremba, A. (2012). Figure–ground discrimination in the avian brain: The nucleus rotundus and its inhibitory complex. *Vision Research*, *70*, 18–26. https://doi.org/10.1016/j.visres.2012.07.023

Ahumada-Galleguillos, P., Fernández, M., Marin, G. J., Letelier, J. C., & Mpodozis, J. (2015). Anatomical organization of the visual dorsal ventricular ridge in the chick (*Gallus gallus*): Layers and columns in the avian pallium. *Journal of Comparative Neurology*, *523*(17), 2618–2636. https://doi.org/10.1002/cne.23808

Alpár, A., & Tömböl, T. (1998). Telencephalic connections of the visual system of the chicken: Tracing the interrelation of the efferents of the visual wulst and the hyperstriatum ventrale. *Annals of Anatomy - Anatomischer Anzeiger*, *180*(6), 529–536. https://doi.org/10.1016/s0940-9602(98)80060-5

Azizi, A. H., Pusch, R., Koenen, C., Klatt, S., Bröker, F., Thiele, S., Kellermann, J., Güntürkün, O., & Cheng, S. (2019). Emerging category representation in the visual forebrain hierarchy of pigeons (*Columba livia*). *Behavioural Brain Research*, *356*, 423–434. https://doi.org/10.1016/j.bbr.2018.05.014

Benowitz, L. I., & Karten, H. J. (1976). Organization of the TECTOFUGAL Visual Pathway in the pigeon: A retrograde transport study. *The Journal of Comparative Neurology*, *167*(4), 503–520. https://doi.org/10.1002/cne.901670407

Becker, T., & Redies, C. (2003). Internal structure of the nucleus rotundus revealed by mapping cadherin expression in the embryonic chicken visual system. *The Journal of Comparative Neurology*, *467*(4), 536–548. https://doi.org/10.1002/cne.10954

Bowmaker, J. K., Heath, L. A., Wilkie, S. E., & Hunt, D. M. (1997). Visual pigments and oil droplets from six classes of photoreceptor in the retinas of birds. *Vision Research*, *37*(16), 2183–2194. https://doi.org/10.1016/s0042-6989(97)00026-6

Braun, K., Scheich, H., Schachner, M., & Heizmann, C. W. (1985). Distribution of parvalbumin, cytochrome oxidase activity and 14C-2-deoxyglucose uptake in the brain of the zebra finch. *Cell and Tissue Research*, *240*(1), 117–127. https://doi.org/10.1007/bf00217564

Braun, K., Scheich, H., Zuschratter, W., Heizmann, C. W., Matute, C., & Streit, P. (1988). Postnatal development of parvalbumin-, calbindin- and adult GABA-immunoreactivity in two visual nuclei of Zebra Finches. *Brain Research*, *475*(2), 205–217. https://doi.org/10.1016/0006-8993(88)90609-9

Clarke, P. G., & Whitteridge, D. (1976). The projection of the retina, including the 'Red Area', on to the optic tectum of the pigeon. *Quarterly Journal of Experimental Physiology and*

Cognate Medical Sciences, *61*(4), 351–358. https://doi.org/10.1113/expphysiol.1976.sp002366

Das, D., Wilkie, S. E., Hunt, D. M., & Bowmaker, J. K. (1999). Visual pigments and oil droplets in the retina of a passerine bird, the canary *Serinus canaria*: Microspectrophotometry and opsin sequences. *Vision Research*, *39*(17), 2801–2815. https://doi.org/10.1016/s0042-6989(99)00023-1

Deng, C., & Rogers, L. J. (1998). Organisation of the Tectorotundal and SP/IPS-Rotundal Projections in the Chick. *Journal of Comparative Neurology*, *394*(2), 171–185. https://doi.org/10.1002/(sici)1096-9861(19980504)394:2<171: aid-cne3>3.0.co;2-#

Deng, C., & Rogers, L. J. (2000). Organization of intratelencephalic projections to the Visual Wulst of the chick. *Brain Research*, *856*(1-2), 152–162. https://doi.org/10.1016/s0006-8993(99)02403-8

Domenici, L., Waldvogel, H. J., Matute, C., & Streit, P. (1988). Distribution of GABA-like immunoreactivity in the Pigeon Brain. *Neuroscience*, *25*(3), 931–950. https://doi.org/10.1016/0306-4522(88)90047-4

Dubbeldam, J. L., Den Boer-Visser, A. M., & Bout, R. G. (1997). Organization and efferent connections of the archistriatum of the Mallard (*Anas platyrhynchos L*): An anterograde and retrograde tracing study. *The Journal of Comparative Neurology*, *388*(4), 632–657. https://doi.org/10.1002/(sici)1096-9861(19971201)388:4<632: aid-cne10>3.0.co;2-n

Ehrlich, D. (1981). Regional specialization of the Chick Retina as revealed by the size and density of neurons in the ganglion cell layer. *The Journal of Comparative Neurology*, *195*(4), 643–657. https://doi.org/10.1002/cne.901950408

Faunes, M., Fernández, S., Gutiérrez-Ibáñez, C., Iwaniuk, A. N., Wylie, D. R., Mpodozis, J., Karten, H. J., & Marín, G. (2013). Laminar segregation of GABAergic neurons in the avian nucleus isthmi pars magnocellularis: A retrograde tracer and comparative study. *Journal of Comparative Neurology*, *521*(8), 1727–1742. https://doi.org/10.1002/cne.23253

Fernández, M., Ahumada-Galleguillos, P., Sentis, E., Marín, G., & Mpodozis, J. (2019). Intratelencephalic projections of the avian visual dorsal ventricular ridge: Laminarly segregated, reciprocally and topographically organized. *Journal of Comparative Neurology*, *528*(2), 321–359. https://doi.org/10.1002/cne.24757

Fernández, M., Morales, C., Durán, E., Fernández-Colleman, S., Sentis, E., Mpodozis, J., Karten, H. J., & Marín, G. J. (2019). Parallel Organization of the avian sensorimotor arcopallium: Tectofugal visual pathway in the pigeon (*Columba livia*). *Journal of Comparative Neurology*, *528*(4), 597–623. https://doi.org/10.1002/cne.24775

Fredes, F., Tapia, S., Letelier, J. C., Marín, G., & Mpodozis, J. (2010). Topographic arrangement of the Rotundo-entopallial projection in the pigeon (*Columba livia*). *The Journal of Comparative Neurology*, *518*(21), 4342–4361. https://doi.org/10.1002/cne.22460

Freund, N., Güntürkün, O., & Manns, M. (2008). A morphological study of the nucleus subpretectalis of the pigeon. *Brain Research Bulletin*, *75*(2-4), 491–493. https://doi.org/10.1016/j.brainresbull.2007.10.031

Frost, B. J., & DiFranco, D. E. (1976). Motion characteristics of single units in the Pigeon Optic tectum. *Vision Research*, *16*(11), 1229–1234. https://doi.org/10.1016/0042-6989(76)90046-8

Gagliardo, A., Vallortigara, G., Nardi, D., & Bingman, V. P. (2005). A lateralized avian hippocampus: Preferential role of the left hippocampal formation in homing pigeon Sun Compass-based spatial learning. *European Journal of Neuroscience*, *22*(10), 2549–2559. https://doi.org/10.1111/j.1460-9568.2005.04444.x

Gamlin, P. D. R., Reiner, A., Keyser, K. T., Brecha, N., & Karten, H. J. (1996). Projection of the nucleus pretectalis to a retinorecipient tectal layer in the pigeon (*Columba livia*). *The Journal of Comparative Neurology*, *368*(3), 424–438. https://doi.org/10.1002/(sici)1096-9861(19960506)368:3<424: aid-cne8>3.0.co;2-7

Gao, M., Lengersdorf, D., Stüttgen, M. C., & Güntürkün, O. (2019). Transient inactivation of the visual-associative nidopallium frontolaterale (NFL) impairs extinction learning and context encoding in pigeons. *Neurobiology of Learning and Memory*, *158*, 50–59. https://doi.org/10.1016/j.nlm.2019.01.012

Garrido-Charad, F., Vega-Zuniga, T., Gutiérrez-Ibáñez, C., Fernandez, P., López-Jury, L., González-Cabrera, C., Karten, H. J., Luksch, H., & Marín, G. J. (2018). "Shepherd's crook" neurons drive and synchronize the enhancing and suppressive mechanisms of the midbrain stimulus selection network. *Proceedings of the National Academy of Sciences*, *115*(32). https://doi.org/10.1073/pnas.1804517115

Goldsmith, T. H., & Butler, B. K. (2005). Color vision of the Budgerigar (*Melopsittacus undulatus*): Hue matches, tetrachromacy, and intensity discrimination. *Journal of Comparative Physiology A*, *191*(10), 933–951. https://doi.org/10.1007/s00359-005-0024-2

González-Cabrera, C., Garrido-Charad, F., Roth, A., & Marín, G. J. (2015). The isthmic nuclei providing parallel feedback connections to the avian tectum have different neurochemical identities: Expression of glutamatergic and cholinergic markers in the chick (*Gallus gallus*). *Journal of Comparative Neurology*, *523*(9), 1341–1358. https://doi.org/10.1002/cne.23739

Gu, Y., Wang, Y., & Wang, S.-R. (2000). Regional variation in receptive field properties of tectal neurons in pigeons. *Brain, Behavior and Evolution*, *55*(4), 221–228. https://doi.org/10.1159/000006654

Güntürkün, O. (1997). Morphological asymmetries of the tectum opticum in the pigeon. *Experimental Brain Research*, *116*(3), 561–566. https://doi.org/10.1007/pl00005785

Gutiérrez-Ibáñez, C., Iwaniuk, A. N., Lisney, T. J., & Wylie, D. R. (2012). Comparative study of visual pathways in owls (aves: Strigiformes). *Brain, Behavior and Evolution*, *81*(1), 27–39. https://doi.org/10.1159/000343810

Hamdi, F. A., & Whitteridge, D. (1954). The representation of the retina on the optic tectum of the pigeon. *Quarterly Journal of Experimental Physiology and Cognate Medical Sciences*, *39*(2), 111–119. https://doi.org/10.1113/expphysiol.1954.sp001053

Hardy, O., Leresche, N., & Jassik-Gerschenfeld, D. (1985). Morphology and laminar distribution of electrophysiologically identified cells in the pigeon's optic tectum: An intracellular study. *The Journal of Comparative Neurology*, *233*(3), 390–404. https://doi.org/10.1002/cne.902330308

Hart, N. S., Partridge, J. C., & Cuthill, I. C. (1998). Visual pigments, oil droplets and cone photoreceptor distribution in the European Starling (*Sturnus vulgaris*). *Journal of Experimental Biology*, *201*(9), 1433–1446. https://doi.org/10.1242/jeb.201.9.1433

Hartmann, B., & Güntürkün, O. (1998). Selective deficits in reversal learning after neostriatum caudolaterale lesions in pigeons: Possible behavioral equivalencies to the mammalian prefrontal system. *Behavioural Brain Research*, *96*(1-2), 125–133. https://doi.org/10.1016/s0166-4328(98)00006-0

Hayes, B. P. (1982). Chapter 7 the Structural Organization of the Pigeon Retina. *Progress in Retinal Research*, *1*, 197–226. https://doi.org/10.1016/0278-4327(82)90009-8

Hellmann, B., Manns, M., & Güntürkün, O. (2001). Nucleus isthmi, pars semilunaris as a key component of the tectofugal visual system in pigeons. *Journal of Comparative Neurology*, *436*(2), 153–166. https://doi.org/10.1002/cne.1058

Hellmann, B., & Gunturken, O. (2000). Structural organization of parallel information processing within the TECTOFUGAL visual system of the pigeon. *The Journal of Comparative Neurology*, *429*(1), 94–112. https://doi.org/10.1002/1096-9861(20000101)429:1<94::aid-cne8>3.0.co;2-5

Hellmann, B., & Güntürkün, O. (1999). Visual-field-specific heterogeneity within the tecto-rotundal projection of the pigeon. *European Journal of Neuroscience*, *11*(8), 2635–2650. https://doi.org/10.1046/j.1460-9568.1999.00681.x

Hellmann, B., Güntürkün, O., & Manns, M. (2004). Tectal mosaic: Organization of the descending tectal projections in comparison to the ascending tectofugal pathway in the pigeon. *Journal of Comparative Neurology*, *472*(4), 395–410. https://doi.org/10.1002/cne.20056

Hodos, W., & Karten, H. J. (1970). Visual intensity and pattern discrimination deficits after lesions of ectostriatum in pigeons. *The Journal of Comparative Neurology*, *140*(1), 53–68. https://doi.org/10.1002/cne.901400104

Hodos, W., & Karten, H. J. (1974). Visual intensity and pattern discrimination deficits after lesions of the optic lobe in pigeons. *Brain, Behavior and Evolution*, *9*(3), 165–179. https://doi.org/10.1159/000123663

Hodos, W., Weiss, S. R. B., & Bessette, B. B. (1988). Intensity difference thresholds after lesions of ectostriatum in pigeons. *Behavioural Brain Research*, *30*(1), 43–53. https://doi.org/10.1016/0166-4328(88)90007-1

Hsiao, Y.-T., Chen, T.-C., Yu, P.-H., Huang, D.-S., Hu, F.-R., Chuong, C.-M., & Chang, F.-C. (2020). Connectivity between nidopallium caudolateral and visual pathways in color perception of zebra finches. *Scientific Reports*, *10*(1). https://doi.org/10.1038/s41598-020-76542-z

Hu, J., & Wang, S.-R. (2001). Firing patterns and morphological features of neurons in the pigeon nucleus rotundus. *Brain, Behavior and Evolution*, *57*(6), 343–348. https://doi.org/10.1159/000047252

Hu, M., Naito, J., Chen, Y., Ohmori, Y., & Fukuta, K. (2003). Afferent and efferent connections of the Nucleus Rotundus demonstrated by WGA-HRP in the Chick. *Anatomia, Histologia, Embryologia: Journal of Veterinary Medicine Series C*, *32*(6), 335–340. https://doi.org/10.1111/j.1439-0264.2003.00488.x

Hunt, S. P., Streit, P., Künzle, H., & Cuénod, M. (1977). Characterization of the pigeon isthmo-tectal pathway by selective uptake and retrograde movement of radioactive compounds and by golgi-like horseradish peroxidase labeling. *Brain Research*, *129*(2), 197–212. https://doi.org/10.1016/0006-8993(77)90001-4

Husband, S. A., & Shimizu, T. (1999). Efferent projections of the ectostriatum in the pigeon (*Columba livia*). *The Journal of Comparative Neurology*, *406*(3), 329–345. https://doi.org/10.1002/(sici)1096-9861(19990412)406:3<329::aid-cne3>3.0.co;2-a

Johnston, M., Anderson, C., & Colombo, M. (2017). Neural correlates of sample-coding and reward-coding in the delay activity of neurons in the entopallium and Nidopallium Caudolaterale of pigeons (*Columba livia*). *Behavioural Brain Research*, *317*, 382–392. https://doi.org/10.1016/j.bbr.2016.10.003

Karten, H. J., Cox, K., & Mpodozis, J. (1997). Two distinct populations of tectal neurons have unique connections within the retinotectorotundal pathway of the pigeon (*Columba livia*). *The Journal of Comparative Neurology*, *387*(3), 449–465. https://doi.org/10.1002/(sici)1096-9861(19971027)387:3<449::aid-cne10>3.0.co;2-g

Koshiba, M., Kikuchi, T., Yohda, M., & Nakamura, S. (2002). Inversion of the anatomical lateralization of Chick Thalamofugal Visual pathway by light experience. *Neuroscience Letters*, *318*(3), 113–116. https://doi.org/10.1016/s0304-3940(01)02306-0

Krützfeldt, N. O. E., & Wild, J. M. (2003). Definition and connections of the entopallium in the zebra finch (*Taeniopygia guttata*). *Journal of Comparative Neurology*, *468*(3), 452–465. https://doi.org/10.1002/cne.10972

Krützfeldt, N. O. E., & Wild, J. M. (2005). Definition and novel connections of the Entopallium in the pigeon (*Columba livia*). *The Journal of Comparative Neurology*, *490*(1), 40–56. https://doi.org/10.1002/cne.20627

Kususnoki, T. (1969). The chemoarchitectonics of the avian brain. *Journal of Brain Research*, *11*(6), 477–497.

Laverghetta, A. V., & Shimizu, T. (1999). Visual discrimination in the pigeon (*Columba livia*). *NeuroReport*, *10*(5), 981–985. https://doi.org/10.1097/00001756-199904060-00016

Laverghetta, A. V., & Shimizu, T. (2003). Organization of the ectostriatum based on afferent connections in the Zebra Finch (*Taeniopygia guttata*). *Brain Research*, *963*(1-2), 101–112. https://doi.org/10.1016/s0006-8993(02)03949-5

Letelier, J.-C., Marin, G., Sentis, E., Tenreiro, A., Fredes, F., & Mpodozis, J. (2004). The mapping of the visual field onto the dorso-lateral tectum of the pigeon (*Columba livia*) and its relations with retinal specializations. *Journal of Neuroscience Methods*, *132*(2), 161–168. https://doi.org/10.1016/j.jneumeth.2003.09.007

Lisney, T. J., Iwaniuk, A. N., Bandet, M. V., & Wylie, D. R. (2012). Eye shape and retinal topography in owls (aves: Strigiformes). *Brain, Behavior and Evolution*, *79*(4), 218–236. https://doi.org/10.1159/000337760

Luksch, H., Cox, K., & Karten, H. J. (1998). Bottlebrush dendritic endings and large dendritic fields: Motion-detecting neurons in the tectofugal pathway. *The Journal of Comparative Neurology*, *396*(3), 399–414. https://doi.org/10.1002/(sici)1096-9861(19980706)396:3<399::aid-cne9>3.0.co;2-y

Maekawa, F., Komine, O., Sato, K., Kanamatsu, T., Uchimura, M., Tanaka, K., & Ohki-Hamazaki, H. (2006). Imprinting modulates processing of visual information in the Visual Wulst of Chicks. *BMC Neuroscience*, *7*(1). https://doi.org/10.1186/1471-2202-7-75

Marin, G. J., Duran, E., Morales, C., Gonzalez-Cabrera, C., Sentis, E., Mpodozis, J., & Letelier, J. C. (2012). Attentional capture? synchronized feedback signals from the isthmi boost retinal signals to higher visual areas. *Journal of Neuroscience*, *32*(3), 1110–1122. https://doi.org/10.1523/jneurosci.4151-11.2012

Marin, G., Salas, C., Sentis, E., Rojas, X., Letelier, J. C., & Mpodozis, J. (2007). A cholinergic gating mechanism controlled by competitive interactions in the optic tectum of the pigeon. *Journal of Neuroscience*, *27*(30), 8112–8121. https://doi.org/10.1523/jneurosci.1420-07.2007

Martin, G. R. (2007). Visual fields and their functions in birds. *Journal of Ornithology*, *148*(S2), 547–562. https://doi.org/10.1007/s10336-007-0213-6

Martin, G. R., & Katzir, G. (1999). Visual fields in short-toed eagles, *Circaetus gallicus* (Accipitridae), and the function of binocularity in birds. *Brain, Behavior and Evolution*, *53*(2), 55–66. https://doi.org/10.1159/000006582

Martin, G. R., & Young, S. R. (1983). The retinal binocular field of the pigeon (*Columba livia*: English racing homer). *Vision Research*, *23*(9), 911–915. https://doi.org/10.1016/0042-6989(83)90061-5

Martinez-de-la-Torre, M., Martinez, S., & Puelles, L. (1990). Acetylcholinesterase-histochemical differential staining of subdivisions within the nucleus rotundus in the Chick. *Anatomy and Embryology*, *181*(2). https://doi.org/10.1007/bf00198952

Maturana, H. R., & Frenk, S. (1965). Synaptic connections of the centrifugal fibers in the pigeon retina. *Science*, *150*(3694), 359–361. https://doi.org/10.1126/science.150.3694.359

Mcfadden, S. A., & Reymond, L. (1985). A further look at the binocular visual field of the pigeon (*Columba livia*). *Vision Research*, *25*(11), 1741–1746. https://doi.org/10.1016/0042-6989(85)90147-6

Medina, L., & Reiner, A. (1994). Distribution of choline acetyltransferase immunoreactivity in the Pigeon Brain. *The Journal of Comparative Neurology*, *342*(4), 497–537. https://doi.org/10.1002/cne.903420403

Mestres, P., & Delius, J. D. (1982). A contribution to the study of the afferents to the pigeon optic tectum. *Anatomy and Embryology*, *165*(3), 415–423. https://doi.org/10.1007/bf00305577

Meyer, D. B., & Cooper, T. G. (1966). The visual cells of the chicken as revealed by phase contrast microscopy. *American Journal of Anatomy*, *118*(3), 723–734. https://doi.org/10.1002/aja.1001180303

Miceli, D., Repérant, J., Bertrand, C., & Rio, J.-P. (1999). Functional anatomy of the avian centrifugal visual system. *Behavioural Brain Research*, *98*(2), 203–210. https://doi.org/10.1016/s0166-4328(98)00085-0

Mitkus, M., Chaib, S., Lind, O., & Kelber, A. (2014). Retinal ganglion cell topography and spatial resolution of two parrot species: Budgerigar (*Melopsittacus undulatus*) and

Bourke's Parrot (*Neopsephotus bourkii*). *Journal of Comparative Physiology A*, *200*(5), 371–384. https://doi.org/10.1007/s00359-014-0894-2

Moore, B. A., Baumhardt, P., Doppler, M., Randolet, J., Blackwell, B. F., DeVault, T. L., Loew, E. R., & Fernández-Juricic, E. (2012). Oblique color vision in an open-habitat bird: Spectral sensitivity, photoreceptor distribution and behavioral implications. *Journal of Experimental Biology*, *215*(19), 3442–3452. https://doi.org/10.1242/jeb.073957

Morris, V. B., & Shorey, C. D. (1967). An electron microscope study of types of receptor in the Chick Retina. *The Journal of Comparative Neurology*, *129*(4), 313–339. https://doi.org/10.1002/cne.901290404

Mpodozis, J., Cox, K., Shimizu, T., Bischof, H.-J., Woodson, W., & Karten, H. J. (1996). GABAergic inputs to the nucleus rotundus (pulvinar inferior) of the pigeon (*Columba livia*). *The Journal of Comparative Neurology*, *374*(2), 204–222. https://doi.org/10.1002/(sici)1096-9861(19961014)374:2<204::aid-cne4>3.0.co;2-6

Nguyen, A. P. (2004). A dissociation of motion and spatial-pattern vision in the avian telencephalon: Implications for the evolution of "Visual streams". *Journal of Neuroscience*, *24*(21), 4962–4970. https://doi.org/10.1523/jneurosci.0146-04.2004

Okano, T., Kojima, D., Fukada, Y., Shichida, Y., & Yoshizawa, T. (1992). Primary structures of chicken cone visual pigments: Vertebrate rhodopsins have evolved out of cone visual pigments. *Proceedings of the National Academy of Sciences*, *89*(13), 5932–5936. https://doi.org/10.1073/pnas.89.13.5932

O'Rourke, C. T., Hall, M. I., Pitlik, T., & Fernández-Juricic, E. (2010). Hawk eyes I: Diurnal raptors differ in visual fields and degree of Eye Movement. *PLoS ONE*, *5*(9). https://doi.org/10.1371/journal.pone.0012802

Ott, M. (2005). Visual accommodation in vertebrates: Mechanisms, physiological response and stimuli. *Journal of Comparative Physiology A*, *192*(2), 97–111. https://doi.org/10.1007/s00359-005-0049-6

Patton, T. B., Cook, R. G., & Shimizu, T. (2013). Functional segregation of the entopallium in pigeons. *PsycEXTRA Dataset*. https://doi.org/10.1037/e598032013-053

Reiner, A., & Karten, H. J. (1983). The laminar source of efferent projections from the avian wulst. *Brain Research*, *275*(2), 349–354. https://doi.org/10.1016/0006-8993(83)90996-4

Remy, M., & Güntürkün, O. (1991). Retinal afferents to the tectum opticum and the nucleus opticus principalis thalami in the pigeon. *Journal of Comparative Neurology*, *305*(1), 57–70. https://doi.org/10.1002/cne.903050107

Repérant, J., & Angaut, P. (1977). The retinotectal projections in the pigeon. an experimental optical and electron microscope study. *Neuroscience*, *2*(1), 119–140. https://doi.org/10.1016/0306-4522(77)90073-2

Revzin, A. M. (1977). Functional localization in the nucleus rotundus. *PsycEXTRA Dataset*. https://doi.org/10.1037/e586822011-001

Reyes-Pinto, R., Ferrán, J. L., Vega-Zuniga, T., González-Cabrera, C., Luksch, H., Mpodozis, J., Puelles, L., & Marín, G. J. (2021). Change in the neurochemical signature and morphological development of the parvocellular isthmic projection to the avian tectum. *Journal of Comparative Neurology*, *530*(2), 553–573. https://doi.org/10.1002/cne.25229

Rio, J. P., Villalobos, J., Miceli, D., & Repérant, J. (1983). Efferent projections of the visual wulst upon the nucleus of the basal optic root in the pigeon. *Brain Research*, *271*(1), 145–151. https://doi.org/10.1016/0006-8993(83)91375-6

Rogers, L., Koboroff, A., & Kaplan, G. (2018). Lateral asymmetry of brain and behaviour in the zebra finch, *Taeniopygia guttata*. *Symmetry*, *10*(12), 679. https://doi.org/10.3390/sym10120679

Sebesteny, T., Davies, D. C., Zayats, N., Nemeth, A., & Tombol, T. (2002). The ramification and connections of retinal fibres in layer 7 of the domestic chick optic tectum: A golgi impregnation, anterograde tracer and GABA-immunogold study. *Journal of Anatomy*, *200*(2), 169–183. https://doi.org/10.1046/j.0021-8782.2001.00012.x

Schmidt, A., & Bischof, H.-J. (2001). Integration of information from both eyes by single neurons of nucleus rotundus, ectostriatum and lateral neostriatum in the zebra finch (*Taeniopygia guttata castanotis gould*). *Brain Research*, *923*(1-2), 20–31. https://doi.org/10.1016/s0006-8993(01)03192-4

Seifert, M., Baden, T., & Osorio, D. (2020). The retinal basis of vision in Chicken. *Seminars in Cell & Developmental Biology*, *106*, 106–115. https://doi.org/10.1016/j.semcdb.2020.03.011

Shimizu, T., Cox, K., & Karten, H. J. (1995). Intratelencephalic projections of the visual wulst in pigeons (*Columba livia*). *The Journal of Comparative Neurology*, *359*(4), 551–572. https://doi.org/10.1002/cne.903590404

Stacho, M., Herold, C., Rook, N., Wagner, H., Axer, M., Amunts, K., & Güntürkün, O. (2020). A cortex-like canonical circuit in the avian forebrain. *Science*, *369*(6511). https://doi.org/10.1126/science.abc5534

Stavenga, D. G., & Wilts, B. D. (2014). Oil droplets of bird eyes: Microlenses acting as spectral filters. *Philosophical Transactions of the Royal Society B: Biological Sciences*, *369*(1636), 20130041. https://doi.org/10.1098/rstb.2013.0041

Sun, H.-J., & Frost, B. J. (1997). Motion processing in Pigeon Tectum: Equiluminant chromatic mechanisms. *Experimental Brain Research*, *116*(3), 434–444. https://doi.org/10.1007/pl00005771

Theiss, M. P., Hellmann, B., & Güntürkün, O. (2003). The architecture of an inhibitory sidepath within the avian tectofugal system. *NeuroReport*, *14*(6), 879–882. https://doi.org/10.1097/00001756-200305060-00021

Thin, N. D., Egedy, G., & Tombol, T. (1992). Golgi study on neurons and fibers in nucleus rotundus of the thalamus in chicks. *Journal of Brain Research*, *33*, 203–214.

Tömböl, T., & Nemeth, A. (1998). Golgi and electron-microscopic Golgi-GABA immunostaining study of the avian optic tectum. *Cells Tissues Organs*, *162*(4), 209–225. https://doi.org/10.1159/000046436

Tömböl, T., Eyre, M. D., Alpár, A., & Németh, A. (2005). The axon arbourisation of nuclei isthmi neurons in the optic tectum of the chick and pigeon. A golgi and anterograde tracer-study. *Anatomy and Embryology*, *209*(5), 371–380. https://doi.org/10.1007/s00429-004-0450-x

Treubert-Zimmermann, U., Heyers, D., & Redies, C. (2002). Targeting axons to specific fiber tract in vivo by altering cadherin expression. *The Journal of Neuroscience*, *22*(17), 7617–7626. https://doi.org/10.1523/jneurosci.22-17-07617.2002

Tyrrell, L. P., Teixeira, L. B., Dubielzig, R. R., Pita, D., Baumhardt, P., Moore, B. A., & Fernández-Juricic, E. (2019). A novel cellular structure in the retina of insectivorous birds. *Scientific Reports*, *9*(1). https://doi.org/10.1038/s41598-019-51774-w

Uchiyama, H., Aoki, K., Yonezawa, S., Arimura, F., & Ohno, H. (2004). Retinal target cells of the centrifugal projection from the isthmo-optic nucleus. *The Journal of Comparative Neurology*, *476*(2), 146–153. https://doi.org/10.1002/cne.20225

Uchiyama, H., Ito, H., & Tauchi, M. (1995). Retinal neurones specific for centrifugal modulation of vision. *NeuroReport*, *6*(6), 889–892. https://doi.org/10.1097/00001756-199504190-00016

Uchiyama, H., Ohno, H., & Kodama, R. (2012). Lesion of the isthmo-optic nucleus impairs target selection for visually guided reaching. *Behavioural Brain Research*, *233*(2), 359–366. https://doi.org/10.1016/j.bbr.2012.05.008

Uchiyama, H., Ohno, H., Kawasaki, T., Owatari, Y., Narimatsu, T., Miyanagi, Y., & Maeda, T. (2022). Attentional signals projecting centrifugally to the avian retina: A dual contribution to visual search. *Vision Research*, *195*, 108016. https://doi.org/10.1016/j.visres.2022.108016

Wang, Y., & Frost, B. J. (1992). Time to collision is signalled by neurons in the nucleus rotundus of pigeons. *Nature*, *356*(6366), 236–238. https://doi.org/10.1038/356236a0

Wang, Y., Luksch, H., Brecha, N. C., & Karten, H. J. (2005). Columnar projections from the cholinergic nucleus isthmi to the optic tectum in chicks (*Gallus gallus*): A possible substrate for synchronizing tectal channels. *The Journal of Comparative Neurology*, *494*(1), 7–35. https://doi.org/10.1002/cne.20821

Wang, Y.-C., Jiang, S., & Frost, B. J. (1993). Visual processing in pigeon nucleus rotundus: Luminance, color, motion, and looming subdivisions. *Visual Neuroscience*, *10*(1), 21–30. https://doi.org/10.1017/s0952523800003199

Wang, S.-R., Wang, Y.-C., & Frost, B. J. (1995). Magnocellular and parvocellular divisions of pigeon nucleus isthmi differentially modulate visual responses in the Tectum. *Experimental Brain Research*, *104*(3). https://doi.org/10.1007/bf00231973

Watanabe, A., Gignac, P. M., Balanoff, A. M., Green, T. L., Kley, N. J., & Norell, M. A. (2018). Are endocasts good proxies for brain size and shape in archosaurs throughout ontogeny? *Journal of Anatomy*, *234*(3), 291–305. https://doi.org/10.1111/joa.12918

Watanabe, S., Mayer, U., & Bischof, H.-J. (2011). Visual Wulst analyses "where" and entopallium analyses "what" in the Zebra Finch Visual System. *Behavioural Brain Research*, *222*(1), 51–56. https://doi.org/10.1016/j.bbr.2011.03.035

Wu, L.-Q., Niu, Y.-Q., Yang, J., & Wang, S.-R. (2005). Tectal neurons signal impending collision of looming objects in the pigeon. *European Journal of Neuroscience*, *22*(9), 2325–2331. https://doi.org/10.1111/j.1460-9568.2005.04397.x

Xiao, Q., Li, D.-P., & Wang, S.-R. (2006). Looming-sensitive responses and receptive field organization of telencephalic neurons in the pigeon. *Brain Research Bulletin*, *68*(5), 322–328. https://doi.org/10.1016/j.brainresbull.2005.09.003

Yamagata, M., Yan, W., & Sanes, J. R. (2021). A cell atlas of the Chick Retina based on single-cell transcriptomics. *ELife*, *10*. https://doi.org/10.7554/elife.63907

Yazulla, S., & Granda, A. M. (1973). Opponent-color units in the thalamus of the pigeon (*Columba livia*). *Vision Research*, *13*(8). https://doi.org/10.1016/0042-6989(73)90014-x

Chapter 3. Mapping the avian visual tectofugal pathway using 3D reconstruction

Parker J. Straight[1], Paul M. Gignac[2,3], Wayne J. Kuenzel[1]

1 Poultry Sci. Dept., University of Arkansas, Fayetteville, AR; 2 Cellular and Molecular Medicine Dept., University of Arizona Health Sciences, Tucson, AZ; 3 MicroCT Imaging Consortium for Research and Outreach, University of Arkansas, Fayetteville, AR

3.1 Abstract

Image processing in amniotes is usually dominated by either the thalamofugal or tectofugal visual system. In laterally eyed birds, the tectofugal system dominates with retinal ganglion cells projecting to the optic tecum, which then projects to a structure in the dorsal thalamus. The thalamic structure projects to a forebrain structure known as the entopallium, the terminal structure in the tectofugal pathway. The tectofugal system functions include color and motion processing, and spatial orientation, stimulus identification and localization making this system critical for complex avian behavior. Two-week-old chicks were used for serial brain sections in either coronal, sagittal or horizontal planes and stained Nissl and either Gallyas or Luxol Fast Blue. We attempted to divide the nucleus rotundus and the entopallium based on cell and fiber density. Additionally, we employed the emerging technique diffusible iodine-based contrast-enhanced computed tomography (diceCT) on a five-week-old chick for our anatomical investigation. Using the acquired data from serial histochemistry, diceCT and interpretation from the literature, we generated a complete 3D model of the avian tectofugal visual system. Our results indicate that the nucleus rotundus has five subdivisions and the entopallium has three subdivisions. The use of a 3D model will enable complete understanding of the structural components of this system and their spatial organization. We believe pairing diceCT with

traditional histochemistry is beneficial to understanding the anatomical and functional organization of complicated neural pathways such as the tectofugal visual system.

Keywords: tectofugal visual system, 3D modeling, diceCT

Abbreviations: AI, intermediate arcopallium; AId, dorsal subdivision of the of the intermediate arcopallium; AIv, ventral subdivision of the intermediate arcopallium; ARP, arcopallium; CEV, cresylecht violet; cp, posterior commissure; dsv, ventral supraoptic decussation; Eb, belt of the entopallium; Ee, external core of the entopallium; Ei, internal core of the entopallium; Ento, entopallium; GABA, γ-Aminobutyric acid; GSM, gallyas silver myelin; HA, apical hyperpallium; iit, intra-isthmal tract; Imc, nucleus isthmus, magnocellular part; iot, isthmo-optic tract; Ipc, nucleus isthmus, parvocellular part; ISPT, intermediate subpretectal nucleus; LFBS, luxol fast blue; MVL, ventral lateral mesopallium; NCL, caudal lateral nidopallium; NFL, frontal lateral nidopallium; NI, intermediate nidopallium; NIL, intermediate lateral nidopallium; omt, occipital mesencephalic tract; pspt, pretecto-subpretectal tract; PT, pretectal nucleus; RGCs, retinal ganglion cells; ROT/Rt, nucleus rotundus; ROTd, dorsal subdivision of the nucleus rotundus; ROTi, intermediate subdivision of the nucleus rotundus; ROTlp, lateral posterior subdivision of the nucleus rotundus; ROTv, ventral subdivision of the nucleus rotundus; SLu, semilunar nucleus; SP, subpretectal nucleus; SPC, superficial parvocellular nucleus; SROT, subrotundus; T, triangularis; TeO, optic tectum; TGCs, tectal ganglion cells; TPO, temporoparietooccipital area; ttt, tectothalamic tract; vat, ventral arcopallial tract

3.2 Introduction

Neuroanatomical systems that enable vision are highly complex, owing to the multi-factorial ways that vertebrate brains process visual stimuli (e.g., luminance, color, motion, texture, shape). Visual field characteristics are processed by several neural systems, each contributing different

anatomical and functional qualities. This makes them both fascinating and difficult aspects of functional neuroscience to study. Nonetheless, they are critical for the day-to-day survival and developmental success of most vertebrates.

Visual capabilities of avian species, for example, are often comparable to and even surpass those of other visually dependent vertebrates. In the case of birds, the visual systems are critical for complex behaviors such as mating, flight, migration and homing, foraging and predation, and predator detection and avoidance.

Historically, these systems have been investigated using well-established approaches, such as 2D serial histology and gross dissection. These efforts have provided previously unheralded insights into avian neuroscience, including the potential cortex-like canonical organization of the avian forebrain (Stacho et al., 2020), regional functional characteristics of various visual structures (Gu et al., 2000), and characterization of cell-type diversity among species (Wai et al., 2006).

For example, the tectofugal system—a series of midbrain –to-forebrain circuits important to avian vision—has been well described in both anatomical complexity and functionality in the pigeon, chicken, and zebra finch (Benowitz and Karten, 1976; Laverghetta and Shimizu et al., 2003; Hellmann and Gunturken, 2001; Bischof and Niemann, 1990; Tombol et al., 1988; Verhaal and Luksch, 2013; Tombol et al., 1988). The tectofugal system consists of three primary neurons. First, small retinal ganglion cells retinotopically project from the eyeball to the superficial layers of the optic tectum (nos. 2–7) where they synapse with the specialized dendritic arbors of tectal ganglion cells from the deep layer 13 (Karten et al., 1997). Next, different populations of tectal ganglion cells ipsilaterally, contralaterally, and bilaterally project as functional groups to the thalamic nucleus rotundus, where they synapse marking the transition

from a retinotopic to functionotopic projections (Karten et al., 1997; Hellmann and Gunturken 2001). The rotundus is divided into functional domains, each processing a specific visual characteristic (looming, luminance, color, motion; Wang et al., 1992). The third-order neurons that distribute unilaterally from these domains maintain their functional organization as they project to the entopallium (Fredes et al., 2010). The entopallium represents the terminus of the tectofugal circuit; however, neurons of the entopallium do project to higher visual associative areas in the avian pallium, a region of the dorsal cerebrum where more complex processing occurs. Additionally, secondary components within the mesencephalon or midbrain, such as the isthmic nuclei and pretectal/subpretectal complex help modulate and potentially direct visual input to aid in functions such as spatial orientation, and stimulus selection/ propagation (Marin et al., 2012; Acerbo et al., 2012).

Generally, these insights have been made without the benefit of visualizing avian neuroanatomy in three dimensions. Three-dimensional (3D) neuroanatomy is often documented and studied as a series of overlapping 2D histological slides or diagrams. While this approach enables the simplification of complex neurocircuitry, the missing features between each section are, by necessity, assumed to be less informative than those visualized. However, this may not always be the case. For example, 3D visualization may be especially important for the study of brains that are globular in form, harbor especially high cellular densities, and form as tightly integrated nodal networks—like those of birds (Shanahan et al., 2013). Documenting this neuroanatomy in 3D enables us to more fully appreciate the spatial complexity of these brains, understand their variation, better infer functional relationships among brain regions, and study the intricate developmental processes that underpin them.

Recent advancements in visualization techniques provide the opportunity to bridge this gap. One such technique, diffusible iodine-based contrast-enhanced computed tomography (diceCT; Gignac et al., 2016), provides an effective means of imaging vertebrate nervous tissue. Although diceCT employs X-ray-based computed tomography, the use of contrast agents which bind selectively to white and gray matter of the brain ensures that neuroanatomical features can be resolved in 3D (Gignac and Kley, 2014, 2018). DiceCT brain datasets show tissue contrast like those of T1-weighted magnetic resonance imaging (MRI) slices but at resolutions comparable to micro-MRI Gignac et al., 2021b). Moreover, diceCT can be integrated with histological datasets to provide orders of magnitude of structural detail, from cellular to brain to organismal levels of organization (Gignac et al., 2021a,b). As a result, we now have the opportunity to develop 3D, highly detailed, and descriptive models of the neural circuitry controlling various aspects of behavior, including the visual behaviors of birds.

Here we aim to use diceCT to create the first up-to-date interactive 3D model illustrating detailed tectofugal structures in a chicken model (*Gallus gallus*), featuring accurate spatial and structural data that delineates the flow of information within this complex system. To provide a detailed model of the tectofugal system for the avian neuroscience research and education communities, we deploy a combination of diceCT and serial immunohistochemistry for 3D reconstruction of specific areas of the avian brain to produce a comprehensive anatomical characterization of the visual tectofugal neural pathway. To this end, we have three objectives: (1) depict the retinotopic transition from the retina to the superficial optic tectum, (2) reconstruct the tectofugal nuclei of the mesencephalon and their interconnectivity, and (3) reconstruct the tectofugal nuclei of the pallium and their interconnectivity. We hope this model and the methods

used to develop it will promote further research of the avian visual system and other neural systems within the brain.

3.3 Materials and Methods

The 3D chicken brain atlas is based on a multi-modal visualization pipeline that includes histology and diceCT imaging. Each imaging methodology has advantages and disadvantages; however, when integrated the techniques complement one another (e.g., Gignac et al., 2021b). On the one hand, histological sections offer cell-specific staining and exceptionally high resolution, limited by the optical power of a user's light microscope. However, the technique parcels the brain into slices, which reduces its spatial dimensions and separates important neuroanatomical relationships. On the other hand is µCT-based imaging. While µCT provides high-resolution (e.g., ≤ 25 microns) imaging, that resolution is static. A major benefit of µCT imaging is that the brain is represented as a volume, documenting three dimensions of neuroanatomical variation without separating features of interest. Here we describe in detail the primary and secondary components of the visual tectofugal pathway and use them to delineate the axonal flow of information between regions in a 3D interactive and modifiable model.

3.3.1 Serial histochemical brain sections

For histological imaging in this study we used Luxol fast blue (LFBS), cresylecht violet (CEV), Gallyas Silver Myelin (GSM), and Nissl (N) staining of a two-week-old chicken brain. To enable easier identification of brain nuclei, LFBS and CEV stains were paired as were GSM and N stains. Luxol fast blue is a basophilic myelin sheath stain that stains nerve fibers blue as a major constituent of nerve processes is phospholipid. In contrast, CEV is an acidophilic agent that stains Nissl bodies (i.e., rough endoplasmic reticulum) dark purple. Together, these help to determine individual groups of cells defining a nucleus. The GSM method is a silver stain that

stains myelinated fibers (i.e., dendrites and axons) black. The Nissl stain (N; cresyl violet) when used in combination with GSM, enables locating groups of cells that form a nucleus or brain structure. GSM and N, and LFBS and CEV sets of slides represented neuroanatomy in all three orthogonal planes.

3.3.2 Diffusible iodine-based contrast-enhanced computed tomography

Following decapitation, the head of one five-week-old chick was fixed in 10% neutral buffered formalin. Once fixed, the sample was fully submerged in a 1% weight-by-volume (w/v) solution of iodine potassium-iodide (I_2KI, a.k.a., Lugol's iodine) for 40 days at room temperature (Gignac et al., 2016; Gignac and Kley, 2018). To facilitate staining, the calvarium and left lateral region of the braincase were partly removed and trepanned. This minimized the effect of a fully closed braincase to reduce stain diffusion rates, enabling the usage of a relatively low (i.e., 1% w/v) stain concentration necessary for minimizing brain shrinkage (Dawood et al., 2021). Over time, the staining solution loses its dark appearance as the majority of the staining agent becomes bound within the cells of the sample. When necessary, the solution was refreshed completely with new 1% I_2KI.

While in the staining solution, iodine naturally diffuses into a brain sample. The primary aqueous form of Lugol's iodine is triiodide (I_3^-), which has an affinity for sugars and, especially, lipids (Gignac et al., 2016). As the staining agent diffuses into the sample, I_3^- polymers collect in regions high in these constituents, such as the myelinated sheaths of Schwann cells and oligodendrocytes. This is beneficial for X-ray imaging of brain tissue because I_3^- is also radiopaque, enabling it to absorb X-rays during µCT scanning. As a result, white matter (along with other fatty and carbohydrate-rich tissues) can be readily differentiated from surrounding

structures. Altogether, this enables the 3D visualization of nervous, muscular, epithelial, bony, and special sensory structures simultaneously.

3.3.3 Image Acquisition and Processing

The sample was imaged at the MicroCT Imaging Consortium for Research and Outreach (MICRO) at the University of Arkansas, Fayetteville campus, using a 2018 Nikon XT H 225 ST µCT system (Nikon Metrology, Brighton, MI). The sample was sealed into a 50ml low-density, plastic tube filled with water (to prevent dehydration). The tube was positioned within the scanning chamber for µCT imaging. A scout image was used to optimize scan parameters, following Gignac and Kley (2018). The sample was scanned at an isometric voxel size of 19.499 microns, using 211 kV, 91 µ-Amperage, a 708-millisecond exposure setting, and 8x multi-frame averaging with a rotating tungsten target and 0.125 mm thick copper filter. For visualization purposes, the minimize ring artifacts setting was on to limit visible rings from appearing in the scanned images. µCT projections were reconstructed using Nikon µCT software and VG Studio Max (Volume Graphics GmbH, Heidelberg, Germany) on an HP z800 workstation (Hewlett-Packard, Palo Alto, CA, USA). The resulting dataset was exported as a stack of TIFF images for 3D model development (see Gignac and Kley, 2018).

3.3.4 Anatomical Reconstruction

Both the serial histochemical and diceCT datasets were used in the reconstruction of the avian brain and structures of the tectofugal pathway. The inner ear canals, visible in the µCT scan, were digitally rendered in 3D using AvizoLite 2020 (Thermo Fisher Scientific Inc., Waltham, MA). These provided important anatomical references necessary to correctly orient whole brain and skull models consistent with the positioning of the stereotaxic instrument used to standardize the orientation of histological sections (Kuenzel and Masson. 1988). This enabled us to ensure

that sagittal histochemical sections were reoriented to match the 45° (from horizontal) orientation of the skull in the stereotaxic atlas of Kuenzel and Masson (1988).

AvizoLite 2020 was also used to delineate the whole-brain surface and several neural structures within the brain from the diceCT dataset. The whole brain was 3D rendered from the background and surrounding tissues based on differences in grayscale contrast afforded by iodine staining. Likewise, the right eye and internal neuroanatomical features were segmented based on differences in the intensity of iodine staining between gray and white matter (see Gignac and Kley, 2018; Gignac et al., 2021). For segmentation in our histochemical series, manual registration was performed for both the brain surface and neural structures of the tectofugal pathway. Divisions of several of these structures were segmented based on cell and fiber density. Segmentation of each structure was performed in both the coronal and sagittal planes.

For segmentation in our histochemical series, serial histochemical sections were stacked to produce 3D volumes of tectofugal structures, fiber tracts, and commissures. Manual registration of histological slice was performed in Brainmaker (MBF Biosciences, Williston, VT). Neuroanatomical structures and their divisions were then segmented using Brainmaker, based on cell and fiber density.

All 3D models from diceCT and histological samples were exported as surface files (.obj and .stl format). These files were then imported into the image, surface and volumetric visualization and editor tool, Blender (Blender Foundation, Amsterdam, Netherlands), to create a complete representation of the tectofugal visual system.

For spatial alignment of all digital models, 2D histology images were imported into Blender. We first used a midline sagittal section, isometrically scaled, to match the 3D brain surface in size and orientation. Coronal stereotaxic atlas images were also imported, isometrically scaled,

and aligned with these so that they crossed through the midline sagittal section at their respective atlas coordinates from Kuenzel and Masson (1988) (see Fig. 3.2). The surfaces of 3D diceCT and histology-based neuroanatomical structures were then manually aligned to this comprehensive, spatial framework. Development between these temporally similar stages is essentially isometric (Kawabe et al., 2017; Watanabe et al., 2018).

3.3.5 Figure Preparation

Orientations of the brain and the resulting tectofugal neural structures and fibers for figures 3.1–3.12 were chosen to best illustrate as many structures as possible within their appropriate location of the eye and brain. Anatomical 3D reconstructions were captured using the snipping tool software from Windows (version 10.2008.2277.0, Microsoft Corp., Redmont, WA, USA). To enhance the visibility of our static figures, we removed the inherent grey background of the Blender environment, replacing it with higher contrast black. To do this, selected images were imported into GIMP 2.10.30. Using the color selection and crop tools, the grey background was removed and replaced with a transparent background. The smudge tool was used to fix any images or information mistakenly cropped due to the pixels having similar grayscale values to the background that was removed. Images were exported from GIMP as PNG files and imported into PowerPoint. Here, images were placed on a uniform black background to easily distinguish the semitransparent brain surface and solid neural structures and fibers underneath. Similarly, a series of Gallyas Silver and diceCT brain sections from sagittal and coronal sets were selected for figures 3.5 and 3.6. Images were first selected due to their visualization of key tectofugal structures and then paired to respective diceCT images. For the diceCT sections, we chose to upsample images for the sole purpose of figure clarity, using TopazLabs (Dallas, TX, USA) Gigapixel AI image enhancement software. The process of upsampling 2D diceCT images,

which are captured in 16-bit grayscale values ranging from 0–65,535, subdivides each pixel into several smaller subpixels. Gigapixel AI machine learning algorithms interpret the grayscale values of each target pixel along with the surrounding pixels to interpolate a grayscale value for each new subpixel. This enables, for example, a square image that is 100 x 100 pixels to become a 600 x 600 pixel image, showing the same visualization, but with higher interpolated spatial detail. The use of thousands of image datasets to train Gigapixel AI machine learning algorithm also enables the software to scale noise, blur, and luminance to maintain image quality comparable to the original image. Effectively, this process improves image viewability by zooming into 2D images beyond the spatial detail provided by the original detector hardware and helical reconstruction process (e.g., for computed tomography), but with minimal visual artifacts.

3.3.6 Terminology

For neural structures we primarily used the terminology from the atlases of Kuenzel and Masson (1988) and Puelles (2019). For many of the forebrain regions, we adopted the nomenclature of Reiner et al. (2004). Furthermore, we named subdivisions of the entopallium and rotundus by referencing nomenclature from Krutzfeldt and Wild (2004,2005) and Benowitz and Karten (1976) respectively.

3.4 Results

In this section, we describe the neuroanatomy of the chicken tectofugal system following the direction of information flow, starting from the retina. This circuit is comprised of 3 primary neuron projections. The first being the retinal ganglion cells whose soma reside in the ganglion cell layer of the retina. The RGCs receive input from bipolar cells and send axons out of the back of the eyeball forming the optic nerve. These axons decussate through the optic tract and move

toward the contralateral optic tectum where they synapse in the superficial tectal layers 2-7. The second primary projection arises from TGC classes whose soma reside in layer 13 of the optic tectum. The dendrites of these TGCs project up into the intermediate and superficial layers, synapsing on the RGC terminals. The TGCs will send axons toward the midbrain via the tectothalamic tract where they will course rostral and medial to synapse within the nucleus rotundus. The final primary projection arises from the cells of the rotundus. The rotundal cells receive direct and indirect bilateral input from the terminals of TGCs and will project dorsally using the lateral forebrain bundle where they will synapse within the entopallium, the terminal structure of the tectofugal pathway.

3.4.1 Retina

Visual sensory processing in birds begins in the retina, a five-layered structure with several unique types of cells. The layers of the retina consist of the ganglion cell layer, the inner and outer plexiform layers, and the inner and outer nuclear layers. Avian retinae have at least 6 classes of photoreceptors (chicken: Prada et al., 2008; Kram et al., 2010; Okano, 1992; pigeon: Bowmaker, 1977; goose: Fernandez et al., 2012; starling: Cuthill et al., 1998; blue tit: Bennett et al., 2000; zebra finch: Bowmaker et al., 1997; emu: Hart et al., 2016; however, see Tyrell et al., 2019) which selectively respond to visual stimuli. These photoreceptors are distributed in a regular mosaic-like pattern in the retina and consist of four spectrally different single cones, double cones, and rods (Kram et al., 2010). Photoreceptors pass electrical signals to bipolar cells that propagate these signals to different classes of retinal ganglion cells (Naito and Chen, 2004). Retinal ganglion cells (RGCs) have been classified based upon dendritic morphology (Naito and Chen, 1999, 2004), soma size (Ito et al., 1986; Hayes and Holden, 1980), neurotransmitters (Calaza et al., 2009; Karten et al., 1988,) and recently single cell profiling

(Sanes et al., 2020). With respect to the tectofugal system, small retinal ganglion cells project to the optic tectum. Axons of RGCs leave the back of the eye as the optic nerve and decussate in the optic chiasma where nearly 90% of RGCs will synapse in the superficial layers of the optic tectum in a retinotopic fashion (Mpodozis et al., 1997). Many studies have sought to describe the retinotopic map of the superficial tectum (Wylie et al., 2009; Mpodozis et al., 2004; Hamdi and Whitteridge, 1954; Clarke and Whitteridge, 1976; Cowan et al., 1966); however, there is much disparity among them. We sought to clarify this issue by utilizing 3D methods to overlay the retinotopic map upon the tectum. Using the retinal bundles of fibers found from the diceCT data rendering and our interpretations of the literature, we mapped the retinotopy in Fig 3.3. Here we show a sagittal view of the eyeball and brain as it would exist in a stereotaxic instrument and the theorized quadrant divisions of the retina projecting to the respective regions of the optic tectum.

3.4.2 Optic Tectum

The optic tectum (TeO) is a relatively large and highly laminated structure at the lateral expanse of the avian brain. There are 15 layers, each unique with its own connections, neurotransmitters, cell morphology, and functions (Tombol et al., 2002; Hardy et al., 1985; Veenman and Reiner, 1994; Medina and Reiner, 1994). Retinal ganglion cells as described in section **3.4.1 Retina** synapse in the superficial layers 2–7 with most retinal terminals synapsing in layers 3, 5 and 7 (Reperant and Angaut, 1977; Tombol et al., 2002; Karten et al., 1988). Here retinal terminals make monosynaptic and polysynaptic connections with the unique dendritic arbors of several classes of cells whose soma reside in layer 13. The neurons of layer 13 that synapse with retinal ganglion terminals have been named tectal ganglion cells (TGCs; Mpodozis et al., 2003). To date, three classes of TGCs have been well described in both the chicken and

pigeon, with two additional classes of TGCs also described in the pigeon (Karten et al 1998, Mpodozis et al., 1997; Hellmann and Gunturken, 2001). Tectal ganglion cell classes seem to be unique in their connectivity, dendritic morphology, and their potential function. For example, TGC class I neurons have unique bottlebrush dendrites that reach up to layer 5b and synapse with small retinal ganglion cells (Luksch et al., 1998). Layer 13 seems to contain sub-laminae in which different classes of TGCs reside in a highly organized manner (Deng and Rogers, 1998; Fukuta et al., 2003; Karten et al., 1997; Hellmann and Gunturken, 2001). Alternatively, some suggest that the organization of layer 13 is mosaic-like, presenting a mix of TGC classes rather than highly organized sublaminae (Manns et al., 2004). Apart from the anatomy, an extensive amount of research has found that cells of layer 13 play functional roles in stimulus selection, spatial attention, and simple visual characteristic processing (Karten et al., 1998; Wang et al., 2005; Clark et al., 2009; Morgan et al., 1987; DiFranco and Frost, 1976; Sun and Frost, 1997; Wessel et al., 2001; Marin et al., 2018). At the level of the tectum, the retinotopic map seems to translate to a functionotopic map in which different classes of TGCs will project to specific functional domains of the thalamic nucleus rotundus via the tectothalamic tract (ttt). In figure 3.10, we demonstrate the projection of bundles of axons from layer 13 through the ttt where they enter the rotundus at its caudal aspect.

Avian Midbrain

3.4.3 Rotundus

The thalamus is an important relay station in the dorsal diencephalon, and the nucleus rotundus (Rt) is the largest nucleus within the thalamus. It receives substantial input, directly and indirectly, from the optic tectum. Deng and Rogers (1998) et al has shown that TGCs projecting to the Rt can be grouped into those that project ipsilaterally, contralaterally, or bilaterally. We

demonstrate both the direct connections and indirect connections of the tectorotundal pathway in figure 3.10D,G, and H. Collaterals of TGCs split from axons in the ttt and project either to the ipsilateral SP/ISPT complex, ipsilateral pretectal nucleus, or contralateral ROT. The rotundus has been subdivided into as few as three, and as many as seven, functional regions on the basis of tract tracing (Benowitz and Karten, 1976), cadherin expression (Becker and Redies, 2003), acetylcholinesterase staining (Martinez et al., 1990), functionality (Wang et al 1992), and cell and fiber density. Karten et al (1976) was the first to subdivide the nucleus rotundus into five subdivisions (Da, Am, M, V, P) on the basis of tract tracing in the pigeon. However, recent tract tracing studies have reduced these subdivisions to three (Da, Ce, P; Mpodozis et al., 2010). Martinez et al., (1990) used differential acetylcholinesterase staining and divided the chicken ROT into six divisions (Ram, Rvl, Ri, Rpm, Rpl, Rf). Wang et al., (1992) used several types of visual stimuli to subdivide the rotundus into functional domains that favor processing either 2D motion, looming, luminance, or color.

We attempted to divide the chicken ROT into subdivisions based on cell and fiber density using coronal and sagittal series of Nissl and Gallyas stained sections. Figure 3.3 illustrates our rotundal divisions in 3D (left hemisphere) mirrored by a non-divided rotundus (right hemisphere). We delineated the rotundus into four subdivisions as follows: ventral (ROTv, green), dorsal (ROTd, blue), intermediate (ROTi, red), and lateral posterior (ROTlp, pink). Our ventral division contained the most fibers and seemed to have a higher number of cells compared to the intermediate and lateral posterior divisions. The ventral subdivision spanned the rostrocaudal expanse of the rotundus and disappeared toward the final 200 microns of the posterior end of the rotundus. The dorsal anterior division could be delineated from the triangularis (T), the dorso-medial extension of the rotundus that can be identified by its small,

densely packed cells. The dorsal anterior subdivision was more densely packed than the intermediate and posterior subdivisions and there seemed to be a change in cell density between the ROTd and ROTi subdivisions. The lateral posterior division was characterized by a lower number of fibers and a sparse number of cells at its anterior portion as well as by a dense fiber plexus at its posterior end. The intermediate division was characterized by fewer fibers than ROTv and ROTd. Our subdivisions were named with respect to Karten's subdivisions (1976) with our lateral posterior nucleus interpreted as homologous to his posterior subdivision. Additionally, our ROTv and ROTi subdivisions together would compare to the central rotundal subdivision described by Marin et al (2010).

3.4.4 Isthmic Nuclei

The isthmic nuclei consist of the Imc, Ipc, ION, and SLu. However only the Imc, Ipc and SLu are considered a part of the tectofugal system. These nuclei are situated in the caudal mesencephalon, and each differs in cell morphology, connectivity, and functionality.

The parvocellular isthmic nucleus, Ipc, receives topographic visual input from Shepherd crook neurons of layer 10 of the optic tectum (Karten et al., 2006; Cuenod et al., 1977; Karten et al., 1991). The Ipc feeds back on the optic tectum with reciprocal, homotopic projections. These Ipc projections have been shown to modulate optic information transfer at the level of the rotundus, and entopallium (Letelier et al., 2012). The Ipc does this via its reciprocal, columnar paintbrush-like terminals that synapse throughout layers 2–10 of the tectum where visual input is provided. The Ipc selectively directs the retinal input and is likely to be mediated by glutamate (Marin et al., 2016). We rendered the Ipc in both coronal and sagittal Nissl and Gallyas series (Fig 3.9F and 3.10F–K), and it is easily discernible in the diceCT sets (Fig 3.6G–H) because the Ipc is a

gray-matter structure surrounded by higher contrast fibers. We illustrate its reciprocal homotopic projections with the tectum as well as the efferent projections of the Imc to Ipc.

The magnocellular isthmic nucleus, Imc, receives roughly topographic input from Shepherd crook neurons of layer 10 of the optic tectum (Karten et al., 2004). There are two types of neurons found intermingled within the Imc and are classified based on their projections. The Imc-Te neurons feedback upon the intermediate layers of the tectum in a heterotopic manner and provide a modulation of visual input via GABA (Wang et al., 2004). Imc-Is neurons project to both the Ipc and SLu via the intraisthmic tract (iit) (Wang et al., 2004). It has been proposed that Imc provides an inhibitory function at both the level of the tectum and the level of the Ipc and SLu with the latter likely focusing the Ipc feedback for spatial attention and stimulus selection in the superficial tectum. Here we have rendered the Imc in both sagittal and coronal sets of histochemical stains (Figs 3.9f and 3.10F–K). This nucleus, like its counterpart the Ipc, is also readily discernible in the diceCT dataset (Fig 3.6G–H).

The semilunar nucleus, SLu, receives topographic visual input from Shepherd crook neurons of layer 10 of the optic tectum (Hellmann et al., 2001). The SLu feeds back onto the intermediate and deep layers of the tectum in a homotopic manner similar to the Ipc. Additionally, SLu has several extratectal projections including those to the lateral spiriform nucleus (SpL), and the ipsilateral and contralateral nucleus rotundus (ROT) (Hellmann et al., 2001). The SLu therefore acts as an indirect projection of the tectum onto the rotundus. Hellman et al. (2001) have hypothesized that the SLu may act as a system for visuomotor integration via its connections to the tectum and rotundus governing retinal input and its connections to the SpL modulating descending input from the tectum. The SLu is easily discernible in both Nissl and Gallyas stained series in which we reconstructed this nucleus (Figs. 3.9F and 3.10F–K).

The isthmo-optic nucleus, ION, makes up the centrifugal pathway in which dendrites of ION neurons receive input from neurons of layers 9 and 10 of the optic tectum (Reiner and Karten, 1991; Miceli et al., 1999). The ION neurons then project via the isthmo-optic tract (iot) to the contralateral retina and terminate within the ventral half of the retina in which they synapse on amacrine cells (Uchiyama et al., 2004). Though there is a substantial amount of literature investigating the ION, its complete functional role has yet to be revealed but has been hypothesized to involve retinal stabilization during gaze, behavioral attention, or increased selectivity to novel stimuli (Miceli et al., 1999; Uchiyama et al., 2022; Pearlman and Hughes, 1976; Uchiyama et al., 2012; Ibanez et al., 2012). The ION is easily visualized in the Gallyas sets as it is surrounded by a dense fiber plexus and was reconstructed based on cells within the plexus (Figs 3.9H and 3.10H–K).

3.4.5 Pretectal, Subpretectal, and Intermediate-Pretectal-Subpretectal Nuclei

The pretectal nucleus (PT), sits dorsal and caudal to the rotundus and receives excitatory collateral input from layer 13 neurons in the tectum (Gamlin et al., 1996). The PT sends axons carrying reciprocal inhibitory signals to the SP/ISPT complex as well as inhibitory projections to layer 5b of the optic tectum (Gamlin et al., 1996). The functional significance of the projections from PT to the TeO remains unclear, but studies in frogs have shown that the PT plays a role in item selection during feeding behavior and avoidance behaviors (Gamlin et al., 1996). Therefore, the avian PT may function similarly by modulating visuomotor behaviors. The PT was readily identified in all datasets and could be separated into its core and shell components (Figs 3.9H, 3.10H–K, and 3.6I).

The subpretectal and intermediate subpretectal (SP/ISPT) complex is located caudally to the nucleus rotundus and receives excitatory collateral projections from classes of TGCs. The

SP/ISPT complex then sends inhibitory projections to the ROT thereby constituting an indirect circuit between the TeO and ROT. The SP/ISPT complex also maintains reciprocal inhibitory connections with the pretectal nucleus via the pretectal-subpretectal tract (pspt) (Theiss et al., 2003). The SP/ISPT complex has been implicated in bilateral visual integration as well as figure-ground segregation dependent on static cues (Acerbo et al., 2012). Due to the immense number of fibers running through these nuclei, it was difficult to isolate the full extent of this complex within the sagittal series; however, it was possible to delineate within the coronal Gallyas series. The SP maintains a round to oval shape with the ISPT capping it dorsally in a triangular fashion. The SP is detectable in diceCT after manual manipulation of brightness and contrast, whereas the ISPT was not easily detected (Fig 3.5I and 3.6I).

Avian Forebrain

3.4.6 Entopallium

The entopallium is the primary visual center of the dorsal ventricular ridge. It receives numerous projections from the ipsilateral rotundus via the lateral forebrain bundle. Based on molecular markers and connectivity, the entopallium is the proposed homolog of layer 4 of the neocortex in mammals (Krutzfeldt and Wild, 2005). This nucleus is readily identifiable in a Nissl and Gallyas stain and can be divided into a core and shell. Manipulating brightness, contrast, and gamma correction, we can identify the entopallium within the diceCT dataset. However, the border was not obvious in some sections. The entopallium, like the rotundus, can be subdivided based on tract tracings, functionality, differential histochemical staining, cell, and fiber density. Projections maintain their rostrocaudal topography from the rotundus onto the entopallium. The anterior half of the entopallium seems to preferentially process color and luminance stimuli whereas the posterior entopallium processes 2D and looming motion (Xiao et al., 2006; Cook et

al., 2013; Nguyen et al., 2004). However, Krutzfeldt and Wild (2004, 2005) divided the entopallium into dorsoventrally oriented divisions on the basis of cell density in wet mounts, tract tracing, and parvalbumin and cytochrome oxidase staining. From this work, they divide the entopallium into three divisions: Ex, Ei, and Eb.

We attempted to divide the chicken entopallium into subdivisions on the basis of cell and fiber density using coronal and sagittal series of Nissl and Gallyas stained sections. We find that the ventral entopallium contains a high density of fibers (Figs 3.5A and 3.6A–B) and has more densely packed cells. We divided our entopallium into three divisions comparable to those in the reports of Krutzfeldt and Wild: Ee, Ei, and Eb. Our Ei and Eb were named following homologous subdivisions of Krutzfeldt and Wild, while our Ee corresponds to their Ex. These divisions were identified in both sagittal and coronal Nissl and Gallyas series; however, no subdivisions could be made out in the diceCT set (Figs 3.5G and 3.6G-H).

3.4.7 Nidopallium

The visual nidopallium can be divided into four regions: the intermediate nidopallium (NI), the frontolateral nidopallium (NFL), the intermediolateral nidopallium (NIL), and the caudolateral nidopallium (NCL). These four areas are considered higher visually associative regions.

The NI lies dorsal to the entopallium and ventral to the mesopallial lamina. It acts as a relay station for the other visual associative areas. Due to its intra-telencephalic connectivity, the NI has been likened to layers 2/3 of the neocortex (Fernandez et al., 2019). The NI receives input from the entopallial belt and has reciprocal connections with ventrolateral mesopallium (MVL) (Fernandez et al., 2019; Stacho et al., 2020). The NI is major source of projections to the NFL, NIL, and NCL and has been hypothesized to have intermingled populations of unique classes of

cells that project to specific lateral regions of the nidopallium (Fernandez et al., 2019). It receives feedback projections from all three lateral nidopallial regions. We distinguished the NI based on its dorsal and ventral borders, the mesopallial lamina and entopallium, respectively. We confined the lateromedial extent of the NI to be similar to that of the entopallium. Reconstruction of the NI was done in both sagittal and coronal Gallyas series (Figs 3.9I and 3.10I–K).

The NFL, the most rostral division of the lateral nidopallium, maintains a spherical shape and a rostral and lateral position to the entopallium. It receives a major projection from the NI, as well as projects back to the NI (Fernandez et al., 2019). Additionally, NFL sends projections to the NCL, arcopallium (ARP), lateral striatum (LSt), hyperpallium apical (HA) and amygdala (Sadananda and Bischof, 2006). The NFL has been implicated in several complex functions including extinction learning and context encoding (Gao et al., 2019). We rendered the NFL using a series of coronal Gallyas brain sections and compared them with those provided in the literature (Atoji and Wild, 2012; Fernandez et al., 2019).

The NIL, the intermediate division of the lateral nidopallium, maintains a concave shape, bordered by the entopallium medially and the brain surface laterally. It is confined between the caudal end of the NFL and wraps the entopallium caudally. NIL receives a major projection from the NI, and other afferents from NCL, NFL, and interestingly the subrotundus in the thalamus (Sadananda and Bischof, 2006, Fernandez et al., 2019). This projection from the subrotundus to the NIL represents interaction of the thalamofugal and tectofugal system, which potentially suggests modulation of tectofugal information by the thalamofugal system. We delineated the NIL using the atlases of Kuenzel and Masson (1988) our interpretation of the literature (Alpar and Tombol, 2000; Atoji and Wild, 2012; Fernandez et al., 2019) and rendered the NIL using the coronal Gallyas series (Fig 3.9J and 3.10J–K).

The NCL, the caudal portion of the lateral nidopallium, sits caudal to the NIL and has been a proposed homolog of the mammalian prefrontal cortex on the basis of connectivity, dopaminergic innervation, and that it is a multisensory convergence domain (Hartmann and Gunturken 1998, Hsiao et al 2020, Fernandez et al 2019). The NCL has functional significance in color perception, reversal learning, and selection/execution of perceptual responses (Hartmann and Gunturken 1998, Lengersdorf et al 2014, Hsiao et al 2020). The NCL is often paired with the temporo-parieto-occipital area (TPO) as it is difficult to distinguish between the two in our Gallyas stained series. Using atlases and comparable sections from the literature (Fernandez et al 2019, Hartmann and Gunturken 1998, Fernandez et al 2019), we attempted to define the NCL using the coronal series of Gallyas stained sections (Figs 3.9J and 3.10J–K).

3.4.8 Mesopallium

The mesopallium sits dorsal the nidopallium and is clearly separated by the mesopallial lamina. The visually sensitive mesopallium is limited to the ventrolateral (MVL) region and has a distinct ovoid shape (Krutzfeldt and Wild, 2004, 2005). The MVL has reciprocal projections with the NFL, intermediate arcopallium, NIL and entopallium and additionally, the suprarotundus (SpROT) and DLL which are nuclei of the thalamofugal system (Atoji and Wild, 2012; Krutzfeldt and Wild, 2005; Ahumada et al., 2015). The connection of the MVL with the SpROT and DLL is interesting as it represents a point of crosstalk between the tectofugal and thalamofugal systems. Several functional studies have described the MVL as being involved in processing characteristics of moving and static stimuli to a greater capacity than the entopallium and is likely to be involved in processing specifically local feature characteristics (Clark et al., 2022; Stacho et al., 2016; Azizi et al., 2019; Anderson et al., 2020). The MVL is distinguishable

in the coronal Gallyas set as it maintains a comparable ovoid shape with an elongated tail flanking medially (Figs 3.9I and 3.10I–K).

3.4.9 Arcopallium

The arcopallium can be divided into visual, auditory, and trigeminal sensory regions with neurons responding to visual stimuli residing in the intermediate arcopallium (AI) and to a lesser extent the dorsal arcopallium (Scarf et al., 2016). AI receives input directly from the NI and indirectly from the NI via the NCL (Fernandez et al., 2019, Husband and Shimizu, 1999). AI represents the beginning of descending projections to modulate visuomotor behavior. The visual arcopallium, using the occipitomesencephalic tract (omt/vaf), projects to the deep layers of the optic tectum with densest terminations in layer 13 (Dubbledam et al., 1997; Manns et al., 2007; Fernandez et al., 2019). Additionally, the visual arcopallium projects to the superficial parvocellular nucleus (SPC/nTSM) and subrotundus (SROT), both involved in the thalamofugal visual system. The function of the visual arcopallium is still debated, however, it is hypothesized that it performs top-down modulation of ascending sensory input via direct or indirect connections to TGCs or Shepherd's crook neurons, respectively (Fernandez et al., 2019). We delineated and rendered the intermediate ventral and dorsal arcopallium together (AId and AIv) as they were easily distinguishable in the coronal series of Gallyas stained sections (Figs 3.9K and 3.10K).

3.4.10 Fiber Tracts, Decussations and Commissures

Based on the Gallyas fiber staining of sections and intense labeling of myelinated fibers in the diceCT protocol, we reconstructed various fiber projections, commissures, tracts, and decussations utilized by the tectofugal system. Afferent and efferent connections of each structure were manually traced (with a few exceptions) and rendered in 3D. These renderings

were replaced by uniformly smooth projections that mimicked the natural paths axons would take to move from one structure to another. Fig 3.11 shows the rendered fibers alone within the semitransparent brain. Fiber thickness was also manipulated in an attempt to represent major and minor efferent and afferent projections.

3.5 Discussion

In the present study, we utilized diceCT and a series of Gallyas silver-stained brain sections to 3D reconstruct a comprehensive atlas of the avian tectofugal pathway. We identified and bilaterally reconstructed 18 tectofugal structures, subdivided the rotundus into four divisions, subdivided the entopallium into three divisions, and illustrated the many tracts, commissures, and decussations utilized by this visual system. By combining the emerging technique, diceCT, with traditional histochemistry, we were able to visualize better the tectofugal system at the 3D whole-brain level.

3.5.1 Tectofugal System

We investigated the three-dimensional (3D) structure, connectivity, and spatial organization of the tectofugal pathway using several imaging techniques. The tectofugal pathway begins with the photoreceptors of the retina responding to stimuli with differential characteristics in the visual field (Fig 3.1). These photoreceptors create electrical and chemical signals that are passed onto bipolar cells. Bipolar cells propagate these signals to different classes of retinal ganglion cells whose axons form the optic nerve that project to the superficial layers of the contralateral optic tectum as shown in Fig 3.3. We describe this retinotopic transformation from the retina to the tectum using the quadrant theory. We placed the vertical retinal dividing line just superior and nasal to the head of the optic nerve, intersecting the central foveal-like area described in the chicken (Morris, 1982). We then produced a horizontal orthogonal line that passed just above the

head of the optic nerve through the central fovea. Together, these lines create the often-utilized quadrant theory of the retina. We then recreated the quadrant theory on the tectum with respect to the orientation of the retina. Many studies often do not describe the orientation of the eye and the tectum with respect to each other and this has caused disparity among results. Our model addresses this issue by accounting for the orient relationship and providing an overlay of the quadrant theory on both the right retina and left superficial tectum.

The terminals of the retinal ganglion cells are unique in their morphology, connectivity, and the layer where they synapse within the optic tectum. Reperant and Angaut (1977) described five potential classes of retinal ganglion cell (RGC) types whose terminals were differentially classified depending on their terminal field size, shape, and layer where they occurred. These terminals create monosynaptic and polysynaptic connections with the unique dendritic profile of each type of tectal ganglion cell (TGC) found within layer 13. Similar to the RGC terminations, the dendrites of these TGCs vary in dendritic field shape, size, and layer of the optic tectum where a particular synapse occurred. A single TGC dendritic field of any of the three classes can cover over a millimeter of the superficial optic tectum and possess unique brush-like terminal branches (Luksch et al., 1998; Karten et al., 1997). For example, TGC class 1 is thought to be involved in motion detection (Luksch et al., 1998; Hellmann and Gunturken, 2001; Dellen et al., 2010; Sun and Frost,1997) and have an average dendritic field width of 1.5 mm. The unique synaptic connections of the RGC terminals and the TGC dendrites potentially demarcate the transition from a retinotopic to functionotopic organization of parallel streams of visual processing. These streams may potentially begin at the level of the retina as different classes of RGCs. As mentioned above, the Type I TGC, Type II TGC, and Type III TGC form monosynaptic or polysynaptic connections with type 1, type 2, and type 3 retinal terminal classes

respectively (Karten et al., 1997; Reperant and Angaut, 1976). Although several studies have determined several types of RGCs, research is lacking in determining which subclass of RGC produces the respective retinal terminal type and the distribution of these classes within the retina. This would mirror the parallel streams of processing seen in mammals with different classes of RGC's producing different pathways for visual processing (e.g. small bistratified RGCs producing the koniocellular pathway or midget RGCs producing the parvocellular pathway, Kim et al., 2021). The TGC subclasses then transmit the retinal information directly and indirectly to the large thalamic nucleus rotundus.

The rotundus has been divided into three to seven subdivisions whose number and structure depend on the methods used to divide this nucleus. We attempted to divide the rotundus into four subdivisions based on cell and fiber density as shown in Figure 3.7. There is much overlap between our subdivisions and those of studies using differential staining, tract tracing, and electrophysiology (Martinez-de-la-Torre et al., 1990; Fredes et al., 2010; Gao et al., 1995; Wang et al., 1993; Becker and Redies 2003). For example, our intermediate and ventral subdivisions correspond to the medial and ventral divisions of Benowitz and Karten (1976) and together correspond to the central division of Fredes et al., (2010; see Fig 3.4). The differences in the number and structure of these subdivisions are due to the methods used, the species, and age. Each of these subdivisions seem to receive major input from a single class of TGCs, thereby solidifying the functionotopic organization. Type I TGC seems to primarily project to the ventral and intermediate subdivisions of the rotundus, whereas type II TGC seems to primarily project to the dorsomedial triangularis. Other proposed classes of TGC, such as TGC types IV and V project to dorsal and lateral posterior subdivision respectively (Karten et al., 1997; Hellmann and Gunturken, 2001; Hu et al., 2003; Deng and Rogers, 1998). The rotundal neurons roughly

maintain their relative topography as they project to the entopallium (Fredes et al., 2010; Shimizu et al., 2010). The entopallium has also been divided into two to three subdivisions based on tract tracing, differential histochemical staining, electrophysiology, and cell density (Krutzfeldt and Wild, 2004,2005; Ahumada et al., 2015; Suarez et al., 2005; Cook et al., 2013). Many of these studies show different results with some utilizing an anterior-posterior partitioning or a dorsal-ventral partitioning of the entopallium. Very few functional studies, using a limited number of species, have been performed to undoubtedly determine if the entopallium maintains the functional divisions shown in the rotundus. The studies that have attempted to delineate functional entopallial domains often sampled from few areas of the entopallium and do not describe in detail where they are taking cell recordings (Patton et al., 2013; Nguyen et al., 2004; Xiao et al., 2006). This prompts the need for more detailed functional studies utilizing more species, preferably over a range of orders to undoubtedly determine the functional domains of the entopallium

Beyond the entopallium, there is a limited number of studies investigating the mesopallium and specific nidopallial areas associated with vision. The projections of the entopallium to the nidopallium and mesopallium retain their topography, but functional studies have not shown functional domains in either of these higher associative areas. For example, the intermediate nidopallium is composed of a mosaic of different cell types projecting to either the NFL, NIL, or NCL (Fernandez et al., 2019). Many sub-divisions of the nidopallium and mesopallium lack a plethora of research and require further investigations to understand their complete boundaries, structural organization, cell morphology, transmitters, and functionality.

3.5.2 General considerations

DiceCT has been utilized to study many aspects of vertebrates. With respect to birds, diceCT has been used to study the feeding apparatus (Genbrugge et al., 2011; Li and Clarke, 2016), cranial musculoskeletal anatomy (Lautenschlager et al., 2014; To et al., 2021; Hadden et al., 2021; Jones et al., 2019), forelimb musculoskeletal anatomy (Contreras and Sellers, 2017), vocal organs (During et al., 2013), brain ontogeny and function (Gold et al., 2016; Watanabe et al., 2019), and craniofacial pathology (Gignac et al., 2021). DiceCT has many advantages for anatomical investigations compared to traditional and other 3D techniques including cost, ease of access, non-destructiveness and reversible nature, and high-precision visualization of soft tissues (Gignac et al., 2016). These attributes provide diceCT an advantage for comparative studies of avian anatomy and neuroanatomy over other, more traditional approaches. The accessibility of contrast-enhanced imaging tools such as diceCT have given researchers a new way of studying complex morphology without the use of destructive dissection. DiceCT permitted us to produce a highly detailed, comprehensive model of the tectofugal visual pathway that is easily shareable and changeable, allowing future researchers to modify and build upon our work as additional discoveries occur.

Brainmaker was utilized to generate stacks of serial immunocytochemical brain sections in both sagittal and coronal planes to generate 3D volumes of the tectofugal structures. This software program allows users to import a series of brain sections and will automatically place contours or outlines around the brain section. There are a few issues that may prevent or distort these automatic contours including artificial objects in the background, tearing of brain tissue, shifts in the regions of the brain, and diffuse staining in the background surrounding the brain section. The program will also semi-automatically align brain sections using center of the image,

the shape of the image, or the shape of the image and image features. Often users will have to perform additional manual corrections to the alignment of the series of brain sections. The reason for manual corrections is that some sections may have shifted or rotated slightly prior to imaging. After alignment, users will then create a reconstruction of the brain surface from the automatic contours. This program allows for further segmentation through manual contours of areas of interest within the brain sections. The quality of the reconstructions depends on several factors: number of sections in the complete series, distance between brain sections, consistency of number of sections, number of manual contours per area of interest, smoothness of manually drawn contours, and the alignment condition of the series. To generate better models by reducing the issues described above, we recommend the following: (1) Use a complete consistent series of brain sections, (2) use brain sections that are ≤ 50 microns, (3) mount sections as carefully as possible to prevent unnecessary shifts and rotations, (4) when aligning, try to select one or more structures that can act as reference points throughout the series (i.e. third ventricle), and (5) use more vertices when producing manual contours.

Data from both diceCT and histochemical sections were combined in the Blender software. This was accomplished by using several atlas images (Kuenzel and Masson 1988) as references for the alignment of the diceCT endocast and serial ICC reconstructions. We began by setting up the atlas plates to the grid within Blender to ensure there were no odd rotations or scaling issues. Next, we integrated the diceCT whole brain surface reconstruction by scaling and orienting the model to meet the general brain surface outline of the midline sagittal atlas plate. This initial alignment of the whole brain model is important for setting the foundation for the alignment of internal tectofugal structures. To ensure proper orientation and scaling of the segmented tectofugal structures, we first aligned the optic tectum—a large and three-dimensionally complex

feature of the tectofugal system. Using the tectum as a reference, we were able to incorporate the remaining tectofugal structures with accurate relative location, size, and orientation. To ensure this accuracy, we aligned several coronal atlas plates that intersected the midline sagittal plate at their respective coordinates and observed the overlap of tectofugal structures. We found substantial overlap of the reconstructed tectofugal structures and the outline of these structures in the 2D atlas plates. However, we observed a slight lateral bias in a few tectofugal structures, likely due to age differences (i.e. images derived from a two-week old bird versus a five-week-old bird) even with isometric scaling (see Methods section 2.4). For future studies using these methods we would recommend the following: (1) utilize atlas plates to determine correct orientation, scaling, and combination of models, (2) use one or more structures that makes up a portion of the whole brain surface to act as a reference for scaling and orientation of other structures (e.g. optic chiasm and tectum, or vallecula and superficial hyperpallium), and (3) understand how to use the maneuvering mechanics, hide/unhide function, viewport shading tools, and select/unselect tool prior to using Blender. The Blender software provides an excellent means of combining, viewing and interacting with 3D models. Users can interact with our model at varying levels, being able to rotate, orient, scale and view the whole tectofugal system as well as isolate and study components of this system.

3.5.3 The use of 3D modeling for research and education

Neuroanatomy has traditionally been studied using various 2D illustrations, predefined brain sections, and atlases. With the improvement of imaging techniques and visualization software, many 3D brain atlases and models have been created to further enhance the understanding of the structure and function of the brain. Several highly detailed mammalian atlases have been produced such as the brain atlas of the marmoset (Liu et al., 2018), human (Huo et al., 2019), and

mouse (Wang et al., 2020) and are utilized in both research and education. 3D models and atlases have also gained attention in avian species. For example, the Bio-Imaging Lab at the University of Antwerp has created 3D atlases for the zebra finch (i.e. structures of song control, auditory and visual nuclei), starling (i.e. parts of sensory systems and song system), canary (i.e. song perception, learning, and production), and pigeon (i.e. various components of sensory and motor systems) (Gunturken et al., 2012; De Groof et al., 2015; Vellema et al., 2011; Poirier et al., 2008). These 3D media and others alike are indispensable resources that have opened new avenues of research in various fields such as neuroanatomy, neurophysiology, evolutionary biology, and developmental biology. Pertaining to our model, it will allow users to find the best orientation and coordinates to use for placement of tract tracer injections and microelectrodes, readily identify visual structures from any point of view, and determine optimal sectioning for experiments.

Apart from research, 3D models offer students additional information on the spatial organization, connectivity, and functional relationships that traditional 2D media cannot portray. Much research has been undertaken to determine the usefulness of 3D models in anatomical education. Most of these studies determine 3D modeling usefulness using two criteria: student preference and student examination performance. Many studies (Oktem et al., 2019; Park et al., 2018; Hoyek et al., 2014) have shown that 3D media improves students' understanding of anatomical organization and performance on quizzes and exams compared to 2D images and drawings. Oktem et al., (2019), for example, found that students performed significantly better on quizzes over segmentations of the thyroid gland, trachea, and common carotid artery after having been exposed to 3D model training. Park et al., (2018) found that students studying 3D material performed better on open-book simple questions compared to students who only utilized

2D illustrations. Additionally, Hoyek et al., (2014) found that students receiving 3D material to study had significantly improved scores on questions utilizing spatial ability whereas there were no differences on general knowledge questions between students receiving 2D or 3D material. The consensus (although see Roach et al., 2012 for contradictory findings) seems to be that 3D models and atlases often produce equivalent or better results than 2D representations. Currently, 3D models aim to be more of a supplementary resource rather than replacing 2D material altogether. We suggest that when combined, both modalities together provide synergy, with an explanatory capacity that is greater than the sum of their parts.

3.5.4 Future Directions

Pairing diceCT and traditional anatomical methods has allowed for a new avenue of investigation (Early et al., 2020; Racicot et al., 2021; Hedrick et al., 2018). DiceCT provides a whole-brain level of detail and spatial orientation of the tectofugal pathway while traditional histochemistry provides detail disembodied sections of neuroanatomy focused on cellular morphologies. Together, a highly accurate model of the tectofugal visual system was created maintaining the spatial and structural organization of the tectofugal nuclei. This model can be used to educate users about primary and secondary tectofugal components and their connectivity for not only *Gallus domesticus* but other species within the Class Aves. For the purpose of research, the present model can allow for anatomical investigation of the chicken tectofugal visual system outside of the limited defined orientation of the traditional 2D visualization techniques. This model can benefit studies aiming to isolate visual structures for tract tracing, intracellular filling, and electrophysiology. To parallel this, diceCT produces stacks of digitally sliced brain sections that can be modified to produce a series of sections virtually re-sliced at atypical angles to visualize as many preferred structures as possible. DiceCT can also be utilized

to obtain volumetric analyses because the size of each voxel that defines size and shape of neuroanatomical features is known. It would be interesting to generate more tectofugal models across chickens to study the 3D development of this system as well as models for many more avian species to compare interspecific differences and potentially infer functional significance to anatomical differences. This comparison will allow for better understanding of the variations in linear dimensions, structural volume, and connectivity and how this is related to differences in visual ecology of birds.

Acknowledgements

We are grateful to Manon Wilson (University of Arkansas) and the MICRO group for their efforts in performing the CT scans on our specimen. We are thankful to Alex Claxton (OSU-CHS) for his help in initial model manipulations in Blender. This project was funded by grants from the Chancellor's Innovation Grant of UA, 2020-23 to WJK and PG, Arkansas Biosciences Institute Grant, 2022-23 to WJK, and NSF 1457180 and 1725925 to PMG.

Supplementary Information

Please contact PJS for additional datasets, models, and images.

Conflict of Interest

The authors declare no conflict of interest.

Author Contribution

PJS, WJK and PMG designed the overall study and established the specific aims. WJK collected and prepared the specimen. PJS learned the software programs, aligned all structures to attain their appropriate location and size within the actual 3D dimensions of the avian brain. PJS and PMG created the 3D brain and skull reconstructions for the chicken. PJS created the figures in

the manuscript, wrote the first draft and WJK and PMG contributed to subsequent drafts of the manuscript.

3.6 References

Acerbo, M. J., Lazareva, O. F., McInnerney, J., Leiker, E., Wasserman, E. A., & Poremba, A. (2012). Figure–ground discrimination in the avian brain: The nucleus rotundus and its inhibitory complex. *Vision Research*, *70*, 18–26. https://doi.org/10.1016/j.visres.2012.07.023

Ahumada-Galleguillos, P., Fernández, M., Marin, G. J., Letelier, J. C., & Mpodozis, J. (2015). Anatomical organization of the visual dorsal ventricular ridge in the chick (*Gallus gallus*): Layers and columns in the avian pallium. *Journal of Comparative Neurology*, *523*(17), 2618–2636. https://doi.org/10.1002/cne.23808

Alpár, A., & Tömböl, T. (2000). Efferent connections of the Ectostriatal Core. an anterograde tracer study. *Annals of Anatomy - Anatomischer Anzeiger*, *182*(2), 101–110. https://doi.org/10.1016/s0940-9602(00)80067-9

Anderson, C., Parra, R. S., Chapman, H., Steinemer, A., Porter, B., & Colombo, M. (2020). Pigeon nidopallium caudolaterale, entopallium, and mesopallium ventrolaterale neural responses during categorisation of Monet and Picasso Paintings. *Scientific Reports*, *10*(1). https://doi.org/10.1038/s41598-020-72650-y

Angaut, P., & Repérant, J. (1976). Fine structure of the optic fibre termination layers in the pigeon optic tectum: A golgi and electron microscope study. *Neuroscience*, *1*(2). https://doi.org/10.1016/0306-4522(76)90003-8

Atoji, Y., & Wild, J. M. (2012). Afferent and efferent projections of the mesopallium in the pigeon (*Columba livia*). *The Journal of Comparative Neurology*, *520*(4), 717–741. https://doi.org/10.1002/cne.22763

Azizi, A. H., Pusch, R., Koenen, C., Klatt, S., Bröker, F., Thiele, S., Kellermann, J., Güntürkün, O., & Cheng, S. (2019). Emerging category representation in the visual forebrain hierarchy of pigeons (*Columba livia*). *Behavioural Brain Research*, *356*, 423–434. https://doi.org/10.1016/j.bbr.2018.05.014

Becker, T., & Redies, C. (2003). Internal structure of the nucleus rotundus revealed by mapping cadherin expression in the embryonic chicken visual system. *The Journal of Comparative Neurology*, *467*(4), 536–548. https://doi.org/10.1002/cne.10954

Benowitz, L. I., & Karten, H. J. (1976). Organization of the tectofugal visual pathway in the pigeon: A retrograde transport study. *The Journal of Comparative Neurology*, *167*(4), 503–520. https://doi.org/10.1002/cne.901670407

Bischof, H.-J., & Niemann, J. (1990). Contralateral projections of the optic tectum in the zebra finch (*Taenopygia guttata castanotis*). *Cell and Tissue Research*, *262*(2), 307–313. https://doi.org/10.1007/bf00309886

Bowmaker, J. K. (1977). The visual pigments, oil droplets and spectral sensitivity of the pigeon. *Vision Research*, *17*(10), 1129–1138. https://doi.org/10.1016/0042-6989(77)90147-x

Bowmaker, J. K., Heath, L. A., Wilkie, S. E., & Hunt, D. M. (1997). Visual pigments and oil droplets from six classes of photoreceptor in the retinas of birds. *Vision Research*, *37*(16), 2183–2194. https://doi.org/10.1016/s0042-6989(97)00026-6

Bribiesca-Contreras, F., & Sellers, W. I. (2017). Three-dimensional visualisation of the internal anatomy of the Sparrowhawk (*Accipiter nisus*) forelimb using contrast-enhanced micro-computed tomography. *PeerJ*, *5*. https://doi.org/10.7717/peerj.3039

Chen, Y., & Naito, J. (1999). Morphological classification of ganglion cells in the central retina of chicks. *Journal of Veterinary Medical Science*, *61*(5), 537–542. https://doi.org/10.1292/jvms.61.537

Clark, W. J., & Colombo, M. (2020). The functional architecture, receptive field characteristics, and representation of objects in the visual network of the pigeon brain. *Progress in Neurobiology*, *195*, 101781. https://doi.org/10.1016/j.pneurobio.2020.101781

Clark, W., Chilcott, M., Azizi, A., Pusch, R., Perry, K., & Colombo, M. (2022). Neurons in the pigeon visual network discriminate between faces, scrambled faces, and sine grating images. *Scientific Reports*, *12*(1). https://doi.org/10.1038/s41598-021-04559-z

Clarke, P. G., & Whitteridge, D. (1976). The projection of the retina, including the 'Red Area', on to the optic tectum of the pigeon. *Quarterly Journal of Experimental Physiology and Cognate Medical Sciences*, *61*(4), 351–358. https://doi.org/10.1113/expphysiol.1976.sp002366

De Groof, G., George, I., Touj, S., Stacho, M., Jonckers, E., Cousillas, H., Hausberger, M., Güntürkün, O., & Van der Linden, A. (2015). A three-dimensional digital atlas of the Starling Brain. *Brain Structure and Function*, *221*(4), 1899–1909. https://doi.org/10.1007/s00429-015-1011-1

Dellen, B., Wessel, R., Clark, J. W., & Wörgötter, F. (2009). Motion processing with wide-field neurons in the retino-tecto-rotundal pathway. *Journal of Computational Neuroscience*, *28*(1), 47–64. https://doi.org/10.1007/s10827-009-0186-y

Deng, C., & Rogers, L. J. (1998). Organisation of the tectorotundal and SP/IPS-rotundal projections in the chick. *Journal of Comparative Neurology*, *394*(2), 171–185. https://doi.org/10.1002/(sici)1096-9861(19980504)394:2<171::aid-cne3>3.0.co;2-#

Dubbeldam, J. L., Den Boer-Visser, A. M., & Bout, R. G. (1997). Organization and efferent connections of the archistriatum of the Mallard (*Anas platyrhynchos*) L.: An anterograde and retrograde tracing study. *The Journal of Comparative Neurology*, *388*(4), 632–657. https://doi.org/10.1002/(sici)1096-9861(19971201)388:4<632::aid-cne10>3.0.co;2-n

Düring, D. N., Ziegler, A., Thompson, C. K., Ziegler, A., Faber, C., Müller, J., Scharff, C., & Elemans, C. P. H. (2013). The songbird syrinx morphome: A three-dimensional, high-resolution, interactive morphological map of the zebra finch vocal organ. *BMC Biology*, *11*(1). https://doi.org/10.1186/1741-7007-11-1

Early, C. M., Iwaniuk, A. N., Ridgely, R. C., & Witmer, L. M. (2020). Endocast structures are reliable proxies for the sizes of corresponding regions of the brain in extant birds. *Journal of Anatomy*, *237*(6), 1162–1176. https://doi.org/10.1111/joa.13285

Ewert, J.-P. (1984). Tectal mechanisms that underlie prey-catching and avoidance behaviors in toads. *Comparative Neurology of the Optic Tectum*, 247–416. https://doi.org/10.1007/978-1-4899-5376-6_11

Faunes, M., Fernández, S., Gutiérrez-Ibáñez, C., Iwaniuk, A. N., Wylie, D. R., Mpodozis, J., Karten, H. J., & Marín, G. (2013). Laminar segregation of GABAergic neurons in the avian nucleus isthmi pars magnocellularis: A retrograde tracer and comparative study. *Journal of Comparative Neurology*, *521*(8), 1727–1742. https://doi.org/10.1002/cne.23253

Fernández, M., Ahumada-Galleguillos, P., Sentis, E., Marín, G., & Mpodozis, J. (2019). Intratelencephalic projections of the avian visual dorsal ventricular ridge: Laminarly segregated, reciprocally and topographically organized. *Journal of Comparative Neurology*, *528*(2), 321–359. https://doi.org/10.1002/cne.24757

Fernández, M., Morales, C., Durán, E., Fernández-Colleman, S., Sentis, E., Mpodozis, J., Karten, H. J., & Marín, G. J. (2019). Parallel organization of the avian sensorimotor arcopallium: tectofugal visual pathway in the pigeon (*Columbia livia*). *Journal of Comparative Neurology*, *528*(4), 597–623. https://doi.org/10.1002/cne.24775

Fredes, F., Tapia, S., Letelier, J. C., Marín, G., & Mpodozis, J. (2010). Topographic arrangement of the rotundo-entopallial projection in the pigeon (*Columba livia*). *The Journal of Comparative Neurology*, *518*(21), 4342–4361. https://doi.org/10.1002/cne.22460

Frost, B. J., & DiFranco, D. E. (1976). Motion characteristics of single units in the pigeon optic tectum. *Vision Research*, *16*(11), 1229–1234. https://doi.org/10.1016/0042-6989(76)90046-8

Frost, B. J., Cavanagh, P., & Morgan, B. (1988). Deep tectal cells in pigeons respond to kinematograms. *Journal of Comparative Physiology A*, *162*(5), 639–647. https://doi.org/10.1007/bf01342639

Gamlin, P. D. R., Reiner, A., Keyser, K. T., Brecha, N., & Karten, H. J. (1996). Projection of the nucleus pretectalis to a retinorecipient tectal layer in the pigeon (Columba Livia). *The Journal of Comparative Neurology*, *368*(3), 424–438. https://doi.org/10.1002/(sici)1096-9861(19960506)368:3<424::aid-cne8>3.0.co;2-7

Gao, M., Lengersdorf, D., Stüttgen, M. C., & Güntürkün, O. (2019). Transient inactivation of the visual-associative nidopallium frontolaterale (NFL) impairs extinction learning and context encoding in pigeons. *Neurobiology of Learning and Memory*, *158*, 50–59. https://doi.org/10.1016/j.nlm.2019.01.012

Genbrugge, A., Herrel, A., Boone, M., Van Hoorebeke, L., Podos, J., Dirckx, J., Aerts, P., & Dominique, A. (2011). The head of the finch: The anatomy of the feeding system in two species of finches (*Geospiza fortis* and *Padda oryzivora*). *Journal of Anatomy*, *219*(6), 676–695. https://doi.org/10.1111/j.1469-7580.2011.01437.x

Gignac, P. M., Green, T. L., Oehler, D. A., Malatos, J., Paré, J. A., & Hollinger, C. (2021). Diffusible iodine-based contrast-enhanced computed tomography as a necropsy aid: A case report evaluating respiratory disease in Macrocephalon Maleo. *Journal of Zoo and Wildlife Medicine*, *52*(1). https://doi.org/10.1638/2020-0086

Gignac, P. M., & Kley, N. J. (2018). The utility of dicect imaging for high-throughput comparative neuroanatomical studies. *Brain, Behavior and Evolution*, *91*(3), 180–190. https://doi.org/10.1159/000485476

Gignac, P. M., Kley, N. J., Clarke, J. A., Colbert, M. W., Morhardt, A. C., Cerio, D., Cost, I. N., Cox, P. G., Daza, J. D., Early, C. M., Echols, M. S., Henkelman, R. M., Herdina, A. N., Holliday, C. M., Li, Z., Mahlow, K., Merchant, S., Müller, J., Orsbon, C. P., … Witmer, L. M. (2016). Diffusible iodine-based contrast-enhanced Computed Tomography (dicect): An emerging tool for rapid, high-resolution, 3-D imaging of metazoan soft tissues. *Journal of Anatomy*, *228*(6), 889–909. https://doi.org/10.1111/joa.12449

Gold, M. E., Schulz, D., Budassi, M., Gignac, P. M., Vaska, P., & Norell, M. A. (2016). Flying Starlings, pet and the evolution of Volant Dinosaurs. *Current Biology*, *26*(7). https://doi.org/10.1016/j.cub.2016.02.025

González-Cabrera, C., Garrido-Charad, F., Mpodozis, J., Bolam, J. P., & Marín, G. J. (2015). Axon terminals from the nucleus isthmi pars parvocellularis control the ascending retinotectofugal output through direct synaptic contact with tectal ganglion cell dendrites. *Journal of Comparative Neurology*, *524*(2), 362–379. https://doi.org/10.1002/cne.23860

Güntürkün, O., Verhoye, M., De Groof, G., & Van der Linden, A. (2012). A 3-dimensional digital atlas of the ascending sensory and the descending motor systems in the Pigeon Brain. *Brain Structure and Function*, *218*(1), 269–281. https://doi.org/10.1007/s00429-012-0400-y

Gutiérrez-Ibáñez, C., Iwaniuk, A. N., Lisney, T. J., Faunes, M., Marín, G. J., & Wylie, D. R. (2012). Functional implications of species differences in the size and morphology of the ISTHMO optic nucleus (ION) in birds. *PLoS ONE*, *7*(5). https://doi.org/10.1371/journal.pone.0037816

Hadden, P. W., Ober, W. C., Gerneke, D. A., Thomas, D., Scadeng, M., McGhee, C. N., & Zhang, J. (2022). Micro-CT guided illustration of the head anatomy of penguins (Aves: Sphenisciformes: Spheniscidae). *Journal of Morphology*, *283*(6), 827–851. https://doi.org/10.1002/jmor.21476

Hamdi, F. A., & Whitteridge, D. (1954). The representation of the retina on the optic tectum of the pigeon. *Quarterly Journal of Experimental Physiology and Cognate Medical Sciences*, *39*(2), 111–119. https://doi.org/10.1113/expphysiol.1954.sp001053

Hardy, O., Leresche, N., & Jassik-Gerschenfeld, D. (1985). Morphology and laminar distribution of electrophysiologically identified cells in the pigeon's optic tectum: An intracellular study. *The Journal of Comparative Neurology*, *233*(3), 390–404. https://doi.org/10.1002/cne.902330308

Hart, N. S., Mountford, J. K., Davies, W. I., Collin, S. P., & Hunt, D. M. (2016). Visual pigments in a palaeognath bird, the emu (*Dromaius novaehollandiae)*: Implications for spectral

sensitivity and the origin of ultraviolet vision. *Proceedings of the Royal Society B: Biological Sciences*, *283*(1834), 20161063. https://doi.org/10.1098/rspb.2016.1063

Hart, N. S., Partridge, J. C., & Cuthill, I. C. (1998). Visual pigments, oil droplets and cone photoreceptor distribution in the European Starling (*Sturnus vulgaris*). *Journal of Experimental Biology*, *201*(9), 1433–1446. https://doi.org/10.1242/jeb.201.9.1433

Hart, N. S., Partridge, J. C., Cuthill, I. C., & Bennett, A. T. (2000). Visual pigments, oil droplets, ocular media, and cone photoreceptor distribution in two species of passerine bird: The Blue Tit (*Parus caeruleus* L.) and the Blackbird (*Turdus merula* L.). *Journal of Comparative Physiology A: Sensory, Neural, and Behavioral Physiology*, *186*(4), 375–387. https://doi.org/10.1007/s003590050437

Hartmann, B., & Güntürkün, O. (1998). Selective deficits in reversal learning after neostriatum caudolaterale lesions in pigeons: Possible behavioral equivalencies to the mammalian prefrontal system. *Behavioural Brain Research*, *96*(1-2), 125–133. https://doi.org/10.1016/s0166-4328(98)00006-0

Hayes, B. P., & Holden, A. L. (1980). Size classes of ganglion cells in the central yellow field of the pigeon retina. *Experimental Brain Research*, *39*(3). https://doi.org/10.1007/bf00237116

Hedrick, B. P., Yohe, L., Vander Linden, A., Dávalos, L. M., Sears, K., Sadier, A., Rossiter, S. J., Davies, K. T., & Dumont, E. (2018). Assessing soft-tissue shrinkage estimates in museum specimens imaged with diffusible iodine-based contrast-enhanced computed tomography (dicect). *Microscopy and Microanalysis*, *24*(3), 284–291. https://doi.org/10.1017/s143192761800039

Hellmann, B., & Güntürkün, O. (2000). Structural organization of parallel information processing within the tectofugal visual system of the pigeon. *The Journal of Comparative Neurology*, *429*(1), 94–112. https://doi.org/10.1002/1096-9861(20000101)429:1<94::aid-cne8>3.0.co;2-5

Hellmann, B., Güntürkün, O., & Manns, M. (2004). Tectal mosaic: Organization of the descending tectal projections in comparison to the ascending tectofugal pathway in the pigeon. *Journal of Comparative Neurology*, *472*(4), 395–410. https://doi.org/10.1002/cne.20056

Hellmann, B., Manns, M., & Güntürkün, O. (2001). Nucleus isthmi, pars semilunaris as a key component of the tectofugal visual system in pigeons. *Journal of Comparative Neurology*, *436*(2), 153–166. https://doi.org/10.1002/cne.1058

Herold, C., Paulitschek, C., Palomero-Gallagher, N., Güntürkün, O., & Zilles, K. (2017). Transmitter receptors reveal segregation of the arcopallium/amygdala complex in pigeons (*Columba livia*). *Journal of Comparative Neurology*, *526*(3), 439–466. https://doi.org/10.1002/cne.24344

Hoyek, N., Collet, C., Di Rienzo, F., De Almeida, M., & Guillot, A. (2014). Effectiveness of three-dimensional digital animation in teaching human anatomy in an authentic classroom context. *Anatomical Sciences Education*, *7*(6), 430–437. https://doi.org/10.1002/ase.1446

Hsiao, Y.-T., Chen, T.-C., Yu, P.-H., Huang, D.-S., Hu, F.-R., Chuong, C.-M., & Chang, F.-C. (2020). Connectivity between nidopallium caudolateral and visual pathways in color perception of zebra finches. *Scientific Reports*, *10*(1). https://doi.org/10.1038/s41598-020-76542-z

Hu, M., Naito, J., Chen, Y., Ohmori, Y., & Fukuta, K. (2003). Afferent and efferent connections of the nucleus rotundus demonstrated by WGA-HRP in the chick. *Anatomia, Histologia, Embryologia: Journal of Veterinary Medicine Series C*, *32*(6), 335–340. https://doi.org/10.1111/j.1439-0264.2003.00488.x

Hunt, S. P., Streit, P., Künzle, H., & Cuénod, M. (1977). Characterization of the pigeon isthmo-tectal pathway by selective uptake and retrograde movement of radioactive compounds and by golgi-like horseradish peroxidase labeling. *Brain Research*, *129*(2), 197–212. https://doi.org/10.1016/0006-8993(77)90001-4

Huo, Y., Xu, Z., Xiong, Y., Aboud, K., Parvathaneni, P., Bao, S., Bermudez, C., Resnick, S. M., Cutting, L. E., & Landman, B. A. (2019). 3D whole brain segmentation using spatially localized atlas network tiles. *NeuroImage*, *194*, 105–119. https://doi.org/10.1016/j.neuroimage.2019.03.041

Husband, S. A., & Shimizu, T. (1999). Efferent projections of the ectostriatum in the pigeon (*Columba livia*). *The Journal of Comparative Neurology*, *406*(3), 329–345. https://doi.org/10.1002/(sici)1096-9861(19990412)406:3<329::aid-cne3>3.0.co;2-a

Ikushima, M., Watanabe, M., & Ito, H. (1986). Distribution and morphology of retinal ganglion cells in the Japanese quail. *Brain Research*, *376*(2), 320–334. https://doi.org/10.1016/0006-8993(86)90195-2

Jones, M. E., Button, D. J., Barrett, P. M., & Porro, L. B. (2019). Digital dissection of the head of the rock dove (*Columba livia*) using contrast-enhanced computed tomography. *Zoological Letters*, *5*(1). https://doi.org/10.1186/s40851-019-0129-z

Karten, H. J., Cox, K., & Mpodozis, J. (1997). Two distinct populations of tectal neurons have unique connections within the retinotectorotundal pathway of the pigeon (*Columba livia*). *The Journal of Comparative Neurology*, *387*(3), 449–465. https://doi.org/10.1002/(sici)1096-9861(19971027)387:3<449::aid-cne10>3.0.co;2-g

Kawabe, S., Tsunekawa, N., Kudo, K., Tirawattanawanich, C., Akishinonomiya, F., & Endo, H. (2017). Morphological variation in brain through domestication of Fowl. *Journal of Anatomy*, *231*(2), 287–297. https://doi.org/10.1111/joa.12623

Kim, U. S., Mahroo, O. A., Mollon, J. D., & Yu-Wai-Man, P. (2021). Retinal ganglion cells—diversity of cell types and clinical relevance. *Frontiers in Neurology*, *12*. https://doi.org/10.3389/fneur.2021.661938

Kram, Y. A., Mantey, S., & Corbo, J. C. (2010). Avian cone photoreceptors tile the retina as five independent, self-organizing mosaics. *PLoS ONE*, *5*(2). https://doi.org/10.1371/journal.pone.0008992

Kuenzel, W. J., & Masson, M. (1988). *A stereotaxic atlas of the brain of the chick (Gallus domesticus)*. Johns Hopkins University Press.

Laforsch, C., Imhof, H., Sigl, R., Settles, M., He, M., & Wanninger, A. (2012). Applications of computational 3D–modeling in organismal biology. *Modeling and Simulation in Engineering*. https://doi.org/10.5772/31092

Lautenschlager, S., Bright, J. A., & Rayfield, E. J. (2013). Digital dissection using contrast-enhanced computed tomography scanning to elucidate hard- and soft-tissue anatomy in the common buzzard (*Buteo buteo*). *Journal of Anatomy*, *224*(4), 412–431. https://doi.org/10.1111/joa.12153

Laverghetta, A. V., & Shimizu, T. (2003). Organization of the ectostriatum based on afferent connections in the Zebra Finch (*Taeniopygia guttata*). *Brain Research*, *963*(1-2), 101–112. https://doi.org/10.1016/s0006-8993(02)03949-5

Lengersdorf, D., Pusch, R., Güntürkün, O., & Stüttgen, M. C. (2014). Neurons in the pigeon nidopallium caudolaterale signal the selection and execution of perceptual decisions. *European Journal of Neuroscience*, *40*(9), 3316–3327. https://doi.org/10.1111/ejn.12698

Letelier, J.-C., Marin, G., Sentis, E., Tenreiro, A., Fredes, F., & Mpodozis, J. (2004). The mapping of the visual field onto the dorso-lateral tectum of the pigeon (*Columba livia*) and its relations with retinal specializations. *Journal of Neuroscience Methods*, *132*(2), 161–168. https://doi.org/10.1016/j.jneumeth.2003.09.007

Li, Z., & Clarke, J. A. (2015). The craniolingual morphology of waterfowl (Aves, Anseriformes) and its relationship with feeding mode revealed through contrast-enhanced X-ray computed tomography and 2D morphometrics. *Evolutionary Biology*, *43*(1), 12–25. https://doi.org/10.1007/s11692-015-9345-4

Liu, C., Ye, F. Q., Yen, C. C.-C., Newman, J. D., Glen, D., Leopold, D. A., & Silva, A. C. (2018). A digital 3D atlas of the marmoset brain based on multi-modal MRI. *NeuroImage*, *169*, 106–116. https://doi.org/10.1016/j.neuroimage.2017.12.004

Luksch, H., Cox, K., & Karten, H. J. (1998). Bottlebrush dendritic endings and large dendritic fields: Motion-detecting neurons in the tectofugal pathway. *The Journal of Comparative Neurology*, *396*(3), 399–414. https://doi.org/10.1002/(sici)1096-9861(19980706)396:3<399::aid-cne9>3.0.co;2-y

Luksch, H., Karten, H. J., Kleinfeld, D., & Wessel, R. (2001). Chattering and differential signal processing in identified motion-sensitive neurons of parallel visual pathways in the chick tectum. *The Journal of Neuroscience*, *21*(16), 6440–6446. https://doi.org/10.1523/jneurosci.21-16-06440.2001

López-López, R., López-Gallardo, M., Pérez-Álvarez, M. J., & Prada, C. (2008). Isolation of chick retina cones and study of their diversity based on oil droplet colour and nucleus position. *Cell and Tissue Research*, *332*(1), 13–24. https://doi.org/10.1007/s00441-007-0572-6

Maggesissi, R. S., Gardino, P. F., Guimarães-Souza, E. M., Paes-de-Carvalho, R., Silva, R. B., & Calaza, K. C. (2009). Modulation of GABA release by nitric oxide in the chick retina: Different effects of nitric oxide depending on the cell population. *Vision Research*, *49*(20), 2494–2502. https://doi.org/10.1016/j.visres.2009.08.004

Manns, M., & Güntürkün, O. (1997). Development of the retinotectal system in the pigeon: A cytoarchitectonic and tracing study with cholera toxin. *Anatomy and Embryology*, *195*(6), 539–555. https://doi.org/10.1007/s004290050074

Manns, M., Freund, N., Patzke, N., & Güntürkün, O. (2007). Organization of telencephalotectal projections in pigeons: Impact for lateralized top-down control. *Neuroscience*, *144*(2), 645–653. https://doi.org/10.1016/j.neuroscience.2006.09.043

Marin, G. J., Duran, E., Morales, C., Gonzalez-Cabrera, C., Sentis, E., Mpodozis, J., & Letelier, J. C. (2012). Attentional capture? Synchronized feedback signals from the isthmi boost retinal signals to higher visual areas. *Journal of Neuroscience*, *32*(3), 1110–1122. https://doi.org/10.1523/jneurosci.4151-11.2012

Martinez-de-la-Torre, M., Martinez, S., & Puelles, L. (1990). Acetylcholinesterase-histochemical differential staining of subdivisions within the nucleus rotundus in the chick. *Anatomy and Embryology*, *181*(2). https://doi.org/10.1007/bf00198952

Marín, G., Letelier, J. C., Henny, P., Sentis, E., Farfán, G., Fredes, F., Pohl, N., Karten, H., & Mpodozis, J. (2003). Spatial organization of the pigeon tectorotundal pathway: An interdigitating topographic arrangement. *Journal of Comparative Neurology*, *458*(4), 361–380. https://doi.org/10.1002/cne.10591

McGill, J., Powell, T., & Cowan, W. (1966). The retinal representation upon the optic tectum and isthmo-optic nucleus in the pigeon. *Journal of Anatomy*, *100*(1), 5–33.

Medina, L., & Reiner, A. (1994). Distribution of choline acetyltransferase immunoreactivity in the pigeon brain. *The Journal of Comparative Neurology*, *342*(4), 497–537. https://doi.org/10.1002/cne.903420403

Miceli, D., Repérant, J., Bertrand, C., & Rio, J.-P. (1999). Functional anatomy of the avian centrifugal visual system. *Behavioural Brain Research*, *98*(2), 203–210. https://doi.org/10.1016/s0166-4328(98)00085-0

Moore, B. A., Baumhardt, P., Doppler, M., Randolet, J., Blackwell, B. F., DeVault, T. L., Loew, E. R., & Fernández-Juricic, E. (2012). Oblique color vision in an open-habitat bird: Spectral sensitivity, photoreceptor distribution and behavioral implications. *Journal of Experimental Biology*, *215*(19), 3442–3452. https://doi.org/10.1242/jeb.073957

Naito, J., & Chen, Y. (2004). Morphologic analysis and classification of ganglion cells of the chick retina by intracellular injection of Lucifer yellow and retrograde labeling with dii. *The Journal of Comparative Neurology*, *469*(3), 360–376. https://doi.org/10.1002/cne.11010

Nguyen, A. P. (2004). A dissociation of motion and spatial-pattern vision in the avian telencephalon: Implications for the evolution of "visual streams". *Journal of Neuroscience*, *24*(21), 4962–4970. https://doi.org/10.1523/jneurosci.0146-04.2004

Okano, T., Kojima, D., Fukada, Y., Shichida, Y., & Yoshizawa, T. (1992). Primary structures of chicken cone visual pigments: Vertebrate rhodopsins have evolved out of cone visual pigments. *Proceedings of the National Academy of Sciences*, *89*(13), 5932–5936. https://doi.org/10.1073/pnas.89.13.5932

Öktem, H., Sencelikel, T., Akcicek, E., Kocyigit, A. S., Penekli, U. S., Sungur, S., Tanriyakul, B., & Ulusoy, B. N. (2019). Contribution of 3D modeling to anatomy education: A pilot study. *Anatomy*, *13*(2), 116–121. https://doi.org/10.2399/ana.19.054

Park, S., Kim, Y., Park, S., & Shin, J.-A. (2019). The impacts of three-dimensional anatomical atlas on learning anatomy. *Anatomy & Cell Biology*, *52*(1), 76. https://doi.org/10.5115/acb.2019.52.1.76

Patton, T. B., Cook, R. G., & Shimizu, T. (2013). Functional segregation of the entopallium in pigeons. *PsycEXTRA Dataset*. https://doi.org/10.1037/e598032013-053

Pearlman, A. L., & Hughes, C. P. (1976). Functional role of efferents to the avian retina. I. Analysis of retinal ganglion cell receptive fields. *The Journal of Comparative Neurology*, *166*(1), 111–122. https://doi.org/10.1002/cne.901660108

Poirier, C., Vellema, M., Verhoye, M., Van Meir, V., Wild, J. M., Balthazart, J., & Van Der Linden, A. (2008). A three-dimensional MRI atlas of the zebra Finch Brain in stereotaxic coordinates. *NeuroImage*, *41*(1), 1–6. https://doi.org/10.1016/j.neuroimage.2008.01.069

Puelles, L., Martinez-de-la-Torre, M., Paxinos, G., Watson, C., & Martinez, S. (2019). *The Chick Brain in stereotaxic coordinates and alternate stains: Featuring neuromeric divisions and mammalian homologies*. Academic Press, an imprint of Elsevier.

Pujol, S., Baldwin, M., Nassiri, J., Kikinis, R., & Shaffer, K. (2016). Using 3D modeling techniques to enhance teaching of difficult anatomical concepts. *Academic Radiology*, *23*(4), 507–516. https://doi.org/10.1016/j.acra.2015.12.012

Racicot, R. (2021). Evolution of whale sensory ecology: Frontiers in nondestructive anatomical investigations. *The Anatomical Record*, *305*(3), 736–752. https://doi.org/10.1002/ar.24761

Reiner, A., Perkel, D. J., Bruce, L. L., Butler, A. B., Csillag, A., Kuenzel, W., Medina, L., Paxinos, G., Shimizu, T., Striedter, G., Wild, M., Ball, G. F., Durand, S., Gütürkün, O., Lee, D. W., Mello, C. V., Powers, A., White, S. A., Hough, G., … Jarvis, E. D. (2004). Revised nomenclature for avian telencephalon and some related brainstem nuclei. *The Journal of Comparative Neurology*, *473*(3), 377–414. https://doi.org/10.1002/cne.20118

Roach, V. A., Brandt, M. G., Moore, C. C., & Wilson, T. D. (2012). Is three-dimensional videography the cutting edge of surgical skill acquisition? *Anatomical Sciences Education*, *5*(3), 138–145. https://doi.org/10.1002/ase.1262

Scarf, D., Stuart, M., Johnston, M., & Colombo, M. (2016). Visual response properties of neurons in four areas of the avian pallium. *Journal of Comparative Physiology A*, *202*(3), 235–245. https://doi.org/10.1007/s00359-016-1071-6

Sebesteny, T., Davies, D. C., Zayats, N., Nemeth, A., & Tombol, T. (2002). The ramification and connections of retinal fibres in layer 7 of the domestic chick optic tectum: A golgi impregnation, anterograde tracer and GABA-immunogold study. *Journal of Anatomy*, *200*(2), 169–183. https://doi.org/10.1046/j.0021-8782.2001.00012.x

Shanahan, M., Bingman, V. P., Shimizu, T., Wild, M., & Güntürkün, O. (2013). Large-scale network organization in the avian forebrain: A connectivity matrix and theoretical analysis. *Frontiers in Computational Neuroscience*, *7*. https://doi.org/10.3389/fncom.2013.00089

Shimizu, T., Patton, T. B., & Husband, S. A. (2010). Avian visual behavior and the organization of the Telencephalon. *Brain, Behavior and Evolution*, *75*(3), 204–217. https://doi.org/10.1159/000314283

Stacho, M., Herold, C., Rook, N., Wagner, H., Axer, M., Amunts, K., & Güntürkün, O. (2020). A cortex-like canonical circuit in the avian forebrain. *Science*, *369*(6511). https://doi.org/10.1126/science.abc5534

Sun, H.-J., & Frost, B. J. (1997). Motion processing in pigeon tectum: Equiluminant chromatic mechanisms. *Experimental Brain Research*, *116*(3), 434–444. https://doi.org/10.1007/pl00005771

Theiss, M. P., Hellmann, B., & Güntürkün, O. (2003). The architecture of an inhibitory sidepath within the avian tectofugal system. *NeuroReport*, *14*(6), 879–882. https://doi.org/10.1097/00001756-200305060-00021

To, K. H., O'Brien, H. D., Stocker, M. R., & Gignac, P. M. (2021). Cranial musculoskeletal description of black-throated finch (Aves: Passeriformes: Estrildidae) with diceCT. *Integrative Organismal Biology*, *3*(1). https://doi.org/10.1093/iob/obab007

Tömböl, T., Maglóczky, Z., Stewart, M. G., & Csillag, A. (1988). The structure of chicken ectostriatum. I. Golgi study. *Journal fur Hirnforschung*, *29*(5), 525–546

Tyrrell, L. P., Teixeira, L. B. C., Dubielzig, R. R., Pita, D., Baumhardt, P., Moore, B. A., & Fernández-Juricic, E. (2019). A novel cellular structure in the photoreceptors of insectivorous birds. *Nature - Scientific Reports*. https://doi.org/10.1101/551945

Uchiyama, H., Aoki, K., Yonezawa, S., Arimura, F., & Ohno, H. (2004). Retinal target cells of the centrifugal projection from the isthmo-optic nucleus. *The Journal of Comparative Neurology*, *476*(2), 146–153. https://doi.org/10.1002/cne.20225

Uchiyama, H., Ohno, H., & Kodama, R. (2012). Lesion of the isthmo-optic nucleus impairs target selection for visually guided reaching. *Behavioural Brain Research*, *233*(2), 359–366. https://doi.org/10.1016/j.bbr.2012.05.008

Uchiyama, H., Ohno, H., Kawasaki, T., Owatari, Y., Narimatsu, T., Miyanagi, Y., & Maeda, T. (2022). Attentional signals projecting centrifugally to the avian retina: A dual contribution to visual search. *Vision Research*, *195*, 108016. https://doi.org/10.1016/j.visres.2022.108016

Veenman, C. L., & Reiner, A. (1994). The distribution of GABA-containing perikarya, fibers, and terminals in the forebrain and midbrain of pigeons, with particular reference to the basal ganglia and its projection targets. *The Journal of Comparative Neurology*, *339*(2), 209–250. https://doi.org/10.1002/cne.903390205

Vellema, M., Verschueren, J., Van Meir, V., & Van der Linden, A. (2011). A customizable 3-dimensional digital atlas of the Canary Brain in multiple modalities. *NeuroImage*, *57*(2), 352–361. https://doi.org/10.1016/j.neuroimage.2011.04.033

Verhaal, J., & Luksch, H. (2013). Mapping of the receptive fields in the optic tectum of chicken (*Gallus gallus*) using sparse noise. *PLoS ONE*, *8*(4). https://doi.org/10.1371/journal.pone.0060782

Wai, M. S., Lorke, D. E., Kung, L. S., & Yew, D. T. (2006). Morphogenesis of the different types of photoreceptors of the chicken (*gallus domesticus*) retina and the effect of amblyopia in neonatal chicken. *Microscopy Research and Technique*, *69*(2), 99–107. https://doi.org/10.1002/jemt.20279

Wang, Q., Ding, S.-L., Li, Y., Royall, J., Feng, D., Lesnar, P., Graddis, N., Naeemi, M., Facer, B., Ho, A., Dolbeare, T., Blanchard, B., Dee, N., Wakeman, W., Hirokawa, K. E., Szafer, A., Sunkin, S. M., Oh, S. W., Bernard, A., … Ng, L. (2020). The Allen Mouse Brain Common Coordinate Framework: A 3D reference atlas. *Cell*, *181*(4). https://doi.org/10.1016/j.cell.2020.04.007

Wang, Y., Luksch, H., Brecha, N. C., & Karten, H. J. (2006). Columnar projections from the cholinergic nucleus isthmi to the optic tectum in chicks (*Gallus gallus*): A possible substrate for synchronizing tectal channels. *The Journal of Comparative Neurology*, *494*(1), 7–35. https://doi.org/10.1002/cne.20821

Wang, Y., Major, D. E., & Karten, H. J. (2003). Morphology and connections of nucleus isthmi pars magnocellularis in chicks (*Gallus gallus*). *The Journal of Comparative Neurology*, *469*(2), 275–297. https://doi.org/10.1002/cne.11007

Wang, Y.-C., Jiang, S., & Frost, B. J. (1993). Visual processing in pigeon nucleus rotundus: Luminance, color, motion, and looming subdivisions. *Visual Neuroscience*, *10*(1), 21–30. https://doi.org/10.1017/s0952523800003199

Watanabe, A., Gignac, P. M., Balanoff, A. M., Green, T. L., Kley, N. J., & Norell, M. A. (2019). Are endocasts good proxies for brain size and shape in archosaurs throughout ontogeny? *Journal of Anatomy*, *234*(3), 291–305. https://doi.org/10.1111/joa.12918

Watanabe, A., Gignac, P. M., Balanoff, A. M., Green, T. L., Kley, N. J., & Norell, M. A. (2018). Are endocasts good proxies for brain size and shape in archosaurs throughout ontogeny? *Journal of Anatomy*, *234*(3), 291–305. https://doi.org/10.1111/joa.12918

Woodson, W., Reiner, A., Anderson, K., & Karten, H. J. (1991). Distribution, laminar location, and morphology of tectal neurons projecting to the isthmo-optic nucleus and the nucleus isthmi, pars parvocellularis in the pigeon (*Columba livia*) and chick (*Gallus domesticus*): A retrograde labelling study. *The Journal of Comparative Neurology*, *305*(3), 470–488. https://doi.org/10.1002/cne.903050310

Wu, L.-Q., Niu, Y.-Q., Yang, J., & Wang, S.-R. (2005). Tectal neurons signal impending collision of looming objects in the pigeon. *European Journal of Neuroscience*, *22*(9), 2325–2331. https://doi.org/10.1111/j.1460-9568.2005.04397.x

Wylie, D. R., Gutierrez-Ibanez, C., Pakan, J. M., & Iwaniuk, A. N. (2009). The optic tectum of birds: Mapping our way to understanding visual processing. *Canadian Journal of Experimental Psychology/Revue Canadienne De Psychologie Expérimentale*, *63*(4), 328–338. https://doi.org/10.1037/a0016826

Xiao, Q., Li, D.-P., & Wang, S.-R. (2006). Looming-sensitive responses and receptive field organization of telencephalic neurons in the pigeon. *Brain Research Bulletin*, *68*(5), 322–328. https://doi.org/10.1016/j.brainresbull.2005.09.003

Yamagata, M., Yan, W., & Sanes, J. R. (2021). A cell atlas of the chick retina based on single-cell transcriptomics. *ELife*, *10*. https://doi.org/10.7554/elife.63907

Legends, Figures, and Tables

Fig 3.1. **A**: Right lateral view of the chicken's right eye with the brain situated behind it. Within the eye, key structures such as the lens, pecten, and head of the optic nerve are shown. A color-coded quadrant system illustrating retinotopy has been overlaid on the retina (red: superiotemporal quadrant; green: superionasal quadrant; yellow: inferiotemporal quadrant; blue: inferionasal quadrant). **B:** Right lateral view of the diceCT rendered chicken's right eye, its lens and when magnified, the pectin appears to the left of the lens. The brain is situated behind the eye. **C**: DiceCT image showing the pecten within the eyeball and sagittal view of the brain situated dorsal and posterior to it. **D**: Unstained image of the retina of the chick.

Fig 3.2. Standardization protocol for registering histology and diceCT visualizations to ensure accurate size, orientation, and position of the brain and relevant tectofugal structures of the chicken. **A,B:** Left lateral view of the rendered diceCT brain and eyeball in their approximate positions in the absence of the skull. This was accomplished by using both surface and wireframe projections within the Blender environment and placement of half of the brain within the midline atlas plate L 0.2 of a stereotaxic atlas of the chick (Kuenzel and Masson, 1988). **C,D,E:** Left anterolateral view of the rendered diceCT brain, interposed by midline atlas plate L 0.2 and corresponding coronal sections of the stereotaxic atlas (**C,** A11.0, **D**, A6.4, **E**, A2.2). **F:** The same left anterolateral view as **C,D,E** showing three interposed coronal sections (A11.0, A6.4, A2.2) intersecting the midline sagittal atlas plate (L0.2).

Fig 3.3. Retinotopic projections of the retina onto the optic tectum by quadrant in left lateral view. **A:** Shows the right eye and brain as positioned in the skull of a bird with a stereotaxic instrument and its beak lowered 45 degrees (e.g. by a bird viewing an object on the ground. **B:** Similar features are seen as (a); however, the surface of the eyeball and brain have been made semitransparent to visualize better the quadrant theory of the retina (striped red: superiotemporal quadrant; striped green: superionasal quadrant; striped yellow: inferiotemporal quadrant striped blue: inferionasal quadrant) and how quadrants are hypothesized to project onto corresponding quadrants (i.e., by color) of the superficial optic tectum. For example, RGCs located in the superiotemporal quadrant of the eye project to the anterior ventral

Fig 3.4. Comparison of the divisions of the rotundus in sagittal sections and entopallium in coronal sections between the current study and the past studies. **A**: Divisions of the rotundus according to cell and fiber density (current study: v, ventral; i, intermediate; d, dorsal; lp, lateral posterior). B,C: Divisions of the rotundus according to tract tracing in the pigeon (Benowitz and Karten, 1976: da, dorsal anterior; am, anteromedial; m, medial; v, ventral; p, posterior) and zebra finch (Laverghetta and Shimizu, 2003: Da, dorsal anterior; Ce, central; P, posterior) **D:** Divisions of the entopallium according to cell and fiber density (current study; Ei: internal entopallium core; Ee: external entopallium core; Eb: entopallium belt). **E,F:** Divisions of the entopallium

according to parvalbumin, cytochrome oxidase, and calretinin histochemistry as well as fiber density (Krutzfeldt and Wild 2004,2005; Ei: internal entopallium core; Ex: external entopallium core; Eb: entopallium belt). Scale bars = 500 μm

Fig 3.5. Series of rostral-to-caudal coronal brain sections in Gallyas silver stain (**A–C**) and diceCT (**D–I**) visualization protocols with various tectofugal structures highlighted showing similar features in both preparation methods. **G,H,I:** diceCT scanned sections with overlay of tectofugal structures (orange: entopallium; green: nucleus rotundus; grey: triangularis; red: subpretectal nucleus). Scale bar = 2 mm.

Fig 6. Series of rostral-to-caudal sagittal brain sections in Gallyas silver stain (**A–C**) and diceCT (**D–I**) visualization protocols showing similar features in both preparations. **G,H,I:** diceCT scanned sections with overlay of tectofugal structures (orange: entopallium; blue: Ipc; yellow: Imc; green: nucleus rotundus; purple: pretectal nucleus; red: subpretectal nucleus). Scale bar = 2 mm.

Fig 3.7. Frontal view of the diceCT eyeball and brain. **A:** Structures rendered as fully opaque as a reference visualization. **B:** Rendered brain surface and eye have been made semitransparent to illustrate the nucleus rotundus as a whole structure (right hemisphere) and as its subdivided components (left hemisphere) (dark orange: nucleus rotundus; green: ventral subdivision; red: intermediate subdivision; blue: dorsal subdivision; pink: lateral-posterior subdivision; white: triangularis).

Fig 3.8. Frontal view of the diceCT eyeball and brain. **A:** Structures rendered as fully opaque as a reference visualization. **B:** Rendered brain surface and eye have been made semitransparent to illustrate the entopallium as a whole structure (right hemisphere; light orange) and subdivided entopallial components (left hemisphere; internal entopallium core: green; external entopallium core: red; entopallial belt: white).

Fig 3.9. 3D reconstruction of the tectofugal nuclei. Structures are displayed in a semitransparent brain from a three-quarters left profile view. **A:** solid rendering of the diceCT brain as a reference visualization. **B:** semitransparent rendering of the diceCT brain with all the tectofugal nuclei rendered opaque. **C:** Optic tectum with the retinotopic quadrant theory overlay (inferior anterior quadrant: striped red; inferior posterior: striped green; superior anterior: striped yellow; superior posterior: striped blue). **D:** Nucleus Rotundus (dark orange). **E:** Entopallium (light orange. **F:** Isthmi Nuclei (Ipc: cyan; Imc: dark purple; SLu: dark blue). **G:** SP/ISPT complex (SP: red; ISPT: dark yellow. **H:** Pretectal nucleus, Isthmo-optic nucleus, and lateral spiriform nucleus (PT: white; ION: dark green; SpL: light green). **I:** Intermediate Nidopallium and visual mesopallium (NI: light pink; MVL: light purple). **J:** Lateral Nidopallium (NFL: light blue; NIL: brown; NCL: dark pink). **K:** Arcopallium (dark grey).

Fig 3.10. 3D reconstruction of the tectofugal nuclei with their interconnectivity in a three-quarters profile view. **A:** solid rendering of the diceCT brain as a reference visualization. **B:** semitransparent rendering of the diceCT brain. **C:** Retinal ganglion cell projections via the optic tract to the optic tectum (striped yellow, blue, red, green). **D:** Addition of bilateral projections of tectal ganglion cells onto the rotundus (dark orange). **E:** Addition of ipsilateral projections from rotundus to entopallium (light orange). **F:** Addition of isthmi nuclei (Ipc: cyan; Imc: dark purple;

SLu: dark blue) and their connectivity to the tectum and between themselves. **G:** Addition of SP/ISPT complex (SP: red; ISPT: dark yellow) and its bilateral connectivity to the tectum and rotundus. **H:** Addition of pretectal nucleus (white) and its bilateral connectivity to the tectum and SP/ISPT complex. **I:** Addition of visual intermediate nidopallium (light pink) and mesopallium (light purple) and their connectivity to the entopallium. **J:** Addition of lateral nidopallium visual associative areas (NFL: light blue; NIL: brown; NCL: dark pink) and their reciprocal connections to the intermediate nidopallium. **K:** Addition of the arcopallium (dark grey) and its connections. All tracts are represented by black to stand out against tectofugal nuclei and semitransparent brain. Tract thickness has been changed in an attempt to illustrate major and minor projections between structures.

Fig 3.11. Semitransparent diceCT brain in three-quarters profile view illustrating a 3D reconstruction of the fiber tracts, decussations, and commissures used by the tectofugal pathway. Projections between tectofugal structures are color-coded to represent afferent projections from one nucleus to the next. A reference image showing the tectofugal structures is shown at the bottom right (see Figure 3.9b for structure identifications). The striped red, green, yellow, and blue tubes project from the retina to the superficial optic tectum using the optic tract. The light grey tubes project from layer 13 TGC's to ipsilateral and contralateral ROT, SP/ISPT, and PT using the ttt, pspt, and dsv. Yellow tubes project from layer 10 shepherd's crook neurons to the isthmi nuclei (Imc, Ipc, SLu, and ION) using the ttt and iit. The cyan tube projects from Ipc back onto the tectum using the iit and ttt. The dark blue tube projects from the SLu to the tectum via iit and ttt. The dark purple tubes project from the Imc to the Ipc and SLu via the iit, and project from the Imc back to the tectum via iit and ttt. Dark green tubes project from ION to the contralateral retina via iot. White tubes project from PT to the ipsilateral SP/ISPT complex and contralateral tectum via pspt and cp. Red tubes project from the SP/ISPT complex to the ipsilateral PT and ROT. Light blue tubes project from NFL to NI. Brown tubes project from NIL to NI. Light orange tubes project from Ento to NI and MVL. Dark pink tubes project from the NCL to the NI and AI. Light purple tubes project from MVL to Ento.

Fig 3.12. Semi-lateral view of the primary components of the tectofugal system in the semitransparent diceCT rendered eye and brain with callout boxes of detailed neuroanatomy of 2D sagittal sections of the optic tectum, nucleus rotundus, and entopallium. Callout boxes display important neuron synapses of RGC and TGC, TGC and rotundal neurons, and rotundal neurons and entopallia neurons. Scale bar in each figure is 500 um.

Table 3.1. Rendered tectofugal structures, their abbreviations, and color code.

Table 3.2. Rendered rotundal divisions, their abbreviations, and color code.

Table 3.3. Rendered entopallial divisions, their abbreviations, and color code.

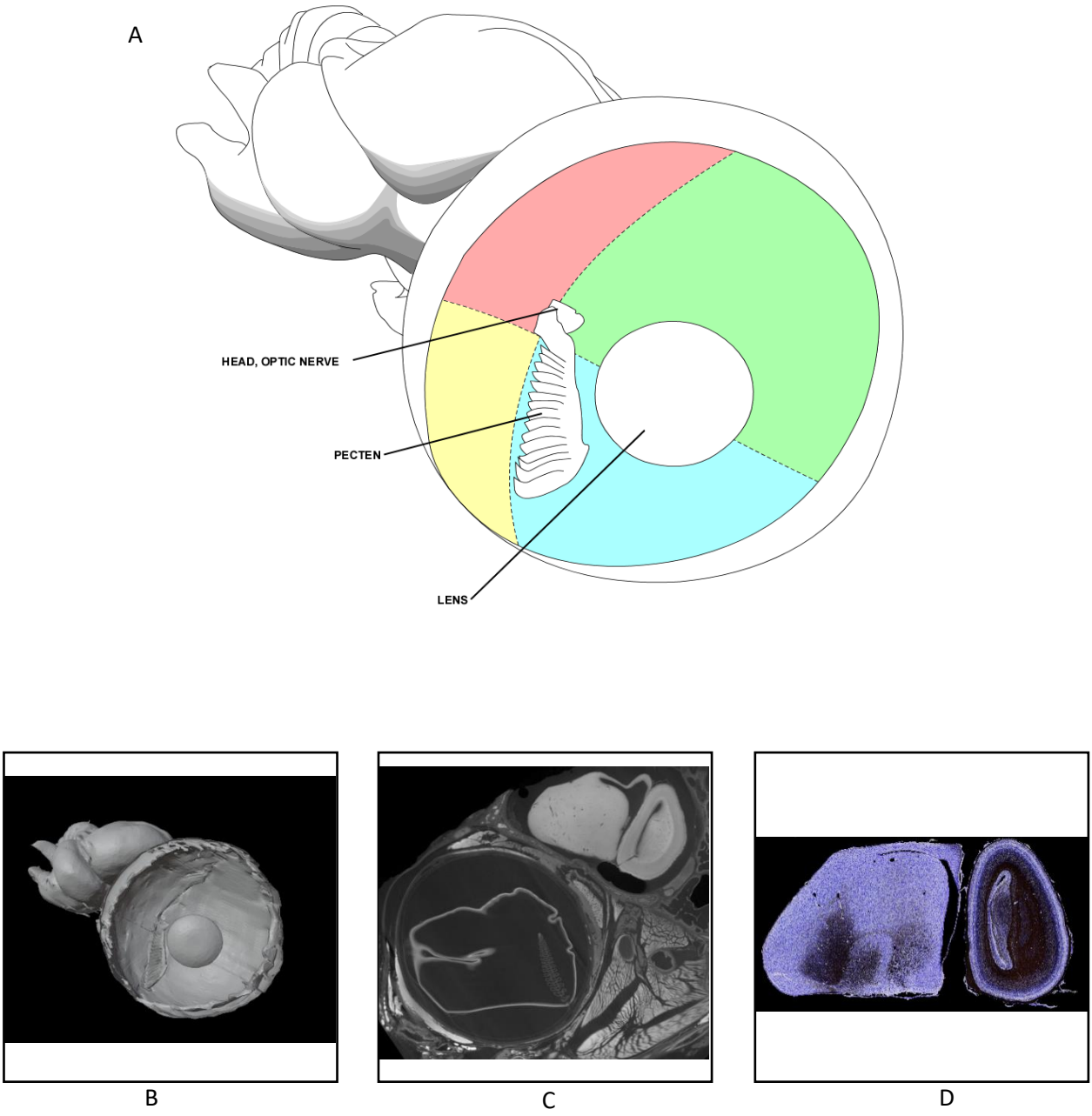

Figure 3.1

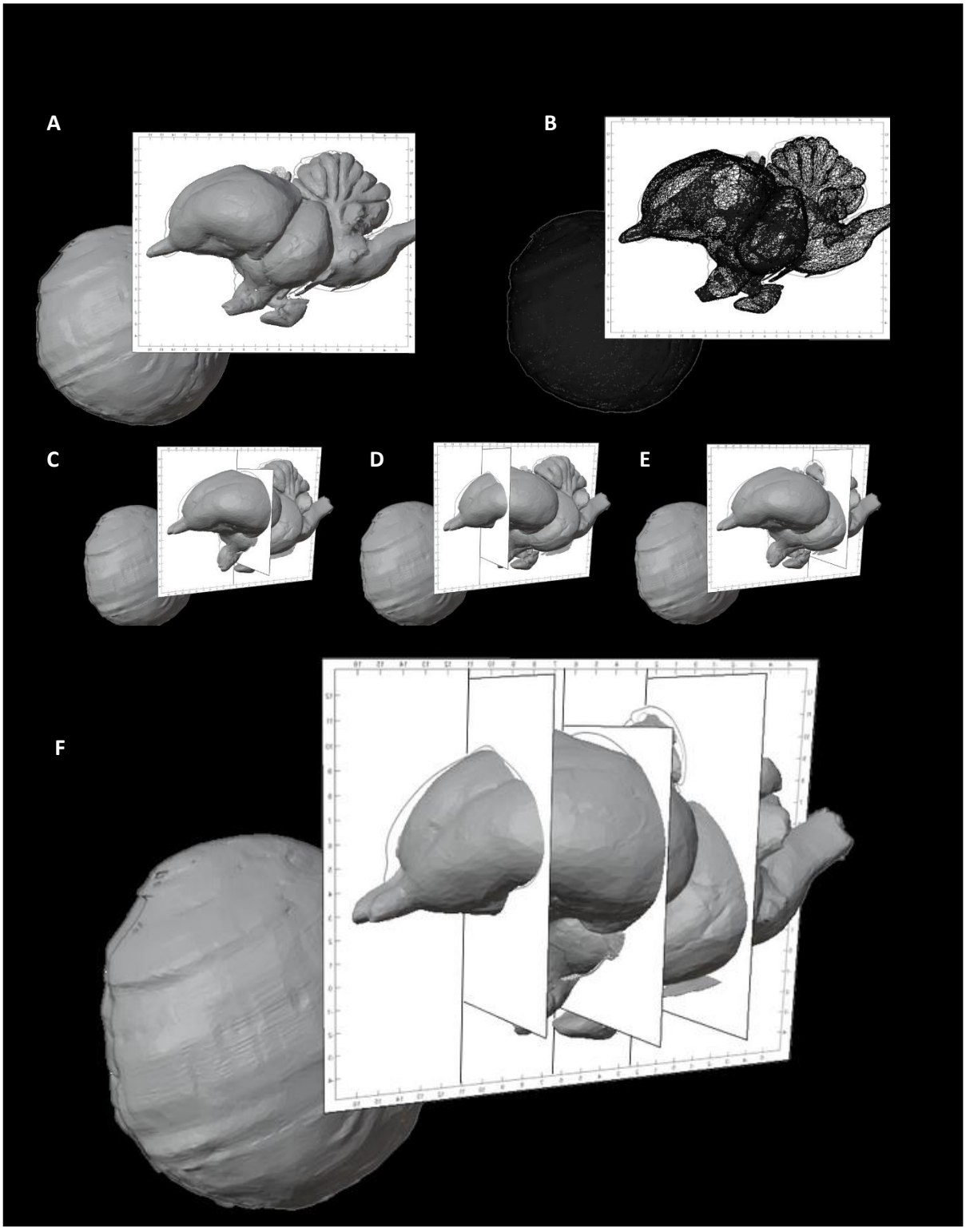

Figure 3.2

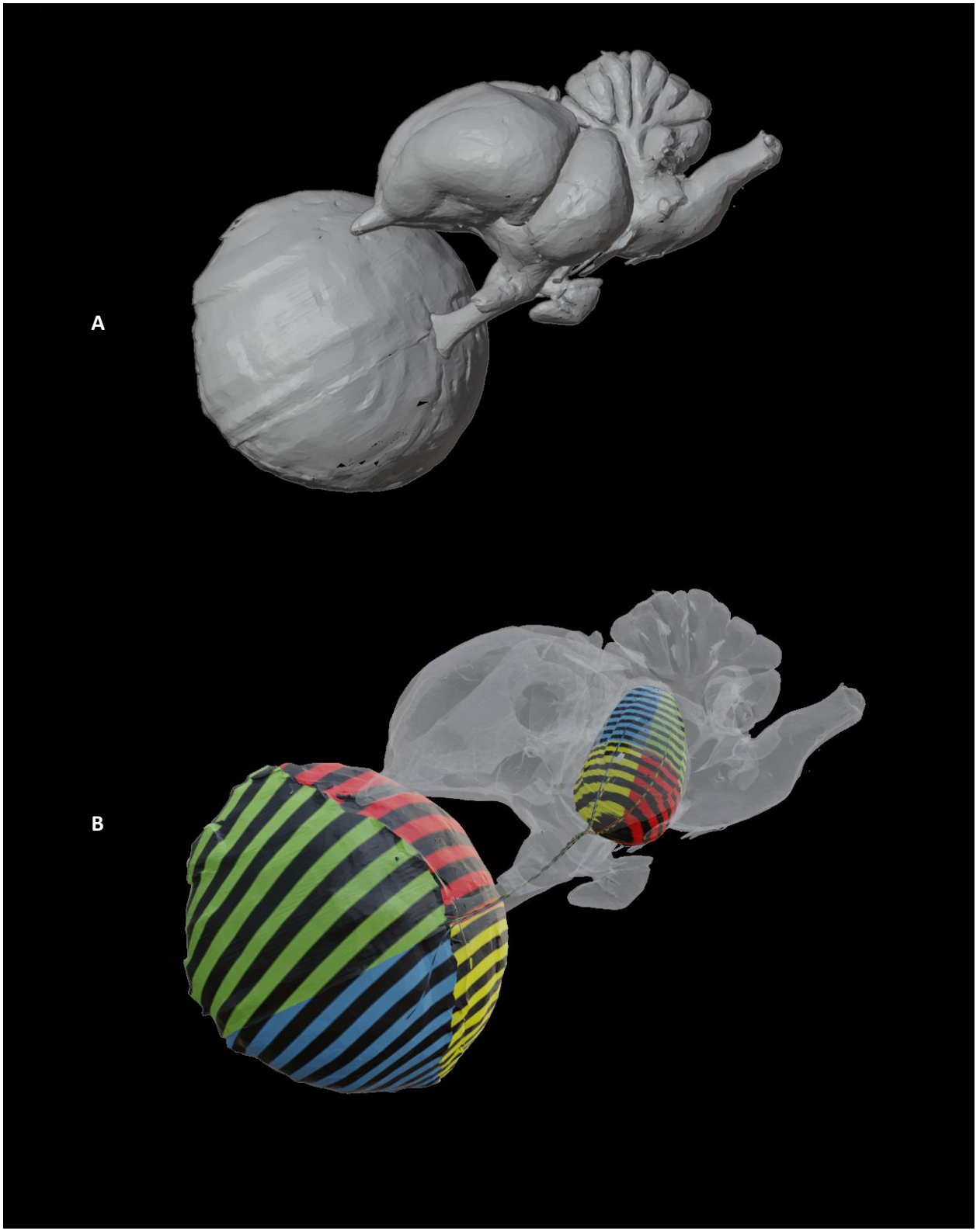

Figure 3.3

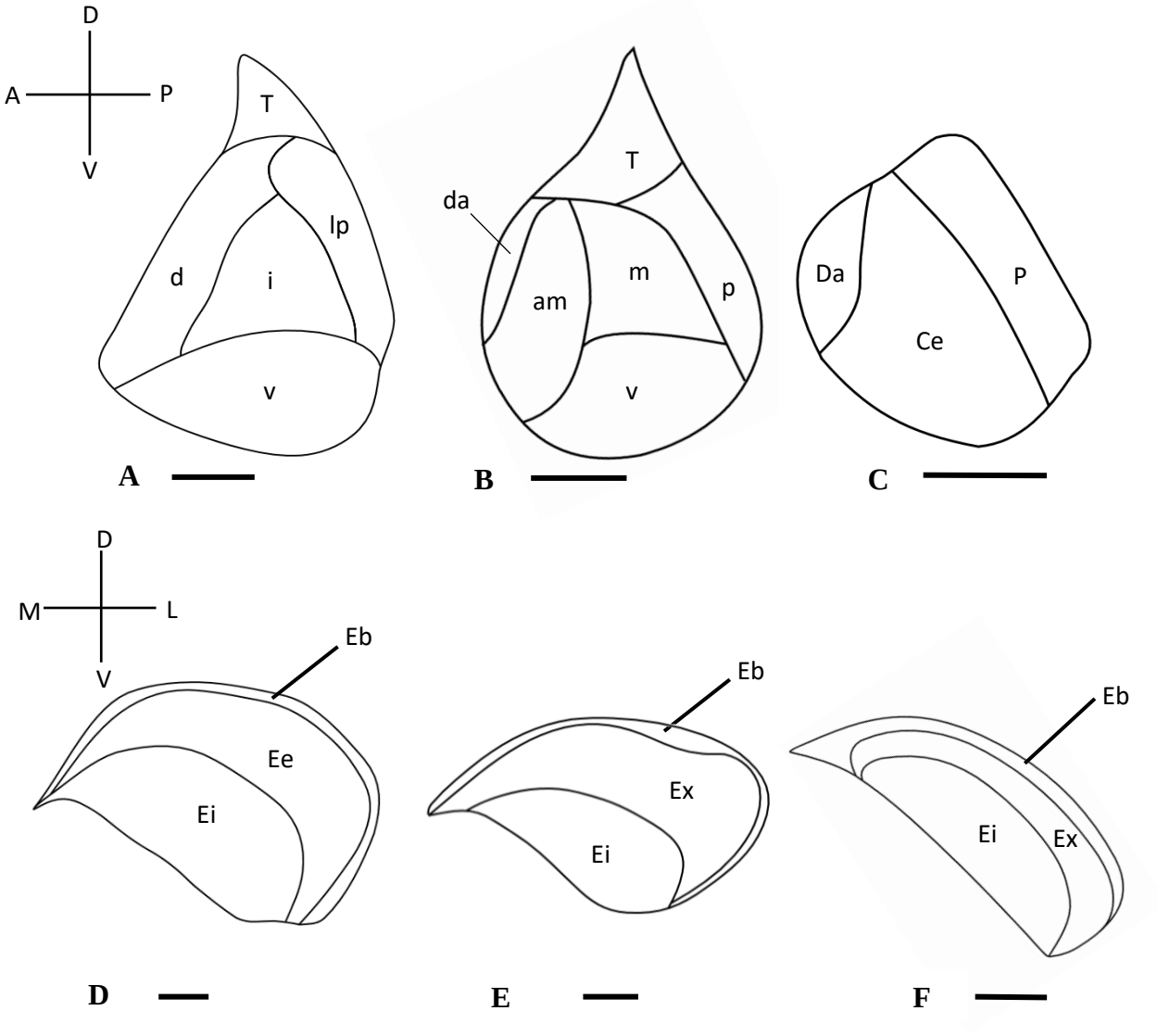
D
A
P
V
T
lp
d
i
v
A
da
T
am
m
p
v
B
Da
P
Ce
C
D
M
L
V
Eb
Ee
Ei
D
Eb
Ex
Ei
E
Eb
Ei
Ex
F

Figure 3.4

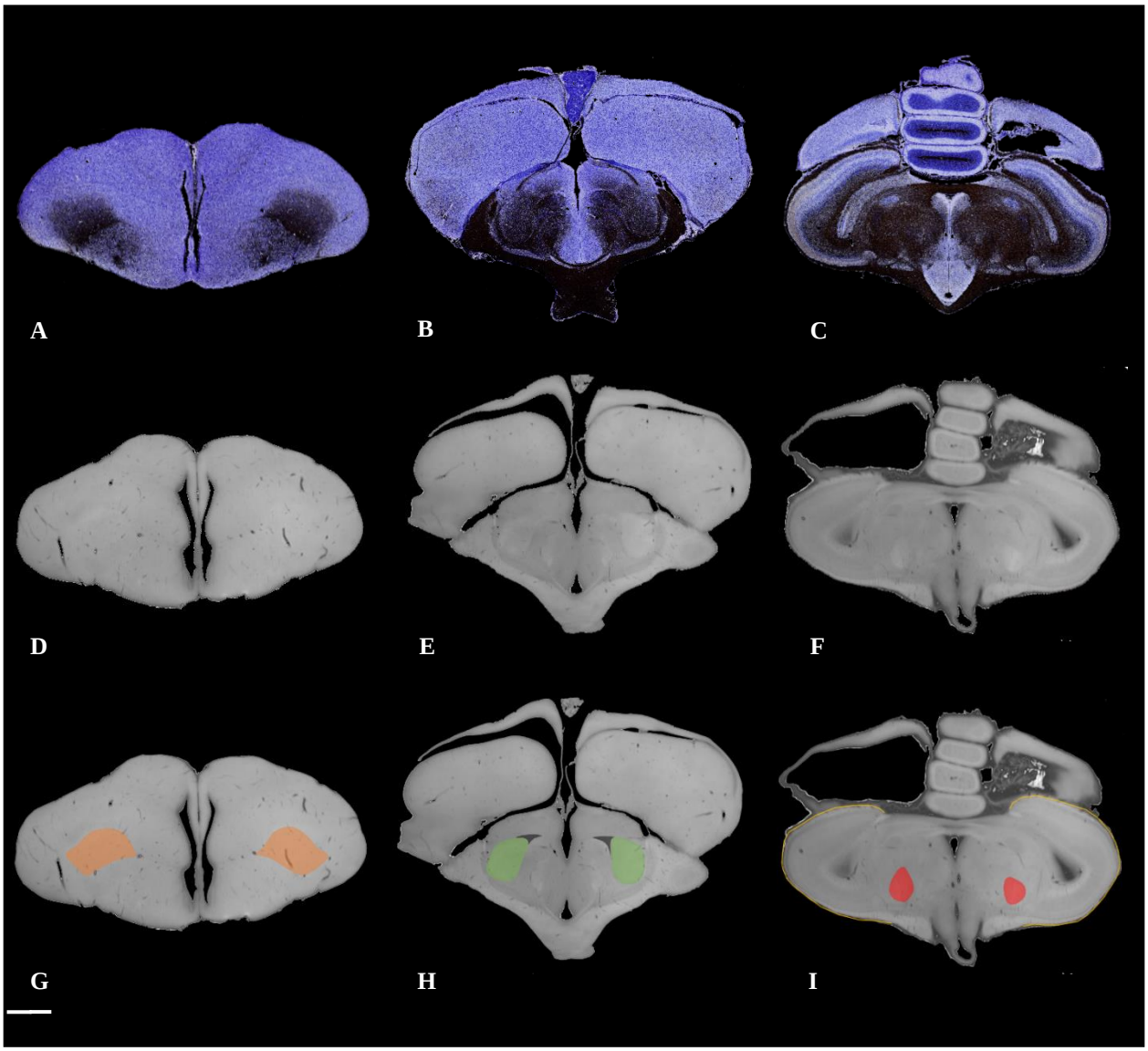

Figure 3.5

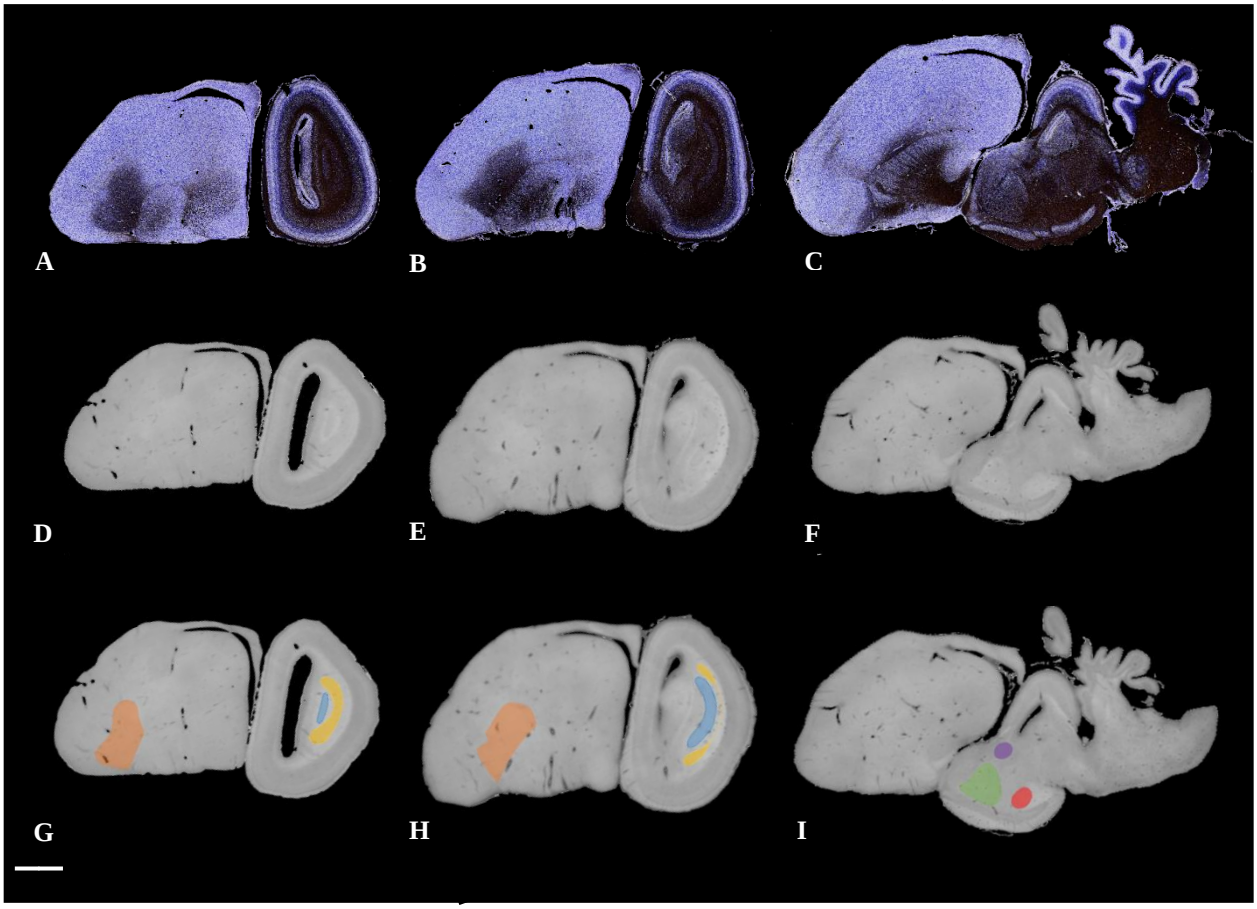

Figure 3.6

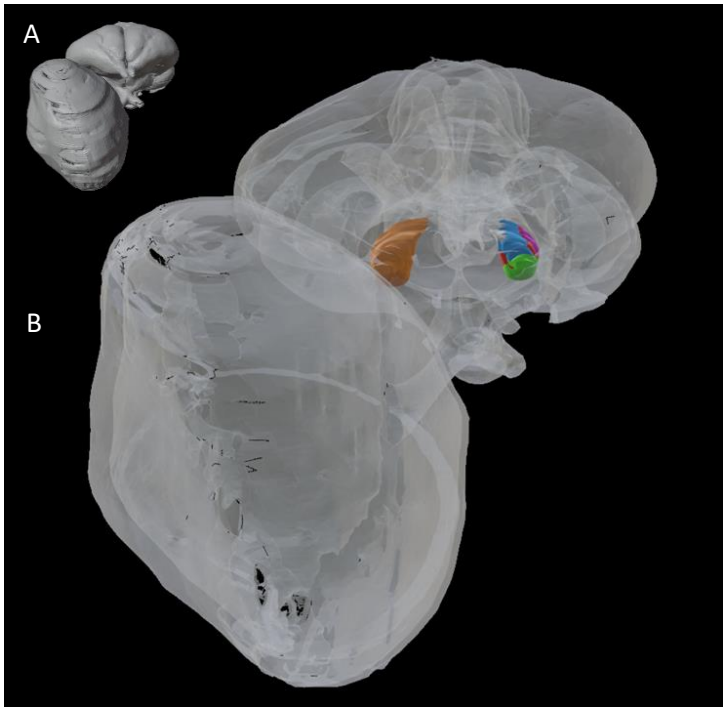

Figure 3.7

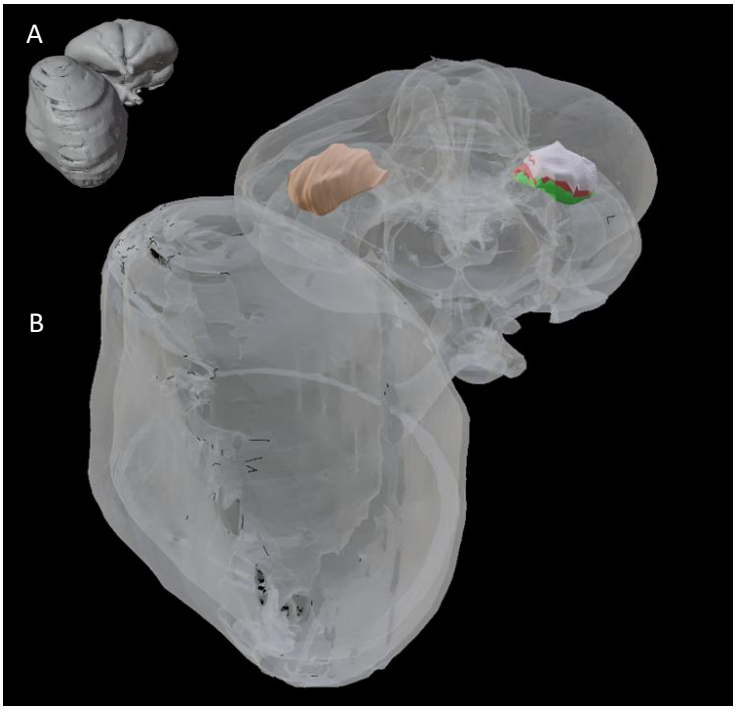

Figure 3.8

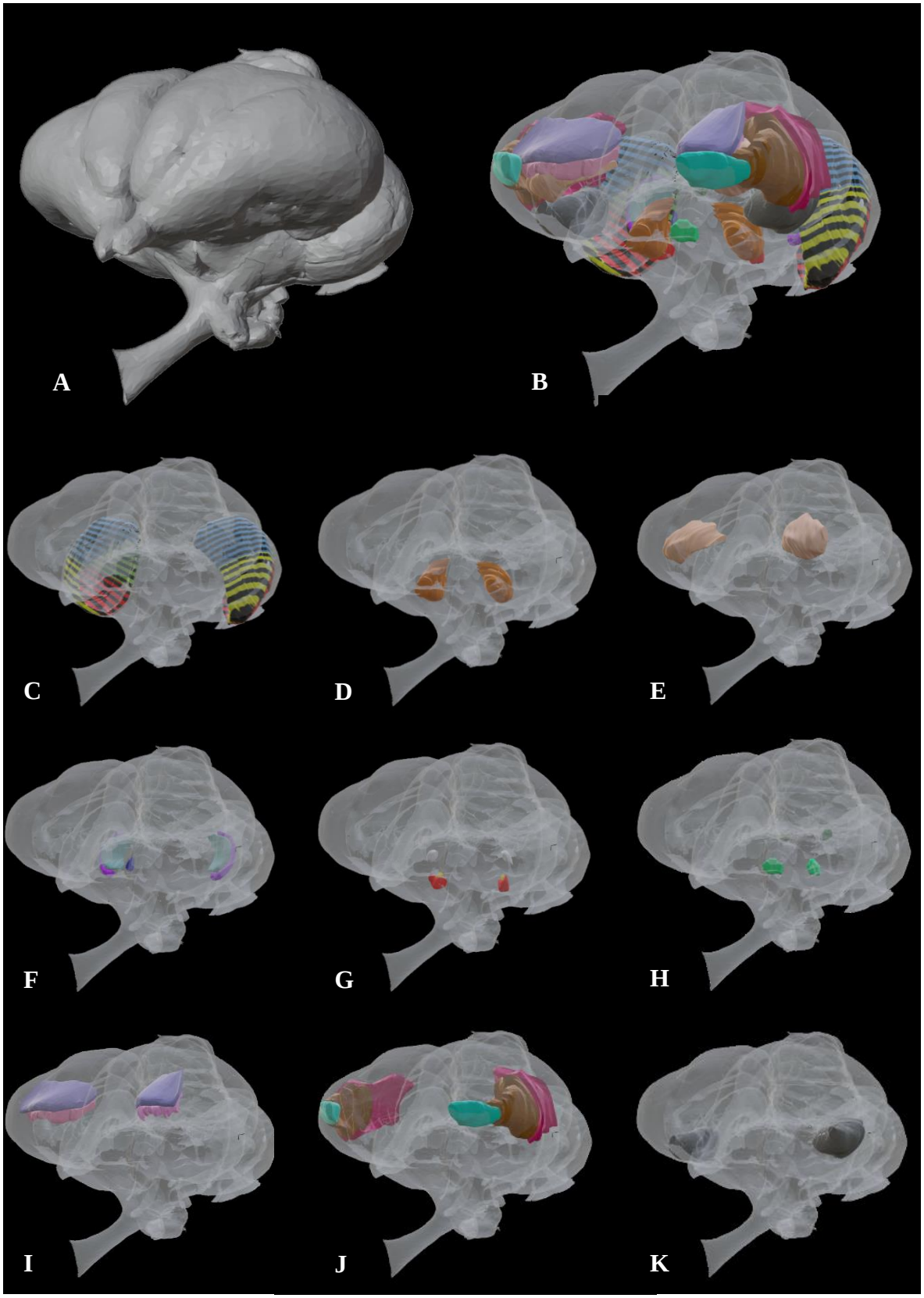

Figure 3.9

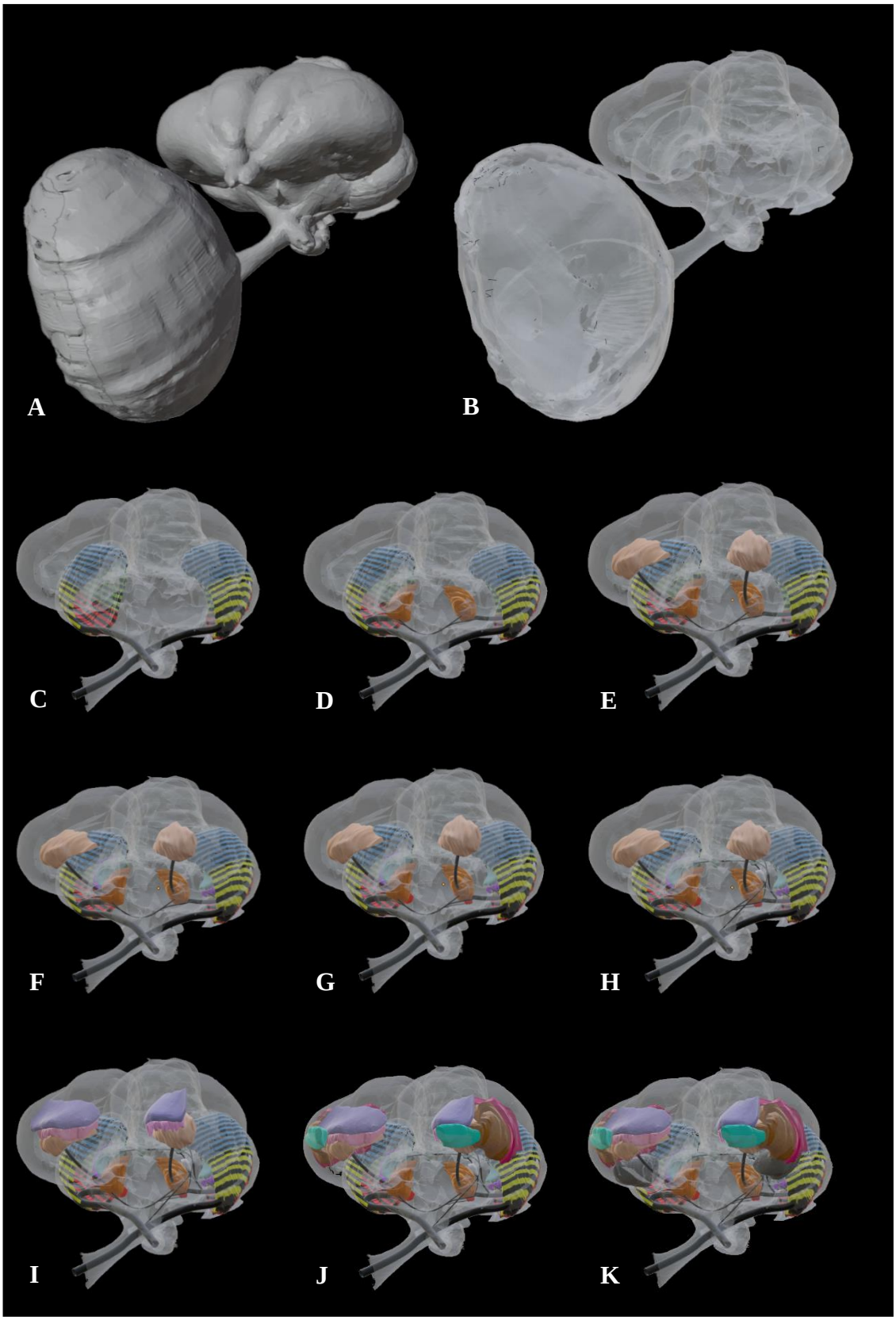

Figure 3.10

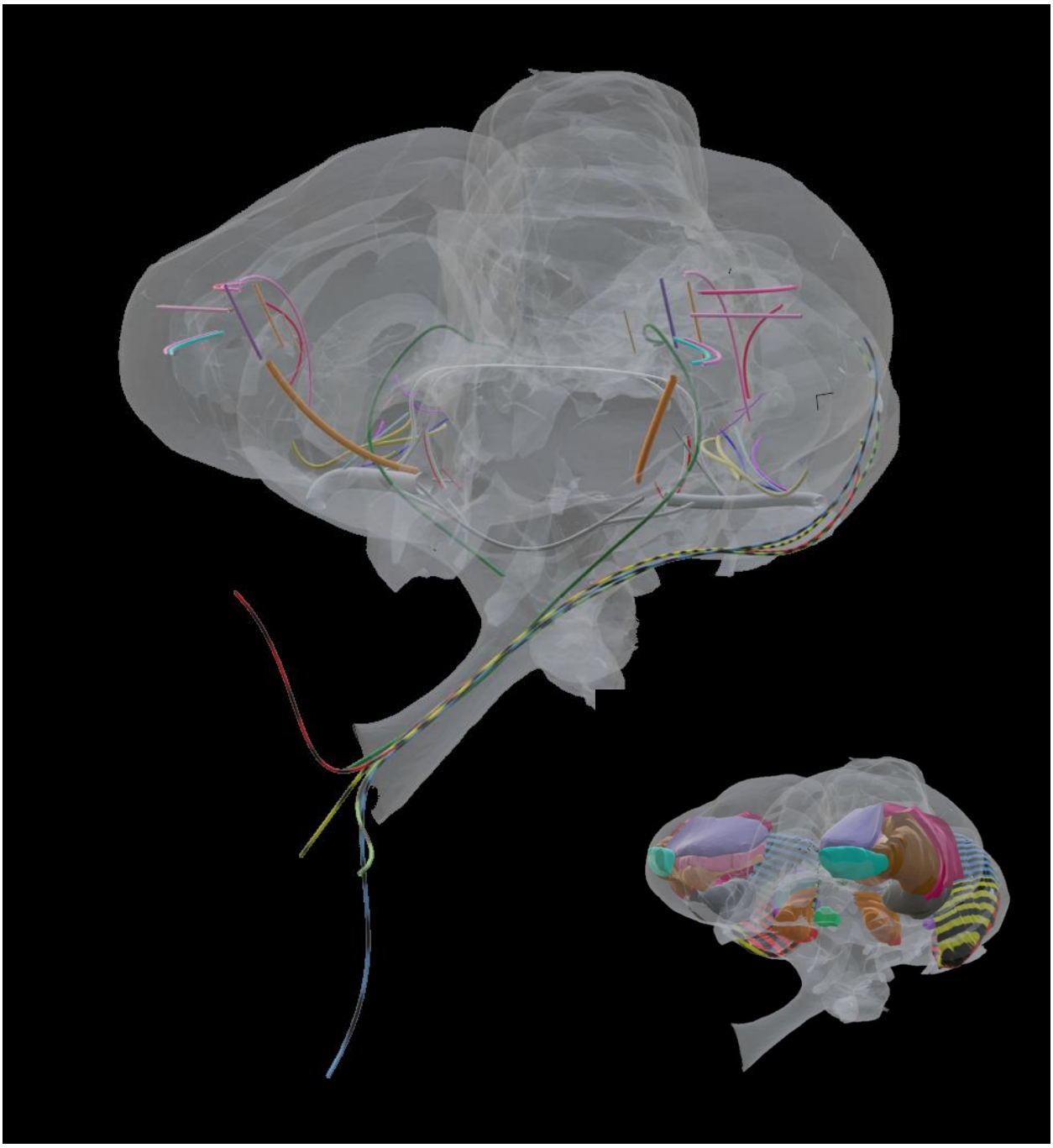

Figure 3.11

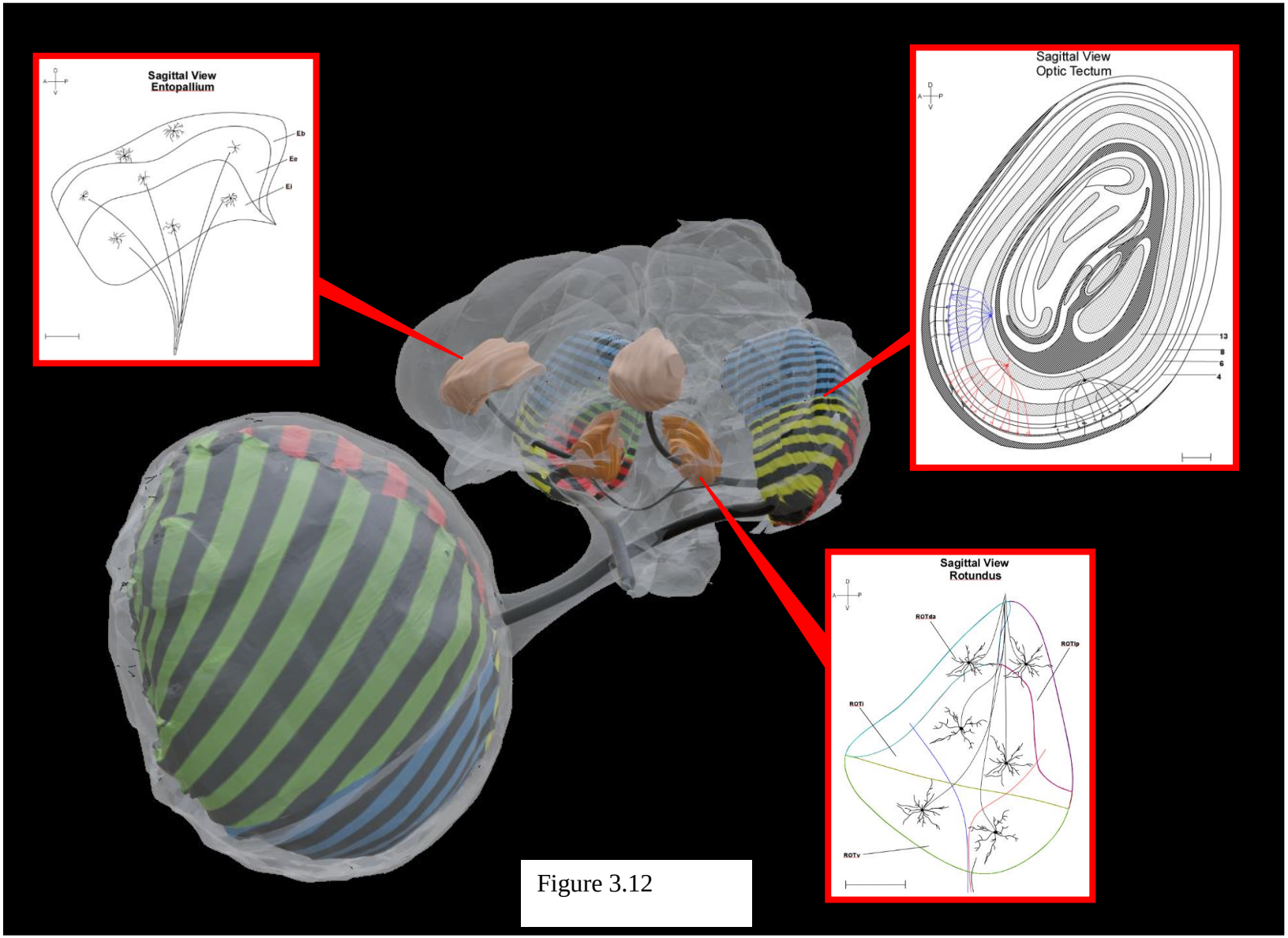
Sagittal View
Entopallium
Eb
Ee
Ei
Sagittal View
Optic Tectum
13
8
6
4
Sagittal View
Rotundus
ROTda
ROTip
ROTl
ROTv

Figure 3.12

Table 3.1

Structure	Abbreviation	Color
Arcopallium intermediate	AI	
Entopallium	E	
intermediate subpretectal nucleus	ISPT	
nucleus isthmi, magnocellular part	Imc	
nucleus isthmi, parvocellular part	Ipc	
isthmo-optic nucleus	ION	
Layer 13	LXIII/SGC	
Layer 5	LV/SGFS	
ventrolateral mesopallium	MVL	
caudolateral mesopallium	NCL	
frontolateral nidopallium	NFL	
intermediate nidopallium	NI	
intermediolateral nidopallium	NIL	
Optic Tectum	TeO	
pretectal nucleus	PT	
nucleus rotundus	ROT	
semilunar nucleus	SLu	
lateral spiriform nucleus	SpL	
subpretectal nucleus	SP	

Table 3.2

Structure	Abbreviation	Color
Dorsal Rotundus	ROTd	
Intermediate Rotundus	ROTi	
Lateral Posterior Rotundus	ROTlp	
Rotundus	ROT	
Triangularis	T	
Ventral Rotundus	ROTv	

Table 3.3

Structure	Abbreviation	Color
Entopallium	E	
Entopallium Belt	Eb	
Internal Core	Ei	
External Core	Ee	

Chapter 4. Visualizing the avian thalamofugal visual pathway in 3D

Parker J. Straight[1], Paul M. Gignac[2,3], Wayne J. Kuenzel[1]

1 Poultry Sci. Dept., University of Arkansas, Fayetteville, AR; 2 Cellular and Molecular Medicine Dept., University of Arizona Health Sciences, Tucson, AZ; 3 MicroCT Imaging Consortium for Research and Outreach, University of Arkansas, Fayetteville, AR

4.1 Abstract

Visual processing in amniotes is typically dominated by one of two visual pathways: the tectofugal pathway or the thalamofugal pathway. In mammals, the thalamofugal pathway dominates with retinal afferents projecting to the lateral geniculate nucleus which then projects to the forebrain. In birds, the thalamofugal pathway plays a lesser role with retinal afferents projecting to the principal optic thalami, a complex of several nuclei that resides in the thalamus. This thalamic complex sends projections to a forebrain structure called the Wulst, the terminal structure of the thalamofugal visual system. The thalamofugal pathway in birds serves many functions such as pattern discrimination, spatial memory, and migration. Many studies utilizing several avian species were reviewed focusing on structures in the avian thalamofugal pathway, their interaction and possible function. Several different subdivisions in the thalamic/pallial structures were found, depending on species examined, age, and techniques utilized. Sections of two-week-old chick brains were cut in either coronal, sagittal, or horizontal planes and stained with Nissl and either Gallyas silver or Luxol Fast Blue. The thalamic principal optic complex and pallial Wulst were subdivided on the basis of cell and fiber density. We utilized the technique of diffusible iodine-based contrast-enhanced computed tomography (diceCT) on a 5-week-old chick, including its eyeball, for our anatomical investigation. Using data from diceCT, our differentially stained histologic sections, and literature, we reconstructed a comprehensive

three-dimensional model of the avian thalamofugal pathway using software from MBF Biosciences Institute. The use of a 3D model provides a clearer understanding of the structural and spatial organization of the thalamofugal system. The ability to integrate histochemical sections with diceCT 3D modeling is critical to better understand the anatomical and physiologic organization of complex pathways such as the thalamofugal visual system.

Keywords: thalamofugal visual system, 3D modeling, diceCT

Abbreviations: ac, anterior commissure; AD, dorsal arcopallium; AI, intermediate arcopallium; ARP, arcopallium; CEV, cresylecht violet; csm, corticoseptomesencephalic tract; dat, dorsal arcopallial tract; diceCT, diffusible iodine-based contrast-enhanced computed tomography; DLAlr, dorsolateral anterior thalamus, lateral rostral part; DLAmc, dorsolateral anterior thalamus, magnocellular part; DLL, dorsolateral anterior thalamus, lateral part; DLLd, dorsal division of the dorsolateral anterior thalamus, lateral part; DLLv, ventral division of the dorsolateral anterior thalamus, lateral part; dsd, dorsal supraoptic decussation; lfb, lateral forebrain bundle; GLd, dorsal lateral geniculate nuclear complex; GSM, gallyas silver myelin; HA, apical hyperpallium; HAI, intercalated nucleus of the apical hyperpallium; HD, densocellular hyperpallium; Hp, hippocampal formation; HIS, superior intercalated hyperpallium; LdOPT, lateral dorsal principal optic thalamus; LFBS, luxol fast blue; N, nissl; NCL, caudolateral nidopallium; NFL, frontolateral nidopallium; NI, intermediate nidopallium; NIL, intermediolateral nidopallium; OPT, nucleus principal optic thalamus; RGCs, retinal ganglion cell; SPC, superficial parvocellular nucleus; SpROT, suprarotundus; W, wulst.

4.2 Introduction

The complex nature of neuroanatomical pathways that facilitate vision afford a number of ways that vertebrates process visual stimuli. Several neural systems are responsible for

processing various visual stimuli, with each system offering distinct anatomical and functional properties. These systems are critical for the development, reproduction, and survival of most vertebrates, making them an important aspect of neurobiological research. The visual capabilities of avian species often are comparable to or exceed those of other vertebrates and are crucial for complex behaviors such as predator detection, migration and homing, mating, flight, and foraging and predation. This makes avian species a great model organism for studying the pathways of vision.

Most of our current knowledge of the avian visual systems have been revealed using traditional approaches, such as gross dissection or 2D histology. These approaches have yielded much information previously unknown within avian neuroscience including characterization of photoreceptor diversity among species (Lopez et al., 2008), reciprocal columnar organization in the forebrain (Stacho et al., 2020), and unique anatomical subdivisions of various visual structures (Martinez de la Torre et al., 1990). For example, the thalamofugal system—a sequence of circuits important to visual processing—has been thoroughly described in the pigeon, chicken, owl and to some degree the zebra finch in terms of its intricate anatomy and to a lesser extent, functionality. The thalamofugal pathway consists of two primary neuronal projections. The first of these projections arise from retinal ganglion cells (RGCs) whose axons form optic nerve and decussate to the contralateral brain where the axons will curve into the thalamus to reach nuclei of the dorsal lateral geniculate nuclear complex (GLd) (Remy and Gunturken, 1991). The second projection arises from differing cell populations of the GLd that will project ipsilaterally, contralaterally, or bilaterally to the Wulst (Wilson, 1980; Miceli et al., 1990; Koshiba et al., 2005; Miceli and Reperant, 1975). The Wulst can be divided into at least four regions, depending on cell morphology, cell density, connectivity, and differential staining (Shimizu and Karten,

1990; Karten et al., 1973; Deng and Rogers, 2000). The Wulst represents the terminus of the thalamofugal circuit; however, the Wulst has several intratelencephalic projections to higher visual associative regions for more complex processing and spatial memory formation (Shimizu et al., 1995; Alpar and Tombol, 1998; Rio et al., 1983). Additionally, the Wulst has several extratelencephalic targets such as the optic tectum and nuclei within the GLd likely performing top-down modulation (Manns et al., 2007; Shimizu et al., 1990).

Notably, these past investigations utilized traditional 2D imaging techniques to study the anatomy of the thalamofugal system. In an attempt to capture 3D relationships, 2D images were often aligned in series to document this pathway in 3D; however, this method falls short in producing a complete 3D visualization, usually due to section alignment issues, sample damage during histological preparation, and relatively larger inter-slice spacing. Altogether, these issues can result in an incomplete understanding of delicate neuroanatomical features and an underappreciation of this complex system. This prompted the need for better 3D visualization techniques that are especially important for documenting highly integrated neural circuits within the brain. For example, the ability to investigate avian neuroanatomy in 3D should enable a more detailed understanding of neural systems and allow for a deeper appreciation of spatial complexity, structural relationships, brain region variation, and developmental mechanisms that define them.

With recent developments in imaging techniques, we now have the opportunity to fill this gap. One such technique, diffusible iodine-based contrast-enhanced computed tomography (diceCT; Gignac et al., 2016), offers an effective mode of visualizing vertebrate nervous tissue. A primary strength of diceCT is the use of contrast agents that selectively bind to white and grey brain matter allowing improved visualization of these neuroanatomical regions of the brain (Gignac

and Kley 2014, 2018). DiceCT, similar to T1-weighted magnetic resonance imaging, displays brain datasets with tissue contrast at resolutions comparable to micro-MRI. Additionally, diceCT can be paired with traditional histological datasets to generate gradual increase in detail from cellular to organism levels (Gignac et al., 2021a,b). Together, this provides the capability for developing a highly detailed, comprehensive 3D model of the visual thalamofugal pathway.

Here we aim to use diceCT to create a current, comprehensive and interactive 3D model illustrating detailed thalamofugal structures utilizing the chick (*Gallus gallus*) as a biomodel to feature accurate, structural data and spatial organization that delineates the flow of information within this complicated system. To provide a detailed model of the tectofugal system for future use in avian neurobiological research and education, we utilize a combination of serial stacked histochemical brain sections and diceCT for 3D reconstruction of visual components of the avian brain to produce a comprehensive anatomical description of the visual thalamofugal pathway. To achieve this, we developed three objectives: (1) reconstruct the thalamofugal nuclei of the dorsolateral geniculate complex, (2) reconstruct the visual Wulst and other telencephalic areas implicated in visual function within the thalamofugal system, and (3) display the interconnectivity among these structures. We hope the methods used to generate a 3D biomodel of the thalamofugal pathway will benefit further research of the avian visual system and other neural systems within the bird brain.

4.3 Materials and Methods

A 3D chicken brain pathway atlas was developed by the use of a multi-modal visualization protocol that is composed of traditional histology and diceCT imaging combined with a stereotaxic atlas of the chick brain in order to have an accurate placement of structures within a brain at their appropriate spatial location and size. Each imaging technique has advantages and

disadvantages, but when combined, the techniques become synergistic. Traditional histology sections the brain into serial slices, allowing for high-resolution, detailed cellular visualization. However, the technique affects spatial relationships and often separates critical neuroanatomical pathways. Alternatively, diceCT offers high-resolution imaging of soft tissue which can be represented as a volume. This allows for the investigation of neuroanatomical features and relationships without separating structures of interest. Here we describe in detail the primary constituents of the visual thalamofugal pathway as well as the axonal flow of information in an interactive 3D model.

4.3.1 Serial histochemical brain sections

We used Luxol fast blue (LFBS), cresylecht violet (CEV), Gallyas Silver Myelin (GSM), and Nissl (N) staining of a two-week-old chicken brain for this study. LFB and CEV as well as GSM and N were paired for better identification of brain nuclei. Luxol fast blue is a basophilic myelin sheath stain that stains nerve fibers blue as a major constituent of nerve processes is phospholipid. In contrast, CEV is an acidophilic agent that stains Nissl bodies (i.e., rough endoplasmic reticulum) dark purple. The GSM method is a silver stain that stains myelinated fibers (i.e., dendrites and axons) black. Pairing LFBS and CEV, and GSM and N together help to determine individual groups of cells defining a nucleus. GSM and N, and LFBS and CEV sets of slides were likewise available in three planes.

4.3.2 Diffusible iodine-based contrast-enhanced computed tomography

Following anesthesia, a 5-week-old chick was perfused with 0.1M phosphate buffered saline followed by 4% paraformaldehyde. After fixation, the sample was completely submerged in a 1% weight-by-volume (w/v) solution of iodine potassium-iodide (I_2KI, a.k.a., Lugol's iodine) for 40 days at room temperature (Gignac et al., 2016; Gignac and Kley, 2018). To promote staining,

the calvarium and left lateral region of the braincase were partly removed and trepanned. This minimized the effect of a fully closed braincase to reduce stain diffusion rates, enabling usage of a relatively low (i.e., 1% w/v) concentration necessary for minimizing brain shrinkage (Dawood et al., 2021). When necessary, the solution was refreshed with an additional 1% I_2KI, and this was performed to prevent the color of the Lugol's iodine staining from becoming paler over time.

While in the staining solution, iodine naturally diffuses into a brain sample. The primary aqueous form of Lugol's iodine is triiodide (I_3^-), which has an affinity for sugars and, especially, lipids (Gignac et al., 2016). As the staining agent diffuses into the sample, the dark-colored I_3^- polymers collect in regions high in these constituents, such as the myelinated sheaths of oligodendrocytes and Schwann cells. Over time, the staining solution loses its dark appearance as the majority of I_3^- becomes bound within the cells of the sample. This is beneficial for X-ray imaging of brain tissue because I_3^- is also radiopaque, enabling it to absorb X-rays during µCT scanning. As a result, white matter (along with other fatty and carbohydrate rich tissues) can be readily differentiated from surrounding structures. Altogether, this enables the 3D visualization of nervous, muscular, epithelial, bony, and special sensory structures simultaneously.

4.3.3 Image Acquisition and Processing

The diceCT sample was imaged using a 2018 Nikon XT H 225 ST µCT system (Nikon Metrology, Brighton, MI) at the MicroCT Imaging Consortium for Research and Outreach (MICRO) at the University of Arkansas, Fayetteville campus. The sample was sealed separately into 50ml low-density, plastic tube filled with water (to prevent dehydration). The tube was positioned within the scanning chamber for µCT imaging. To optimize scan parameters a scout image was performed, following Gignac and Kley (2018). The sample was scanned at an

isometric voxel size of 19.499 microns, using 211 kV, 91 µ-Amperage, a 708-millisecond exposure setting, and 8x multi-frame averaging with a rotating tungsten target and 0.125 mm thick copper filter. The minimize ring artifacts setting was on to reduce the number of visible rings that may appear on scanned images. µCT volumes were reconstructed using Nikon µCT software and VG Studio Max (Volume Graphics GmbH, Heidelberg, Germany) on an HP z800 workstation (Hewlett- Packard, Palo Alto, CA, USA). The resulting dataset was exported as a stack of TIFF images for development of 3D models (see Gignac and Kley, 2018).

4.3.4 Anatomical Reconstruction

Both the serial histochemical and diceCT datasets were used in the reconstruction of the whole brain and important structures of the thalamofugal pathway. To provide anatomical reference needed for the correct orientation of the whole brain and skull models, the inner ear canals, visible in the µCT scan, were rendered in 3D using AvizoLite 2020 (Thermo Fisher Scientific Inc., Waltham, MA). The reference orientation was consistent with the positioning of the brain and skull in a stereotaxic instrument and was used to standardize the positioning of histological sections. This enabled us to ensure that sagittal histochemical sections were reoriented to match the 45° (from horizontal) orientation of the skull in the stereotaxic atlas of Kuenzel and Masson (1988).

AvizoLite 2020 was also used with the diceCT dataset to delineate the whole brain, including several thalamofugal structures. The whole brain surface and feature of the thalamofugal system were 3D rendered from the background and surrounding tissues based on differences in grayscale contrast afforded by differential iodine staining of white and gray matter (see Gignac and Kley, 2018, Gignac et al., 2021). For segmentation in our histochemical series, manual registration was performed for both the brain surface and neural structures of the thalamofugal

pathway. Segmentation of thalamofugal constituents was performed in coronal sections; however, sagittal and horizontal sections were available for reference.

Serial histochemical sections were stacked after segmentation within Brainmaker (MBF Biosciences, Williston, VT) to produce 3D volumes of thalamofugal structures and the important fiber systems they use. All 3D models from diceCT and serial histology were exported as surface files (.obj and .stl format). Files were imported into Blender (Blender Foundation, Amsterdam, Netherlands) and combined to create a complete representation of the thalamofugal visual system.

For spatial alignment of the datasets, stereotaxic images were imported into Blender. We first imported a midline sagittal atlas section and isometrically scaled it to match the brain surface in size and orientation. We then imported a series of coronal stereotaxic atlas sections and isometrically scaled them to align with the brain surface so that they crossed through the midline sagittal section at their respective atlas coordinates of Kuenzel and Masson (1988) (see Fig. 4.1).

4.3.5 Figure Preparation

Orientations of the brain and the segmented thalamofugal components and fiber systems for figures 4.2-4.8 were chosen to best visualize as many structures as possible within their appropriate location of the eye and brain. The Windows snipping tool software (version 10.2008.2277.0, Microsoft Corp., Redmont, WA, USA) was used to capture static images of the reconstructed 3D model. Due to the inherent grey background of the Blender environment, and the semitransparent nature of the whole brain rendering, we chose to replace the background. Selected images were imported into GIMP 2.10.30. Using the color selection and crop tools, the grey background was removed and replaced with a transparent background. The smudge tool

was used to fix mistakenly cropped information whose pixels had similar grayscale values to the background that was removed. The select and fill tools were used to add a uniform black background to easily distinguish the semitransparent brain surface and solid neural structures and fibers underneath. Additionally, series of histological and diceCT brain sections from coronal datasets were selected for figure 4.2. Histologic brain sections were selected due to their visualization of key thalamofugal structures and then paired to respective diceCT images. For the diceCT sections, we chose to upsample images for the sole purpose of figure clarity, using TopazLabs (Dallas, TX, USA) Gigapixel AI image enhancement software. The process of upsampling 2D diceCT images subdivides each pixel into several smaller subpixels. Gigapixel AI machine learning algorithms interpret the grayscale values of each target pixel along with the surrounding pixels to interpolate a grayscale value for each new subpixel. This enables, for example, a square image that is 100 x 100 pixels to become a 600 x 600 pixel image, showing the same visualization, but with higher interpolated spatial detail. The use of thousands of image datasets to train Gigapixel AI machine learning algorithm also enables the software to scale noise, blur, and adjust luminance values to maintain image quality comparable to the original image. Effectively, this process permits zooming into 2D images beyond the spatial detail provided by the original detector hardware and helical reconstruction process (e.g., for computed tomography), but with minimal visual artifacts.

4.3.6 Terminology

For thalamofugal structures we primarily used the terminology from the atlas of Kuenzel and Masson (1988). For many of the forebrain regions, we adopted the nomenclature of Reiner et al. (2004). Furthermore, we used recent literature for nomenclature of thalamofugal structures.

4.4 Results

In this section, we describe the neuroanatomy of the chicken thalamofugal system following the direction of information flow, starting from the retina. The circuit is composed of two primary neuron projections. The first begins with the retinal ganglion cells (RGCs) whose cell bodies reside in the ganglion cell layer of the retina. The RGCs receive input from bipolar neurons and send projections out of the back of the eye as the optic nerve. The RGC axons will move through the optic chiasma to the contralateral hemisphere where the terminals will synapse in various visual nuclei that make up the dorsal lateral geniculate (GLd) complex. These nuclei comprise the second primary neuronal projection that will then send ipsilateral, contralateral, or bilateral input to the visual Wulst.

4.4.1 Retina

Processing of visual information begins at the level of the retina, a multilayered structure with several unique sets of cells that reside within various sublaminae. Visual field properties are processed by several classes of photoreceptors who send these signals to RGCs via bipolar cell mediators (chicken: Lopez-Lopez et al., 2008; Kram et al., 2010; Okano, 1992; pigeon: Bowmaker, 1977; zebra finch: Hunt et al., 1996). Retinal ganglion cells primarily from the yellow field, the large central region of the retina, project via the optic tract to the contralateral dorsal geniculate nuclear complex (Remy and Gunturken, 1991; Miceli et al., 2006). Each nuclear component of the GLd receives a different distribution of contralateral visual input.

Avian Midbrain

4.4.2 DLAlr

The dorsolateral anterior thalamus, lateral rostral part (DLAlr) is the most anterior nucleus of the GLd complex. The DLAlr receives comparatively weak retinal innervation (Miceli et al.,

2006). DLAlr appears at atlas plate A8.0 and is a small round nucleus that primarily projects to the contralateral Wulst. It was difficult to determine the boundaries of this nucleus toward its caudal end, but we were able to segment it and produce a 3D volume in Figs 4.4b and 4.6e-n

4.4.3 DLAmc

The dorsolateral anterior thalamus, magnocellular part (DLAmc) resides in the anterior half of the GLd, located caudally to the DLAlr. This structure maintains a round shape and first appears in coronal sections at atlas plate A 7.8. The DLAmc receives weak retinal innervation compared to other nuclei of the GLd complex. The DLAmc consists of mixed populations of cells that project either ipsilaterally using the lateral forebrain bundle, or contralaterally using the dorsal supraoptic decussation and then the lateral forebrain bundle. We reconstructed the DLAmc in Fig 4.4b and 4.6f-n.

4.4.4 DLL

The dorsolateral anterior thalamus, lateral part (DLL) is the largest component of the GLd complex. It first appears in coronal sections at plate A7.4 and comprises the caudal portion of the GLd. This nucleus can be divided into ventromedial (DLLvm) and dorsolateral (DLLdl) subdivisions on the basis of cell density, differential projections, and choline acetyltransferase and glutamic acid decarboxylase staining (Miceli et al., 2008; Gunturken and Karten, 1991; Koshiba et al., 2005; Miceli et al., 1990). The DLLdl is composed of mostly contralateral projections with minor ipsilateral projections to the Wulst, whereas the DLLvm is composed of mostly ipsilateral projections with minor contralateral projections to the Wulst (Miceli et al. 1990). Interestingly, recent studies in the garden warbler and homing pigeon have implicated this structure in magnetic compass orientation during night-time migration and navigation, respectively (Jorge et al., 2017; Heyers et al., 2007). We were able to identify the DLL in both

LFBS/CEV and GSM/N stains; however, subdivisions were only observable in the LFBS/CEV combination stain due to overwhelming staining of fibers in the GSM/CEV method (Figs 4.4b, 4.6h-n).

4.4.5 SPC

The superficial parvocellular nucleus (SPC) is located dorsal and lateral to the DLL and maintains an elongated oval-like shape. The SPC receives weak retinal innervation from the contralateral retina and projects primarily to the contralateral Wulst (Miceli et al., 1990; Deng and Rogers 1998). The SPC can be divided into dorsal and ventral subdivisions by using cell size as the dorsal subdivision is characterized by small cells and the ventral division characterized by medium-sized cells (Gunturken and Karten, 1991). Unfortunately, we could not make out this demarcation likely due to the passing fibers of the corticoseptomesencephalic (csm) tract that runs through the SPC. The SPC was distinguishable in both sets of coronal series as an oval-like structure with an elongated tail moving medially (Figs 4.4b, 4.6h-n).

4.4.6 SpROT

The suprarotundus (SpROT) is a flat nucleus that resides ventral to the DLL and covers the dorsal anterior nucleus rotundus. This structure is distinct from the dorsal DLL and ventral rotundus because of its darkly stained and tightly packed cells. The SpROT can also be differentiated from surrounding structures based on glutamic acid decarboxylase and neuropeptide Y staining (Gunturken and Karten, 1991). The SpROT sends strictly ipsilateral projections to the Wulst utilizing the lateral forebrain bundle. Due to the easily identifiable nature of the SpROT, we were able to segment and produce a volume for its structure (Figs 4.4b, 4.6j-n).

4.4.7 LdOPT

The lateral dorsal principal optic thalamus (LdOPT), also known as the anterodorsal nucleus, sits ventral to the SPC and lateral to the DLL. This is the smallest nucleus of the GLd that maintains a round to oval shape. The LdOPT receives dense input from the contralateral retina and projects onto the contralateral Wulst (Miceli et al., 2006; Deng and Rogers, 1998; Koshiba et al., 2005). This small nucleus was difficult to determine within our coronal histological series, so we utilized several descriptions from the literature to aid in the segmentation of this structure in Fig 4.4b and 4.6i-n (Deng and Rogers, 1998; Koshiba et al., 2005; Manns et al., 2008).

Avian Forebrain

4.4.8 Wulst

The Wulst is the terminal structure of the thalamofugal pathway and occupies a large extent of the dorsomedial pallium. This structure is multilayered, presenting at least 4 regions (HA, apical hyperpallium; HAI, intercalated nucleus of the apical hyperpallium; HIS, superior intercalated hyperpallium; and HD, densocellular hyperpallium) and is often described as the homolog of the striate cortex (Shimizu and Bowers, 1999). The visual Wulst receives bilateral projections from the nuclei of the GLd and projects to several intratelencephalic regions (NCL, NFL, ARP, Hp) and extratelencephic regions (GLd, TeO) (Shimizu et al., 1995; Deng and Rogers, 2000). Several functional studies have shown involvement of the Wulst in several complex functions such as arena pattern discrimination (Budzynski and Bingman, 2004), color reversal learning, sun compass orientation (Budzynski et al., 2002), and categorization of food vs nonfood (Deng and Rogers, 199). The Wulst occupies much of the dorsomedial brain surface and can be delineated at its ventral aspect using the supreme frontal lamina. We could not identify HAI clearly through

the full series of coronal sections, so for the purpose of our model we combined HAI with HA. We segmented the Wulst and delineated the HA, HIS, and HD subdivisions (Figs 4.5b, 4.6k-n).

4.4.9 Nidopallium

The nidopallium, the region of the forebrain residing between the mesopallial lamina and lamina, consists of 4 regions: the intermediate nidopallium (NI), the frontal lateral nidopallium (NFL), the intermediate lateral nidopallium (NIL), and the caudal lateral nidopallium (NCL). Each of these regions have been implicated in visual function; however, only the NCL and NFL have been shown to be involved in the thalamofugal system.

The NFL lies rostral and lateral to the entopallium and maintains a spherical shape. The NFL has been shown to have reciprocal projections to the Wulst (Deng and Rogers, 2000) as well as sending projections to the NFL and intermediate arcopallium (Shimizu et al., 1995; Deng and Rogers, 2000). The NFL has been shown to be involved in context coding and extinction learning (Gao et al., 2019). We segmented the NFL through a series of Gallyas stained brain sections and generated its 3D volume shown in Fig 4.6m-n.

The NCL, the caudal portion of the visual nidopallium, sits behind the NIL and has reciprocal connections with the Wulst. The NCL has been suggested to be the homolog of the mammalian prefrontal cortex on the basis of dopaminergic innervation, connectivity, and that it is a region of multisensory convergence (Hartmann and Gunturken, 1998; Hsiao et al., 2020; Fernandez et al., 2019). The NCL has been implicated in many visual functions such as reversal learning, color perception, and selection and execution of perceptual responses (Hartmann and Gunturken, 1998; Lengersdorf et al., 2014; Hsiao et al., 2020). The NCL is often affiliated with the temporo-parieto-occipital (TPO) area as the border between the structures is difficult to define. For this reason, we likely include part or all of the TPO in our defined NCL boundaries (Fig 4.6m-n).

4.4.11 Arcopallium

The arcopallium can be divided into auditory, trigeminal, and visual sensory regions with the visual domain residing in the intermediate arcopallium (AI) and to some extent the dorsal arcopallium (AD) (Scarf et al., 2016). The visual arcopallium receives projections from the Wulst and sends reciprocal connections bilaterally back to the Wulst with contralateral projections utilizing the anterior commissure (ac) (Deng and Rogers, 2000; Shimizu et al., 1995). The AI represents the beginning of the descending pathway that modulates visuomotor behaviors. The AI sends projections to the optic tectum, SPC, and SROT, likely modulating ascending visual input at the level of the tectofugal pathway and thalamofugal pathway (Fernandez et al., 2019). For the purpose of the thalamofugal system, we segmented the AI and display its connectivity in Fig 4.6n.

4.4.12 Fiber Tracts, Decussations and Commissures

Based on the Gallyas silver fiber staining of coronal and sagittal sections, and intense labeling of myelinated fibers in the diceCT imaging, we reconstructed various fiber projections, tracts commissures, and decussations utilized by the thalamofugal system. Efferent and afferent connections of each structure were manually traced (with a few exceptions) and rendered in 3D. These renderings were replaced by uniformly smooth tubes that mimicked the natural paths axons would take to move from one structure to another. Fig 4.6 shows the rendered axonal flow of information within the semitransparent brain. Fiber thickness was also manipulated in the model in an attempt to represent major and minor efferent and afferent projections (Fig 4.7).

4.5 Discussion

In the present study, we utilized diceCT and a series of histological brain sections to reconstruct in 3D a highly detailed, comprehensive model of the avian thalamofugal pathway.

We identified and bilaterally reconstructed 10 thalamofugal structures, subdivided the Wulst into three divisions, and illustrated the many tracts, commissures, and decussations utilized by this visual pathway. By integrating diceCT, with traditional histochemistry, we were able to illustrate better the thalamofugal system at the 3D whole-brain level.

4.5.1 Thalamofugal System

We investigated the three-dimensional (3D) structure, spatial organization, and connectivity of the thalamofugal pathway using several imaging methods. The thalamofugal pathway begins with photoreceptors of the retina responding to stimuli with differential qualities in the visual field. These photoreceptors produce electrical signals that are transmitted to bipolar cells. Bipolar cells propagate these signals to classes of retinal ganglion cells whose axons form the optic nerve that project to the contralateral GLd. Initial studies on retinal representation in the GLd found evidence that the dorsotemporal retina, known as the red field in pigeons, has an importance in binocular vision and was shown to project to this region. Subsequent studies found that RGCs from the central and nasal retina project to the GLd rather than RGCs from the dorsotemporal retina in laterally eyed species (Miceli et al., 2006). The reason for this contradiction is due to the amount of binocular field overlap and therefore stereopsis that is often seen in owls and raptors (Iwaniuk et al., 2007). The GLd is composed of six components (however, see Koshiba et al., 2003,2004) that receive differential retinal input and produce differential ipsilateral, contralateral, or bilateral output. The boundaries of these nuclei often overlap, making it difficult to discern the true extent of each of these structures. This has also created difficulty in finding functions for each of these nuclei. Early studies often used large lesions to determine the role of GLd in visual behavior; however, there were two issues with these studies: 1) they were damaging several of the nuclei within the GLd and 2) these studies often used an operant

chamber which utilizes a pecking key as the final operant. The pecking key would be visualized with the dorsotemporal retina, and therefore not pertain to the thalamofugal system. Later studies corrected these issues and have begun to uncover specific functional roles of each of these nuclei (e.g. DLL in navigation); however, there is still a need for more in-depth, fine-tuned functional research. Interestingly, the thalamofugal system seems to play a role in both spatial and pattern discrimination, and this suggests that the GLd nuclei may likely contain parallel pathways that process different visual attributes, similar to the rotundus in the tectofugal pathway. Additional investigation using microelectrodes and microinjections of tracers would potentially clarify this functional organization within the GLd nuclei and suggest possible functional domains within the Wulst. These pathways would then be maintained at the level of the Wulst, specifically as the GLd projections synapse with neurons of the HD, HIS, and HAI. These layers of the Wulst would then project onto the HA, which has reciprocal connections with several telencephalic targets (NFL, NCL, ARP, Hp) that perform more complex visual processing. The Hp, for example, is important for encoding spatial memory from Wulst input and is imperative during navigation (Gagliardo et al., 2005; Hough, 2022). Further research is necessary to explore the underlying mechanisms of the interaction of the thalamofugal pathway and the hippocampal formation in spatial memory and its importance to complex visual behaviors such as migration and homing.

4.5.2 General Considerations

A series of immunohistochemical coronal brain sections were imported into Brainmaker for image stacking to create 3D volumes of thalamofugal structures. Specifically, this software enables users to import series of brain sections for processing to generate volumes of outlined structures. The program will automatically create contours, or outlines, around the brain sections.

Several problems may prevent the software from correctly outlining the brain section including shifts in brain regions, damage to the brain section, stain that has diffused into the background, and artificial objects residing in the background. The issues can be fixed in one of two ways: automatically or manually. To attempt to fix this problem automatically, users can manipulate the smoothing and threshold values for detecting and outlining brain sections. The smoothing function will increase or decrease the sleekness of the outlines around the brain section, while the threshold function will increase or decrease the amount of the image included in the outline (lower threshold will likely include artificial objects or background staining). To fix this problem manually, users can manipulate the vertices of the automatically drawn contour or can delete the existing contour and manually draw a new contour around the brain section. The next step of this process is the alignment of the sections. This program offers an automated alignment process with three options: 1) alignment using the center of the image, 2) alignment using the shape of the image, or 3) alignment using the shape of the image and image features. These options are in order of increasing accuracy of alignment and as accuracy increases, so does the processing time. Typically, additional manual corrections to the automated alignment are also necessary. This is likely due to shifts or rotations of the brain sections. The final step is the reconstruction phase, where the software will produce 3D volumes from the series of contours. The software allows additional segmentation by generating manual contours around neural structures of interest. The quality of reconstruction depends on various aspects: number of brain sections in the imported series, consistency of the number of sections, thickness of the brain sections, alignment condition of the series, number of manual contours per structure of interest, and smoothness of manually drawn contours. To ensure superior reconstruction quality, we suggest the following: mount sections as carefully as possible to avoid damage and distortion of tissue, use brain section

thickness ≤ 50 microns, import a complete and consistent series of brain sections, select several extensive reference points when manually aligning brain sections, and use more vertices when creating manual contours.

DiceCT has been implemented in many studies investigating vertebrate anatomy. Several recent avian anatomical studies have utilized diceCT to gain insight into feeding apparatus (Genbrugge et al., 2011; Li and Clarke, 2016), vocal organs (During et al., 2013), craniofacial pathology (Gignac et al., 2021), cranial musculoskeletal anatomy (Lautenschlager et al., 2014; To et al., 2021; Hadden et al., 2021; Jones et al., 2019), brain ontogeny and function (Gold et al., 2016; Watanabe et al., 2019), and forelimb musculoskeletal anatomy (Contreras and Sellers, 2017). DiceCT offers several attributes that traditional histochemistry often lacks, including low cost, ease of access, high precision imaging of 3D soft tissues, and the reversible and non-destructive nature of this technique. These attributes provide diceCT leverage for comparative neuroanatomical studies compared to conventional approaches. We implemented diceCT in our investigation to generate whole-brain and eye surface volumes as they would naturally exist in the skull. These generated models allowed for easy integration of thalamofugal structures for a comprehensive model of the thalamofugal system with accurate spatial organization, structural information, and connectivity. DiceCT also allows for shareability of data via volume surface files or as their original stacks of TIFF images. This produces the opportunity for adaptation of these data as a foundation for future researchers to build upon.

The datasets produced by diceCT and Brainmaker were integrated within the Blender environment. To accomplish this, we imported several atlas images (Kuenzel and Masson, 1988) as references for the alignment of the diceCT endocast (virtual cast of the braincase) and histochemical reconstructions. Using the grid lines within Blender, we imported a midline

sagittal plate and aligned it with the grid to ensure no unusual rotations or scaling complications. Next, we incorporated our diceCT whole-brain and eye reconstruction and scaled and oriented the volume to meet the brain surface outline of the midline sagittal plate L0.2 (Kuenzel and Masson, 1988). We then imported several coronal atlas plates and scaled and aligned them to intersect the midline sagittal plate at their respective coordinates. These initial steps are critical for aligning the rendered thalamofugal structures ensuring correct orientation and scaling of all imported models. Additionally, we chose to render the optic tectum, a large globular-like structure at the lateral expanse of the midbrain, to act as an additional reference for aligning thalamofugal structures. Using the tectum, we were able to integrate the thalamofugal components with accurate size, orientation, and relative location. We noticed substantial overlap of our 3D rendered structures and the boundaries of these structures in the 2D coronal plates. For future work, we would suggest the following: (1) incorporate 2D atlas plates in at least two planes to aid in scaling, orientation, and integration of several models, (2) use an additional reference structure that occupies a portion of the rendered brain surface for validation of scaling, orientation, and location of structures, and (3) understand the maneuvering mechanics, scaling and rotation tools, and viewport shading tools prior to using Blender. Altogether, the Blender software affords users the means to integrate, view, and interact with 3D models at varying levels using an array of tools to study the thalamofugal pathway.

4.5.3 Future Directions

Combining traditional histology with diceCT has enabled a novel channel for research (refs). DiceCT allows users to obtain large-scale information about the whole brain and certain neural structures, while traditional histology allows for detailed sections of neural tissue for visualization of cell morphology and fiber tracts. Together, these different imaging techniques

were used to create a 3D model of the thalamofugal pathway that is highly accurate in structural and spatial organization. Our model can be utilized in the understanding of the components of the thalamofugal pathway, its spatial organization, structure, and connectivity. For the purpose of research, our model will benefit anatomical investigations of the chicken thalamofugal pathway beyond the predefined orientations of conventional 2D imaging techniques. Specifically, this model can assist studies seeking to investigate a specific region of the thalamofugal pathway using electrophysiology, intracellular filling, and tract tracing. Additionally, diceCT enables virtual re-slicing at unorthodox angles for the purpose of visualizing as many structures as possible. DiceCT also has the capability to obtain volumetric data as the voxel size representing the shape and size of neural structures is known. Generation of more thalamofugal models in the chicken would benefit 3D investigation of the ontogenesis of this pathway as well as the generation of thalamofugal models in other avian species to compare interspecific differences and possibly ascertain the functional implications of these differences. These comparisons will expand our understanding of the alterations of structural volume, spatial organization, linear dimensions, and connectivity of components of the thalamofugal pathway and how these alterations are related to different visual ecologies of birds.

Supplementary Information

Please contact PJS for additional datasets, models, and images.

Acknowledgements

We are grateful to Manon Wilson (University of Arkansas) and the MICRO group for their efforts in performing the CT scans on our specimen. We are thankful to Alex Claxton (OSU-CHS) for his help in initial model manipulations in Blender. This project was funded by grants

from the Chancellor's Innovation Grant of UA, 2020-23 to WJK and PMG, Arkansas Biosciences Institute Grant, 2022-23 to WJK, and NSF 1457180 and 1725925 to PMG.

Conflict of Interest

The authors declare no conflict of interest.

Author Contribution

The project was developed by WJK and PMG. PJS created the figures and wrote the manuscript drafts with assistance from WJK and PMG. PJS and PMG created 3D brain and skull reconstructions for the chicken. WJK sampled and prepared the specimen for diceCT imaging and made available sets of histochemical brain sections of chicks.

4.6 References

Alpár, A., & Tömböl, T. (1998). Telencephalic connections of the visual system of the chicken: Tracing the interrelation of the efferents of the visual wulst and the hyperstriatum ventrale. *Annals of Anatomy - Anatomischer Anzeiger*, *180*(6), 529–536. https://doi.org/10.1016/s0940-9602(98)80060-5

Bowmaker, J. K. (1977). The visual pigments, oil droplets and spectral sensitivity of the pigeon. *Vision Research*, *17*(10), 1129–1138. https://doi.org/10.1016/0042-6989(77)90147-x

Bowmaker, J. K., Heath, L. A., Wilkie, S. E., & Hunt, D. M. (1997). Visual pigments and oil droplets from six classes of photoreceptor in the retinas of birds. *Vision Research*, *37*(16), 2183–2194. https://doi.org/10.1016/s0042-6989(97)00026-6

Budzynski, C. A., & Bingman, V. P. (2004). Participation of the thalamofugal visual pathway in a coarse pattern discrimination task in an open arena. *Behavioural Brain Research*, *153*(2), 543–556. https://doi.org/10.1016/j.bbr.2004.01.011

Budzynski, C. A., Gagliardo, A., Ioalé, P., & Bingman, V. P. (2002). Participation of the homing pigeon thalamofugal visual pathway in sun-compass associative learning. *European Journal of Neuroscience*, *15*(1), 197–210. https://doi.org/10.1046/j.0953-816x.2001.01833.x

Deng, C., & Rogers, L. J. (1997). Differential contributions of the two visual pathways to functional lateralization in Chicks. *Behavioural Brain Research*, *87*(2), 173–182. https://doi.org/10.1016/s0166-4328(97)02276-6

Deng, C., & Rogers, L. J. (1998). Bilaterally projecting neurons in the two visual pathways of Chicks. *Brain Research*, *794*(2), 281–290. https://doi.org/10.1016/s0006-8993(98)00237-6

Deng, C., & Rogers, L. J. (2000). Organization of intratelencephalic projections to the Visual Wulst of the chick. *Brain Research, 856*(1-2), 152–162. https://doi.org/10.1016/s0006-8993(99)02403-8

Fernández, M., Ahumada-Galleguillos, P., Sentis, E., Marín, G., & Mpodozis, J. (2019). Intratelencephalic projections of the avian visual dorsal ventricular ridge: Laminarly segregated, reciprocally and topographically organized. *Journal of Comparative Neurology, 528*(2), 321–359. https://doi.org/10.1002/cne.24757

Fernández, M., Morales, C., Durán, E., Fernández-Colleman, S., Sentis, E., Mpodozis, J., Karten, H. J., & Marín, G. J. (2019). Parallel Organization of the avian sensorimotor arcopallium: Tectofugal visual pathway in the pigeon (*Columba livia*). *Journal of Comparative Neurology, 528*(4), 597–623. https://doi.org/10.1002/cne.24775

Gagliardo, A., Vallortigara, G., Nardi, D., & Bingman, V. P. (2005). A lateralized avian hippocampus: Preferential role of the left hippocampal formation in homing pigeon Sun Compass-based spatial learning. *European Journal of Neuroscience, 22*(10), 2549–2559. https://doi.org/10.1111/j.1460-9568.2005.04444.x

Gao, M., Lengersdorf, D., Stüttgen, M. C., & Güntürkün, O. (2019). Transient inactivation of the visual-associative nidopallium frontolaterale (NFL) impairs extinction learning and context encoding in pigeons. *Neurobiology of Learning and Memory, 158*, 50–59. https://doi.org/10.1016/j.nlm.2019.01.012

Gignac, P. M., & Kley, N. J. (2014). Iodine-enhanced micro-CT imaging: Methodological refinements for the study of the soft-tissue anatomy of post-embryonic vertebrates. *Journal of Experimental Zoology Part B: Molecular and Developmental Evolution, 322*(3), 166–176. https://doi.org/10.1002/jez.b.22561

Gignac, P. M., & Kley, N. J. (2018). The utility of dicect imaging for high-throughput comparative neuroanatomical studies. *Brain, Behavior and Evolution, 91*(3), 180–190. https://doi.org/10.1159/000485476

Gignac, P. M., Green, T. L., Oehler, D. A., Malatos, J., Paré, J. A., & Hollinger, C. (2021). Diffusible iodine-based contrast-enhanced computed tomography as a necropsy aid: A case report evaluating respiratory disease in *Macrocephalon maleo*. *Journal of Zoo and Wildlife Medicine, 52*(1). https://doi.org/10.1638/2020-0086

Gignac, P. M., Kley, N. J., Clarke, J. A., Colbert, M. W., Morhardt, A. C., Cerio, D., Cost, I. N., Cox, P. G., Daza, J. D., Early, C. M., Echols, M. S., Henkelman, R. M., Herdina, A. N., Holliday, C. M., Li, Z., Mahlow, K., Merchant, S., Müller, J., Orsbon, C. P., … Witmer, L. M. (2016). Diffusible iodine-based contrast-enhanced computed tomography (dicect): An emerging tool for rapid, high-resolution, 3-D imaging of metazoan soft tissues. *Journal of Anatomy, 228*(6), 889–909. https://doi.org/10.1111/joa.12449

Gignac, P. M., O'Brien, H. D., Sanchez, J., & Vazquez-Sanroman, D. (2021). Multiscale imaging of the Rat Brain using an integrated dicect and histology workflow. *Brain Structure and Function, 226*(7), 2153–2168. https://doi.org/10.1007/s00429-021-02316-6

Güntürkün, O., & Karten, H. J. (1991). An immunocytochemical analysis of the lateral geniculate complex in the pigeon (*Columba livia*). *Journal of Comparative Neurology*, *314*(4), 721–749. https://doi.org/10.1002/cne.903140407

Hartmann, B., & Güntürkün, O. (1998). Selective deficits in reversal learning after neostriatum caudolaterale lesions in pigeons: Possible behavioral equivalencies to the mammalian prefrontal system. *Behavioural Brain Research*, *96*(1-2), 125–133. https://doi.org/10.1016/s0166-4328(98)00006-0

Heyers, D., Manns, M., Luksch, H., Güntürkün, O., & Mouritsen, H. (2007). A visual pathway links brain structures active during magnetic compass orientation in migratory birds. *PLoS ONE*, *2*(9). https://doi.org/10.1371/journal.pone.0000937

Hough, G. E. (2022). Neural substrates of homing pigeon spatial navigation: Results from Electrophysiology Studies. *Frontiers in Psychology*, *13*. https://doi.org/10.3389/fpsyg.2022.867939

Hsiao, Y.-T., Chen, T.-C., Yu, P.-H., Huang, D.-S., Hu, F.-R., Chuong, C.-M., & Chang, F.-C. (2020). Connectivity between nidopallium caudolateral and visual pathways in color perception of zebra finches. *Scientific Reports*, *10*(1). https://doi.org/10.1038/s41598-020-76542-z

Iwaniuk, A. N., Heesy, C. P., Hall, M. I., & Wylie, D. R. (2007). Relative wulst volume is correlated with orbit orientation and binocular visual field in birds. *Journal of Comparative Physiology A*, *194*(3), 267–282. https://doi.org/10.1007/s00359-007-0304-0

Jorge, P. E., Pinto, B. V., Bingman, V. P., & Phillips, J. B. (2017). Involvement of the avian dorsal thalamic nuclei in homing pigeon navigation. *Frontiers in Behavioral Neuroscience*, *11*. https://doi.org/10.3389/fnbeh.2017.00213

Karten, H. J., Hodos, W., Nauta, W. J., & Revzin, A. M. (1973). Neural connections of the "visual wulst" of the avian telencephalon. experimental studies in the pigeon (*Columba livia*) and owl (*Speotyto cunicularia*). *The Journal of Comparative Neurology*, *150*(3), 253–277. https://doi.org/10.1002/cne.901500303

Koshiba, M., Kikuchi, T., Yohda, M., & Nakamura, S. (2002). Inversion of the anatomical lateralization of Chick Thalamofugal Visual pathway by light experience. *Neuroscience Letters*, *318*(3), 113–116. https://doi.org/10.1016/s0304-3940(01)02306-0

Koshiba, M., Nakamura, S., Deng, C., & Rogers, L. J. (2003). Light-dependent development of asymmetry in the ipsilateral and contralateral thalamofugal visual projections of the chick. *Neuroscience Letters*, *336*(2), 81–84. https://doi.org/10.1016/s0304-3940(02)01162-x

Koshiba, M., Yohda, M., & Nakamura, S. (2005). Topological relation of chick thalamofugal visual projections with hyper pallium revealed by three color tracers. *Neuroscience Research*, *52*(3), 235–242. https://doi.org/10.1016/j.neures.2005.03.017

Kram, Y. A., Mantey, S., & Corbo, J. C. (2010). Avian cone photoreceptors tile the retina as five independent, self-organizing mosaics. *PLoS ONE*, *5*(2). https://doi.org/10.1371/journal.pone.0008992

Kuenzel, W. J., & Masson, M. (1988). *A stereotaxic atlas of the brain of the chick (Gallus domesticus)*. Johns Hopkins University Press, Baltimor and London, 166pp.

Lengersdorf, D., Pusch, R., Güntürkün, O., & Stüttgen, M. C. (2014). Neurons in the pigeon nidopallium caudolaterale signal the selection and execution of perceptual decisions. *European Journal of Neuroscience*, *40*(9), 3316–3327. https://doi.org/10.1111/ejn.12698

López-López, R., López-Gallardo, M., Pérez-Álvarez, M. J., & Prada, C. (2008). Isolation of chick retina cones and study of their diversity based on oil droplet colour and nucleus position. *Cell and Tissue Research*, *332*(1), 13–24. https://doi.org/10.1007/s00441-007-0572-6

López-López, R., López-Gallardo, M., Pérez-Álvarez, M. J., & Prada, C. (2008). Isolation of chick retina cones and study of their diversity based on oil droplet colour and nucleus position. *Cell and Tissue Research*, *332*(1), 13–24. https://doi.org/10.1007/s00441-007-0572-6

Manns, M., Freund, N., & Güntürkün, O. (2008). Development of the diencephalic relay structures of the visual thalamofugal system in pigeons. *Brain Research Bulletin*, *75*(2-4), 424–427. https://doi.org/10.1016/j.brainresbull.2007.10.036

Manns, M., Freund, N., Patzke, N., & Güntürkün, O. (2007). Organization of telencephalotectal projections in pigeons: Impact for lateralized top-down control. *Neuroscience*, *144*(2), 645–653. https://doi.org/10.1016/j.neuroscience.2006.09.043

Martinez-de-la-Torre, M., Martinez, S., & Puelles, L. (1990). Acetylcholinesterase-histochemical differential staining of subdivisions within the nucleus rotundus in the Chick. *Anatomy and Embryology*, *181*(2). https://doi.org/10.1007/bf00198952

Miceli, D., Marchand, L., Repérant, J., & Rio, J.-P. (1990). Projections of the dorsolateral anterior complex and adjacent thalamic nuclei upon the visual wulst in the pigeon. *Brain Research*, *518*(1-2), 317–323. https://doi.org/10.1016/0006-8993(90)90990-s

Miceli, D., Peyrichoux, J., & Repe´rant, J. (1975). The retino-thalamo-hyperstriatal pathway in the pigeon (Columba Livia). *Brain Research*, *100*(1), 125–131. https://doi.org/10.1016/0006-8993(75)90247-4

Miceli, D., Repérant, J., Medina, M., Volle, M., & Rio, J.-P. (2006). Distribution of ganglion cells in the pigeon retina labeled via retrograde transneuronal transport of the fluorescent dye rhodamine β-isothiocyanate from the Telencephalic Visual wulst. *Brain Research*, *1098*(1), 94–105. https://doi.org/10.1016/j.brainres.2006.04.091

Miceli, D., Repérant, J., Ward, R., Rio, J.-P., Jay, B., Médina, M., & Kenigfest, N. B. (2008). Fine structure of the visual dorsolateral anterior thalamic nucleus of the pigeon (*Columba livia*): A hodological and GABA-immunocytochemical study. *The Journal of Comparative Neurology*, *507*(3), 1351–1378. https://doi.org/10.1002/cne.21635

Okano, T., Kojima, D., Fukada, Y., Shichida, Y., & Yoshizawa, T. (1992). Primary structures of chicken cone visual pigments: Vertebrate rhodopsins have evolved out of cone visual pigments. *Proceedings of the National Academy of Sciences*, *89*(13), 5932–5936. https://doi.org/10.1073/pnas.89.13.5932

Remy, M., & Güntürkün, O. (1991). Retinal afferents to the tectum opticum and the nucleus opticus principalis thalami in the pigeon. *Journal of Comparative Neurology*, *305*(1), 57–70. https://doi.org/10.1002/cne.903050107

Rio, J. P., Villalobos, J., Miceli, D., & Repérant, J. (1983). Efferent projections of the visual wulst upon the nucleus of the basal optic root in the pigeon. *Brain Research*, *271*(1), 145–151. https://doi.org/10.1016/0006-8993(83)91375-6

Scarf, D., Stuart, M., Johnston, M., & Colombo, M. (2016). Visual response properties of neurons in four areas of the avian pallium. *Journal of Comparative Physiology A*, *202*(3), 235–245. https://doi.org/10.1007/s00359-016-1071-6

Shimizu, T., & Bowers, A. N. (1999). Visual circuits of the avian telencephalon: Evolutionary implications. *Behavioural Brain Research*, *98*(2), 183–191. https://doi.org/10.1016/s0166-4328(98)00083-7

Shimizu, T., & Karten, H. J. (1990). Immunohistochemical analysis of the Visual Wulst of the pigeon (*Columba livia*). *The Journal of Comparative Neurology*, *300*(3), 346–369. https://doi.org/10.1002/cne.903000307

Shimizu, T., Cox, K., & Karten, H. J. (1995). Intratelencephalic projections of the visual wulst in pigeons (*Columba livia*). *The Journal of Comparative Neurology*, *359*(4), 551–572. https://doi.org/10.1002/cne.903590404

Stacho, M., Herold, C., Rook, N., Wagner, H., Axer, M., Amunts, K., & Güntürkün, O. (2020). A cortex-like canonical circuit in the avian forebrain. *Science*, *369*(6511). https://doi.org/10.1126/science.abc5534

Wilson, P. (1980). The organization of the visual hyperstriatum in the domestic chick. I. Topology and topography of the visual projection. *Brain Research*, *188*(2), 319–332. https://doi.org/10.1016/0006-8993(80)90034-7

Legends, Figures, and Tables

Fig 4.1. Protocol for registering histological and diceCT brain images to ensure accurate size, orientation, and position of relevant neural structures that comprise the avian thalamofugal visual system. **A,B:** Left lateral view of the rendered diceCT chick brain and eyeball in their approximate positions in the absence of the skull. This was accomplished by using both surface and wireframe projections within the Blender software environment and placement of half of the brain at midline that would be comparable to a side view of atlas plate L 0.2 of a stereotaxic brain atlas of the chick (Kuenzel and Masson, 1988). **C,D,E,F:** Left anterolateral view of the rendered diceCT brain, interposed by midline atlas plate L 0.2 and corresponding coronal or cross sections of the stereotaxic atlas (**C,** A13.0; **D**, A11.0; **E**, A8.0; **F**, 6.0).

Fig 4.2. Coronal sections from the approximate locations shown in Fig. 1 D and E are displayed showing three different methods of visualizing neural structures and fibers. (**A,D**) shows an anterior (A) and near midbrain (D) cross section stained with luxol fast blue (dark blue) and cresyl violet (pink/light violet) staining fibers and cell bodies respectively; (**B,E**) showing comparable sections imaged with diceCT displaying fibers as white and cell bodies as grey. The

third set, (**C,F**) shows fibers stained black with Gallyas (**C**, GSM) and perikarya stained blue with Nissl. Datasets representing the wulst include sections **ABC** while the lateral geniculate structures (GLd) are displayed in sections **DEF**.

Fig 4.3. Rostrocaudal series of Luxol fast blue myelin stain of the Wulst (**ABC**) and the dorsal lateral geniculate nucleus (**DEF**). From our interpretations, we have outlined the different nuclei of the GLd and the laminar organization of the Wulst using dotted lines.

Fig 4.4. Frontal view of the diceCT eyeball and brain. **A:** Structures rendered as fully opaque as a reference visualization. **B:** Rendered brain surface and eye have been made semitransparent to illustrate the lateral geniculate nucleus as a whole structure (right hemisphere, black) and as its subdivided nuclei components (left hemisphere; dark green, LA; dark purple, DLL; light green, SPC; light pink, LdOPT; brown, SpROT; dark blue, DLAlr; black, DLAmc). An additional thalamic component, SROT (dark orange) is shown as well.

Fig 4.5. Frontal view of the diceCT eyeball and brain. **A:** Structures rendered as fully opaque as a reference visualization. **B:** Rendered brain surface and eye have been made semitransparent to illustrate the Wulst as a whole structure (right hemisphere, black) and as subcomponents (left hemisphere; yellow, apical hyperpallium (HA); light orange, superior intercalated hyperpallium (HIS); red, densocellular hyperpallium (HD).

Fig 4.6. 3D reconstruction of the thalamofugal nuclei with their interconnectivity in a three-quarters profile view. **A:** solid rendering of the diceCT brain as a reference visualization. **B:** semitransparent rendering of the diceCT brain. **C:** retinal ganglion cells projecting from the retina to the contralateral GLd. **D:** Addition of the lateral anterior thalamus (LA, dark green). **E:** Addition of the dorsolateral anterior thalamus, rostrolateral part (DLAlr, dark blue). **F:** Addition of the dorsolateral anterior thalamus, magnocellular part (DLAmc, black). **G:** Addition of the dorsolateral anterior thalamus, lateral part (DLL, dark purple). **H:** Addition of the superior parvocellular nucleus (SPC, light green). **I:** Addition of dorsal lateral principal optic thalamus (LdOPT, light pink). **J:** Addition of suprarotundus (SpROT, brown) and subrotundus (SROT, dark orange). **K:** Addition of the ipsilateral and contralateral projections of the GLd nuclei to the densocellular hyperpallium (HD, red) and superior intercalated hyperpallium (HIS, light orange) of the Wulst. **L:** Addition of the apical hyperpallium (HA, yellow) and the projections between the HA and HIS/HD. **M:** Addition of the frontolateral nidopallium (NFL, light blue) and caudolateral nidopallium (NCL, dark pink) with the reciprocal projections to the HA. **N:** Addition of the intermediate arcopallium (AI, dark grey) with its reciprocal bilateral projections to the HA.

Fig 4.7. Semitransparent diceCT brain in three-quarters profile view illustrating a 3D reconstruction of the fiber tracts, decussations, and commissures used by the thalamofugal pathway. Projections between thalamofugal structures are color-coded to represent afferent projections from one nucleus to the next. A reference image showing the thalamofugal structures is shown at the bottom right (see Figure 4.5n for structure identifications. Additionally, complete names of all abbreviations of structures are given in the in Fig. legend 4.5). The striped white and black tubes represent the axonal projections from the retina to the contralateral GLd nuclei. Light

pink tubes represent contralateral projections of LdOPT to Wulst using the dsd and lfb. Dark blue tubes represent projections from DLAlr to the contralateral Wulst using the dsd and lfb. Black tubes represent projections from DLAmc to the ipsilateral Wulst using the lfb or to the contralateral Wulst using the dsd and lfb. Dark purple tubes represent projections from the DLL to the ipsilateral Wulst using the lfb or to the contralateral Wulst using the dsd and lfb. Light green tubes represent projections to the ipsilateral Wulst using the lfb or to the contralateral Wulst using the dsd and lfb. Brown tubes represent projections to the ipsilateral Wulst using the lfb. Dark orange tubes represent projections to the ipsilateral Wulst using the lfb. Red tubes represent projections from the HD to the HA. Light orange tubes represent projection from the HIS to the HA. Yellow tubes represent projections of the HA to the ipsilateral NFL, NCL or AI. Additional thick yellow tubes represent HA projecting back down to the thalamus using the csm. Light blue tubes represent projections of NFL to HA. Dark pink tubes represent projections from the NCL to the ipsilateral HA. Grey tubes represent projections of the AI to the ipsilateral Wulst using the dat or to the contralateral Wulst using the ac.

Fig 4.8. Semi-lateral view of the primary components of the thalamofugal system in the semitransparent diceCT rendered eye and brain with callout boxes of detailed neuroanatomy of 2D sagittal sections of the GLd, and Wulst. Call-out boxes display important neuron synapses of RGC and GLd neurons, and GLd and Wulst neurons.

Fig 4.9. Semi-lateral view of the primary components of the thalamofugal system in the semitransparent diceCT rendered eye and brain with callout boxes of detailed neuroanatomy of 2D coronal sections of the dorsal lateral geniculate complex (GLd) and Wulst. Callout boxes display the types of dendritic configurations found at each level. Scale bar in the GLd figure = 50 um. Scale bar in the Wulst figure = 100 um.

Table 4.1. Rendered nuclei of the GLd, their abbreviations, and color code

Table 4.2. Rendered Wulst divisions, their abbreviations, and color code

Table 4.3. Rendered extra thalamofugal structures, their abbreviations, and color code

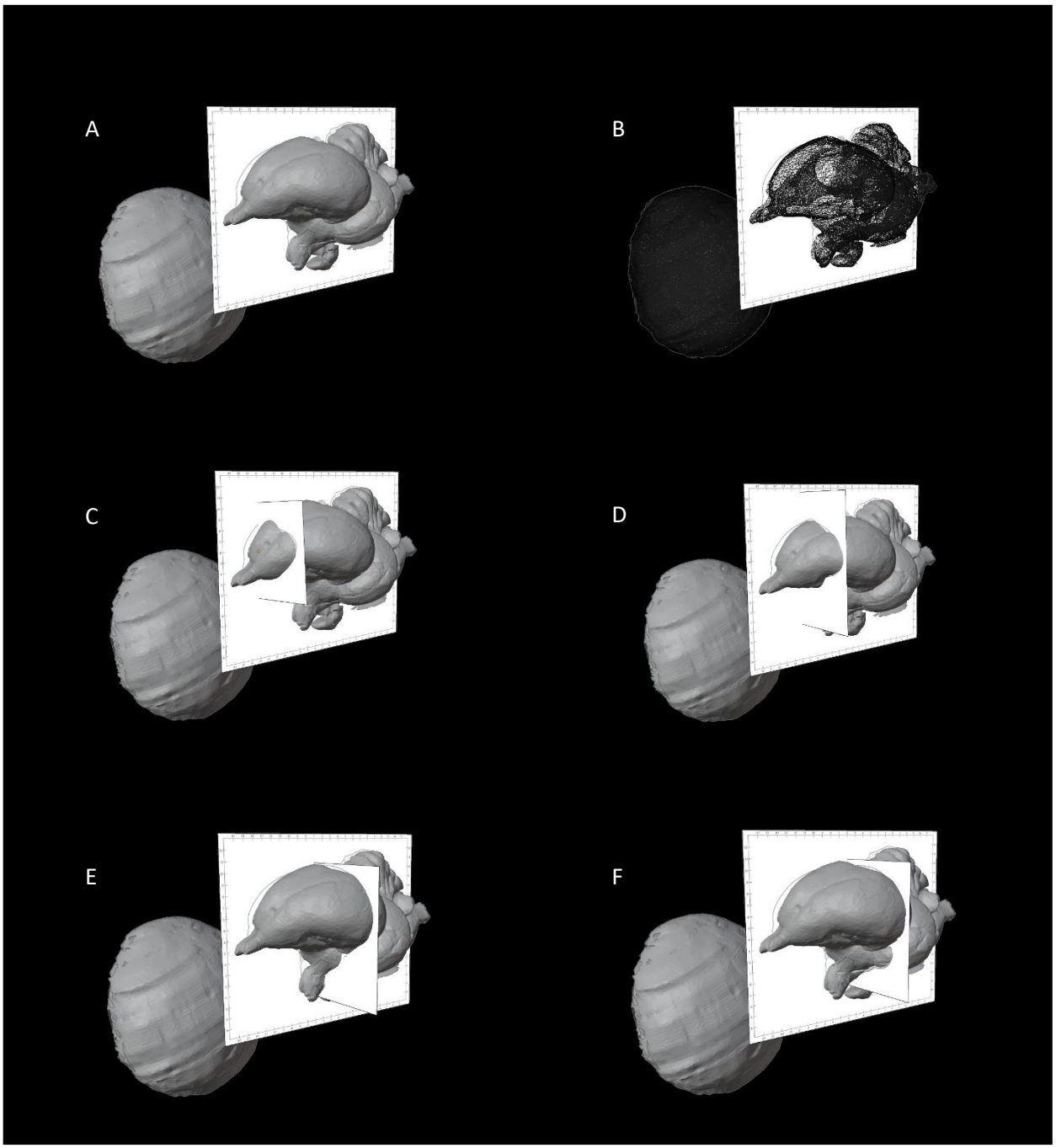

Figure 4.1

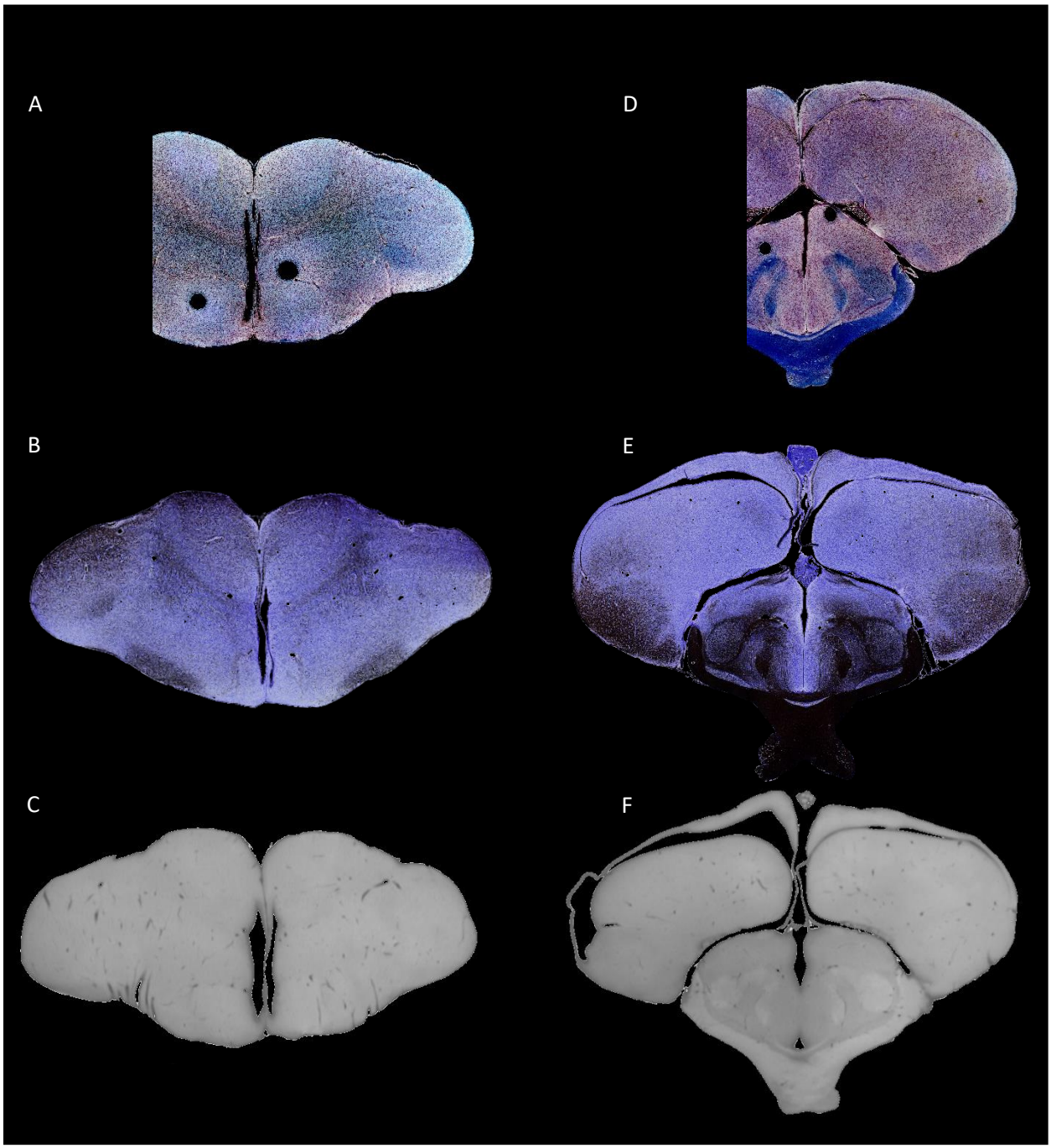

Figure 4.2

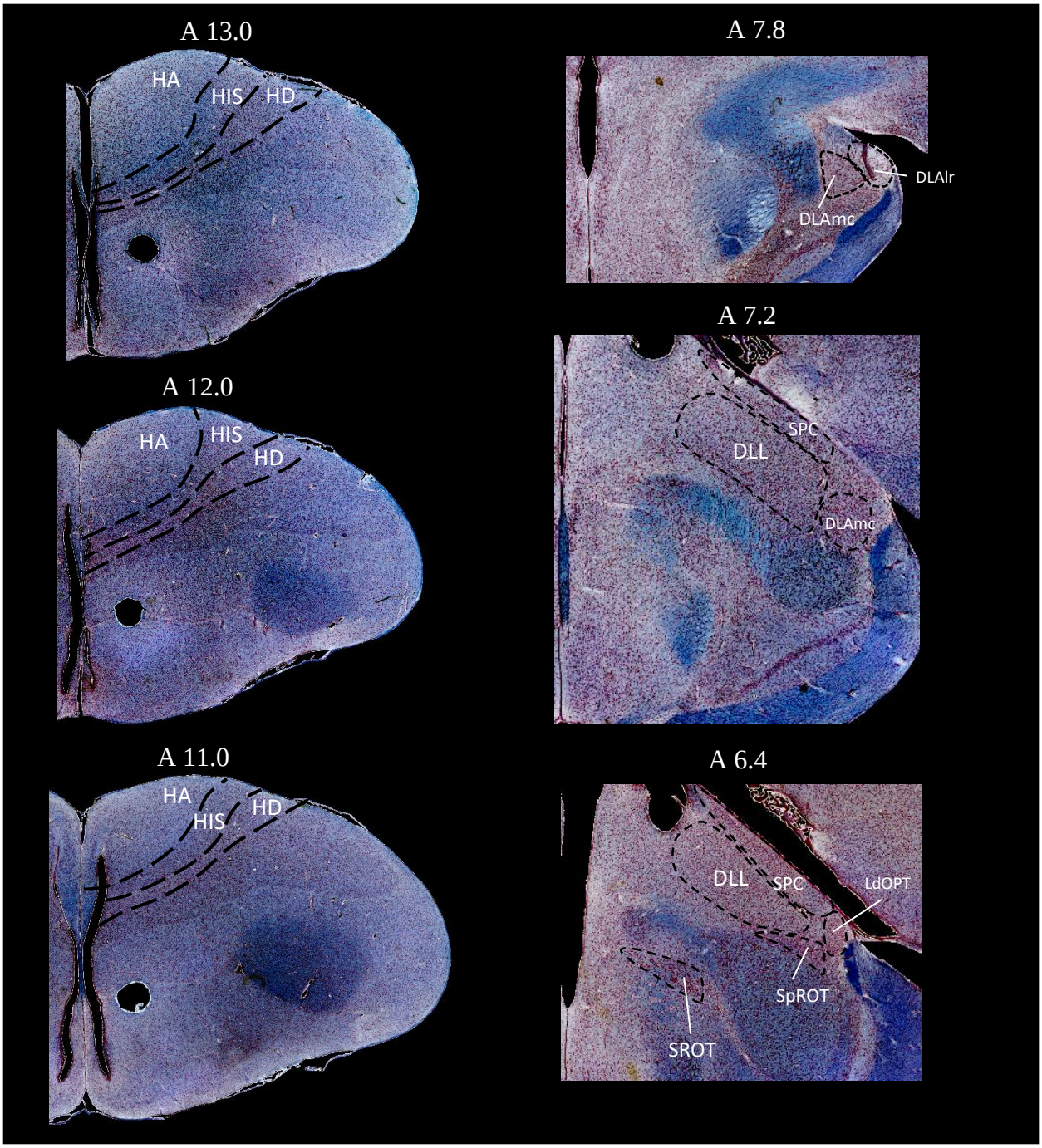
A 13.0
HA
HIS
HD
A 12.0
HA
HIS
HD
A 11.0
HA
HIS
HD
A 7.8
DLAlr
DLAmc
A 7.2
SPC
DLL
DLAmc
A 6.4
DLL
SPC
LdOPT
SpROT
SROT

Figure 4.3

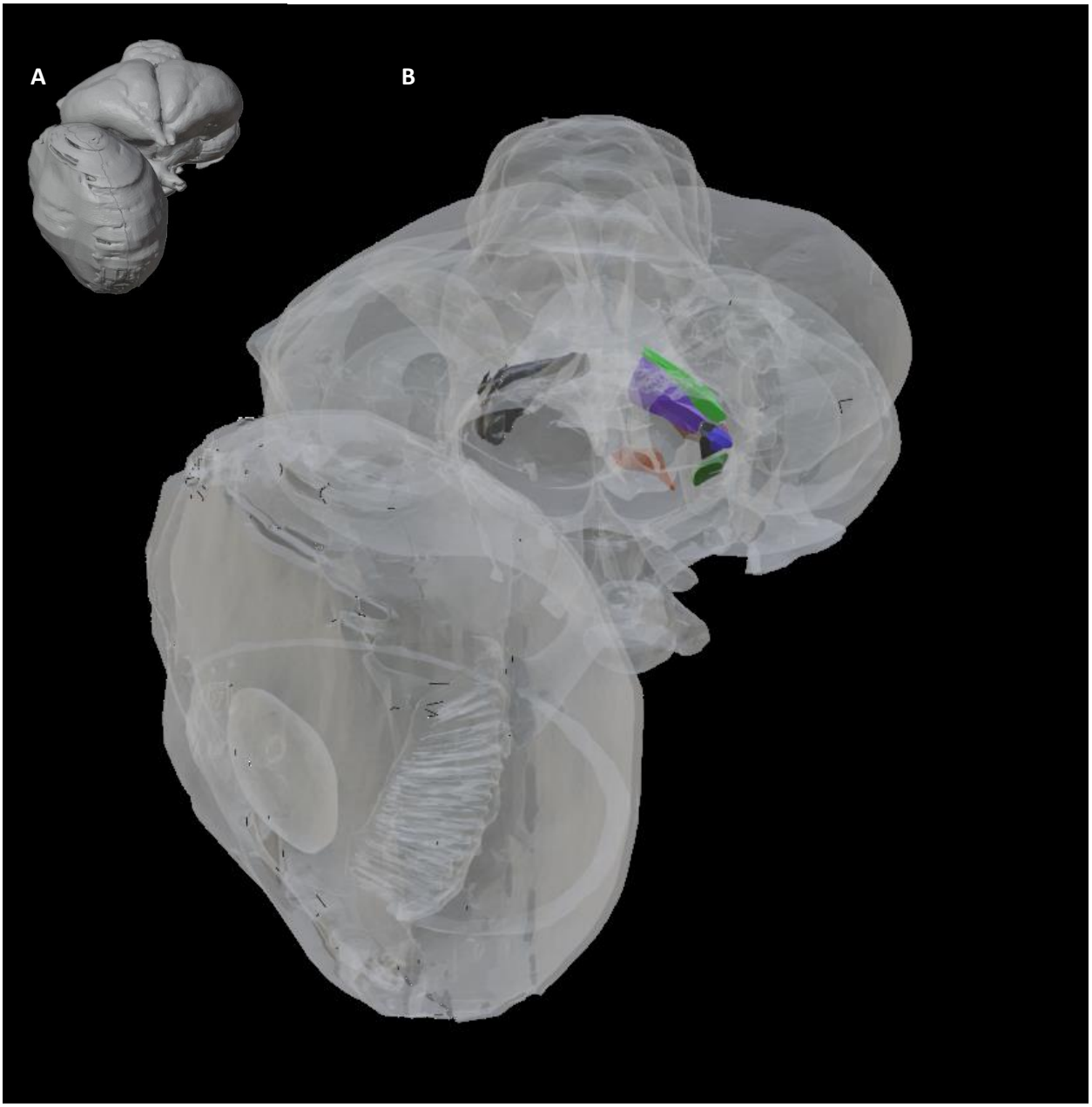

Figure 4.4

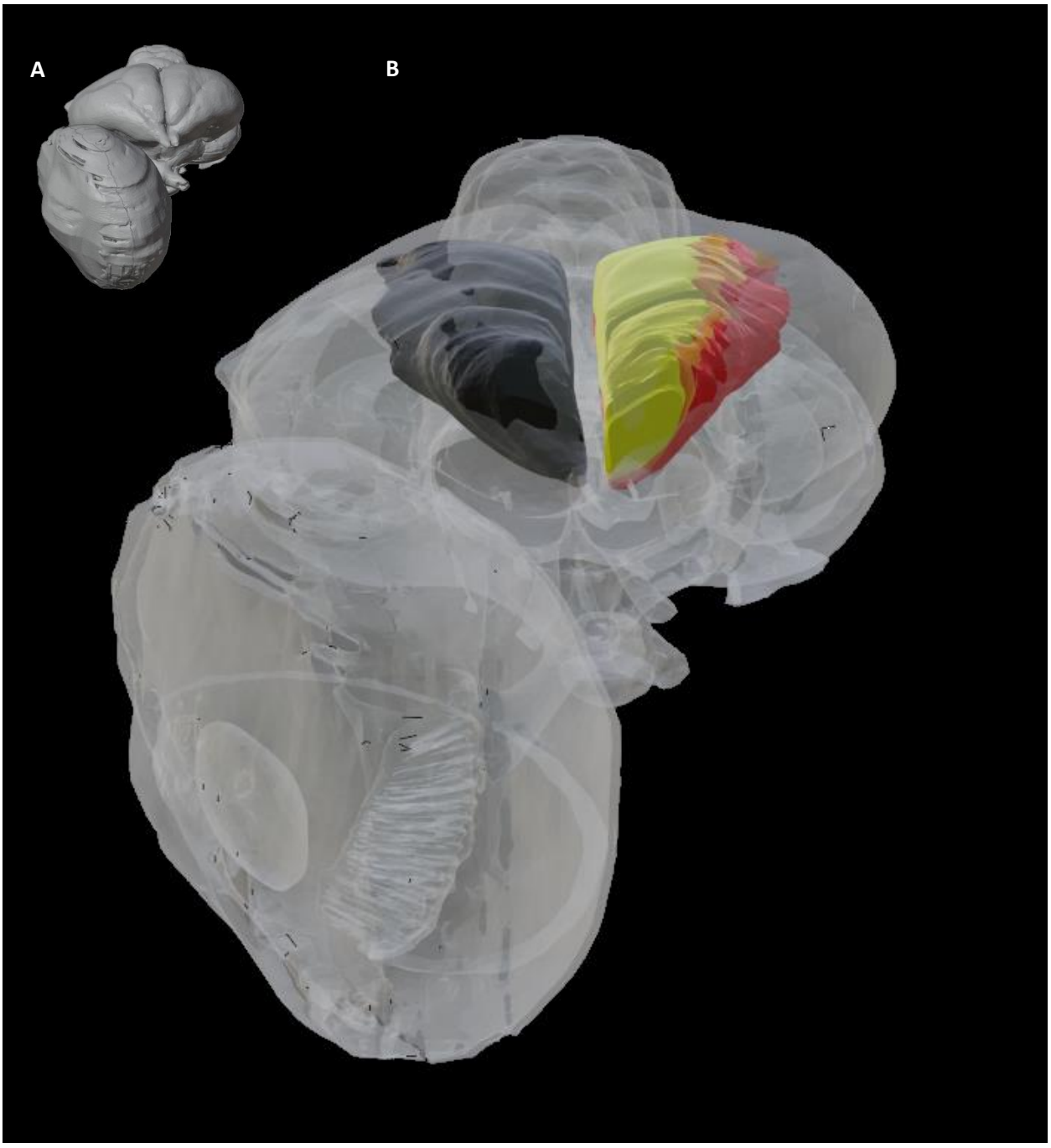

Figure 4.5

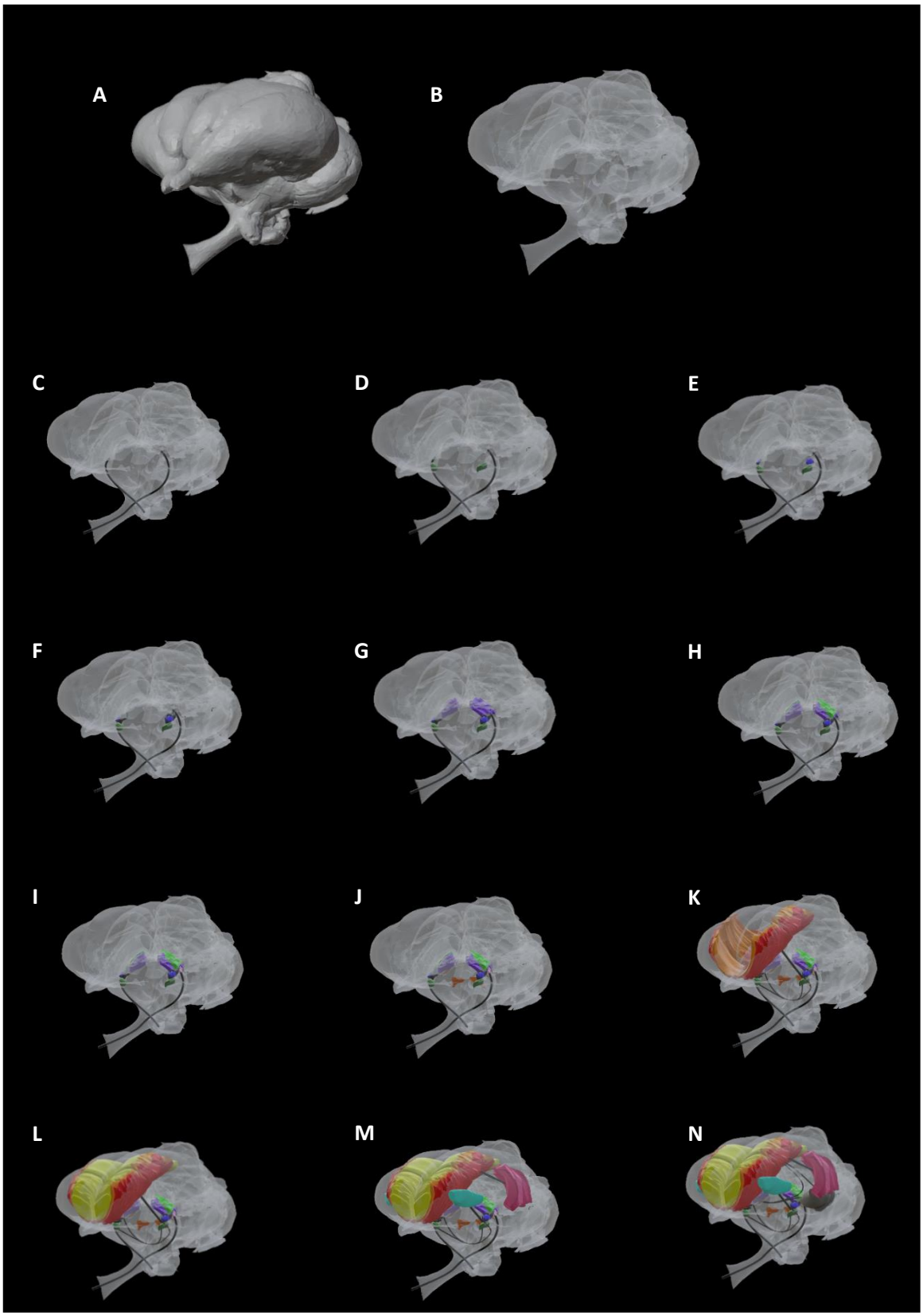

Figure 4.6

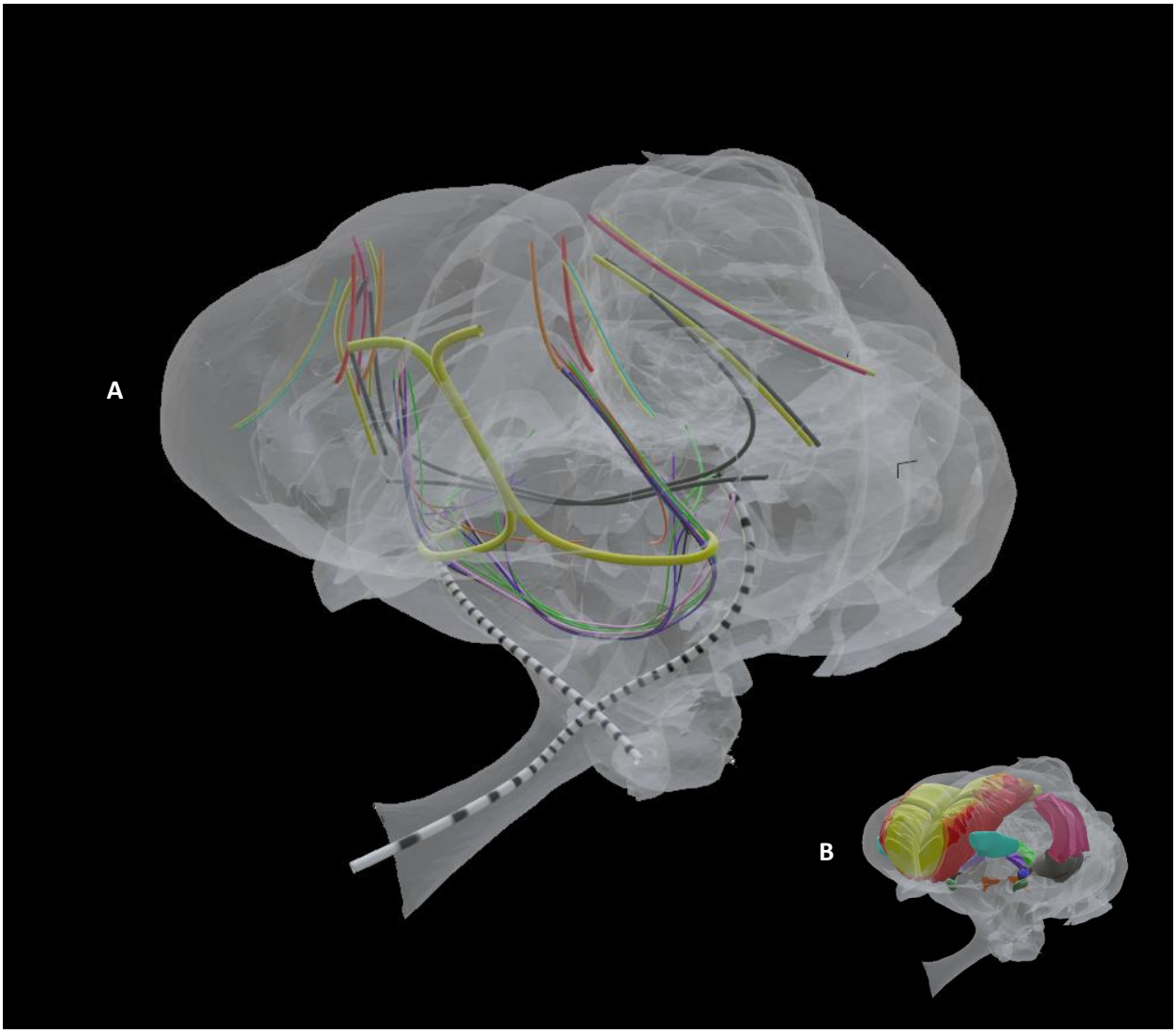

Figure 4.7

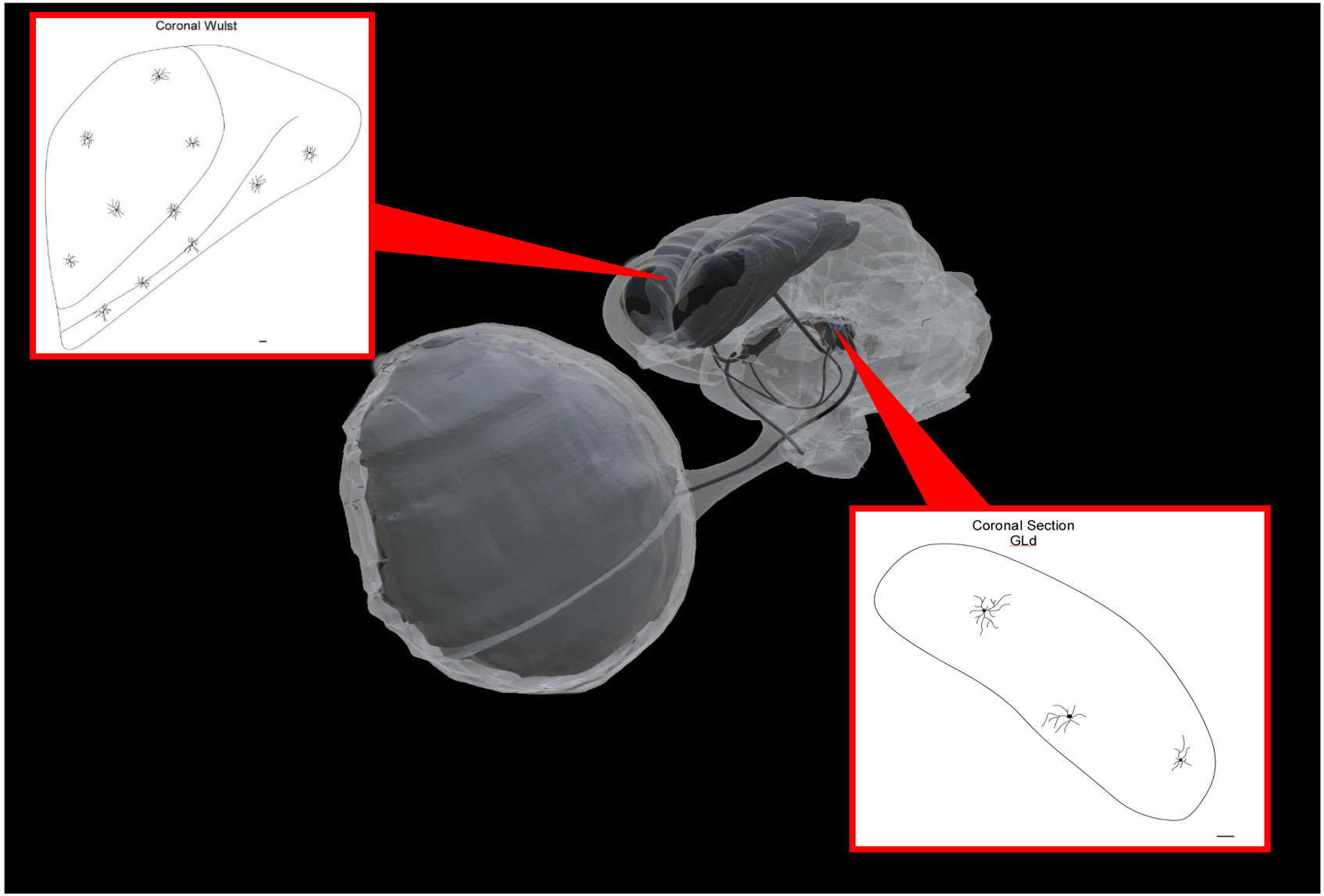

Figure 4.8

Table 4.1

Abbreviation	Structure	Color
DLAlr	dorsolateral anterior thalamus, rostrolateral part	
DLAmc	dorsolateral anterior thalamus, magnocellular part	
DLL	dorsolateral anterior thalamus, lateral part	
LA	lateral anterior thalamus	
LdOPT	dorsolateral principal optic thalamus	
SPC	superficial parvocellular nucleus	
SpROT	suprarotundus	
SROT	subrotundus	

Table 4.2

Abbreviation	Structure	Color
W	Wulst	
HA	apical hyperpallium	
HIS	superior intercalated hyperpallium	
HD	densocellular hyperpallium	

Table 4.3

Abbreviation	Structure	Color
NFL	frontal lateral nidopallium	
NCL	caudal lateral nidopallium	
AI	intermediate arcopallium	

Chapter 5. Conclusion

Most neuroanatomical research investigating the tectofugal and thalamofugal visual systems in birds have been conducted without the use of three-dimensional visualization tools. Though these past studies have made plentiful observations of these systems, there is often an absence of complete comprehension of the spatial organization, structural information and axonal movement. The development of imaging techniques such as diceCT has allowed for non-destructive, reversible visualization of soft tissues at any preferred angle. This allows researchers to maintain the topographic relationships of anatomical structures relative to one another that would often be disrupted when using traditional methods such as serial sectioning. Though these 3D imaging techniques present effective ways of imaging brain tissue, they often cannot present the microlevel detail one might obtain from traditional methodology. Therefore, pairing diceCT with classical techniques such as serial histochemistry provides an excellent means to study neuroanatomical pathways. Integration of these methods can allow for the production of highly detailed, comprehensive neuroanatomical models as we have shown here. Generating these 3D models will permit more efficient means of studying neuroanatomy in the context of research by aiding electrode or tract tracer placement, and in the context of education by supplementing 2D visualizations with 3D models to enhance learning of complex neural systems.